Performance Analysis of Bearings-only Tracking Problems for Maneuvering Target and Heterogeneous Sensor Applications

DISSERTATION

zur

Erlangung des Doktorgrades (Dr. rer. nat.)

der

Mathematisch-Naturwissenschaftlichen Fakultät

der

Rheinischen Friedrich-Wilhelms-Universität Bonn

vorgelegt von

Dipl.-Inform. Julian Hörst

aus

Bochum

Bonn, 2018

Angefertigt mit Genehmigung der Mathematisch-Naturwissenschaftlichen Fakultät der Rheinischen Friedrich-Wilhelms-Universität Bonn

1. Gutachter: Prof. Dr. Wolfgang Koch
2. Gutachter: Prof. Dr. Peter Martini

Tag der Promotion: 16.11.2018
Erscheinungsjahr: 2018

Zusammenfassung

Lokalisierung und Tracking mittels passiver Winkelmessungen (engl. Bearings-only Tracking) spielt in vielen Anwendungsfeldern eine wichtige Rolle. Maßgeblich sind Szenarien, in denen aus taktischen Gründen der Ort der eigenen Aufklärungsplattform nicht preisgegeben werden darf und daher der Einsatz passiver Sensorik bevorzugt wird. Herausforderungen sind dabei zum einen die Verwendung eines nichtlinearen Messmodells, so dass optimale Schätzverfahren nicht existieren. Zum anderen lässt sich durch eine passive Winkelmessung nicht der gesamte Zielzustand bestimmen, da die Messung keine Informationen über die Entfernung zum Ziel beinhaltet. Um Observabilität herzustellen, d.h. den vollständigen Zielzustand bestimmen zu können, müssen mehrere Winkelmessungen fusioniert werden. Die Messungen können entweder räumlich verteilt durch mehrere Sensorplattformen oder zeitlich verteilt durch eine sich bewegende Einzelplattform aufgenommen werden. Darüber hinaus können verschiedene Signalarten – neben den elektromagnetischen auch z.B. akustische Signale – genutzt werden, um durch Ausnutzung der verschiedenen Signallaufzeiten in einem heterogenen Sensor-Setup den Zielzustand bestimmen zu können.

Forschungsaspekte der Dissertation Die Dissertation hat sowohl innovative Ergebnisse in theoretischen Untersuchungen zur Lokalisierung und zum Tracking von manövrierenden Zielen mittels passiver, heterogener Sensorik als auch Ergebnisse aus praktischen Messkampagnen. Diese sollen im Folgenden zusammengefasst werden.

Theoretische Ergebnisse Die theoretischen Betrachtungen sind fokussiert auf Genauigkeits- und Observabilitätsanalysen. Beides spielt in praktischen Anwendungen dahingehend eine wichtige Rolle, als dass die Performanz von passiven, verteilten Aufklärungssystemen vordergründig von der räumlichen Konstellation in Abhängigkeit der nichtlinearen Sensormodelle abhängt. Die Bewertung und Auswahl eines geeigneten Schätzalgorithmus ist daher ohne präzise Kenntnisse der entsprechenden Schätzfehlerschranken (Cramér-Rao Lower Bound, CRLB) nicht sinnvoll [HO10, OH10, HO11a, HO11b, HOK14]. Hierbei müssen die Arbeiten zur Observabilitätsanalyse hervorgehoben werden, die aufzeigen, dass durch die Verwendung heterogener Sensorik, die beispielsweise akustische und optische/elektromagnetische Signale desselben Ereignisses messen, eine gesteigerte Observabiltät erreicht werden kann. Der Schlüssel hierzu liegt in der geschickten Ausnutzung der unterschiedlichen Signallaufzeiten [HGR+16, HK16].

Praktische Ergebnisse Die im theoretischen Teil untersuchten Schätzverfahren zur Lokalisierung und Verfolgung von Zielen mittels verteilter, passiver Sensorik sind im Rahmen des Eigenforschungsprojektes zum vernetzten, dezentralen Schutz von Plattformen implementiert und verglichen worden. In diesem Rahmen wurde für die Fusion verteilter Daten eine Kommunikationsinfrastruktur aufgebaut: Diese wurde mittels eines dezentralen mobilen Ad-hoc-Netzes (MANET) auf WLAN-Basis realisiert. Um robusten Datenaustausch auch unter Abschattungs- bzw. Ausfallbedingungen zu gewährleisten, wurde das Routing mittels OLSRv2 durchgeführt. Das komplexe Zusammenspiel der heterogenen Sensorik und der Kommunikation stellt die wesentliche Forschungsleistung dar. Die Ergebnisse zeigen, dass in diesem System eine Bedrohung erfolgreich lokalisiert werden kann [HGR+16].

Abstract

State estimation, i.e. determining the trajectory, of a maneuvering target from noisy measurements collected by a single or multiple passive sensors (e.g. passive sonar and radar) has wide civil and military applications, for example underwater surveillance, air defence, wireless communications, and self-protection of military vehicles. These passive sensors are listening to target emitted signals without emitting signals themselves which give them concealing properties. Tactical scenarios exists where the own position shall not be revealed, e.g. for tracking submarines with passive sonar or tracking an aerial target by means of electro-optic image sensors like infrared sensors. This estimation process is widely known as *bearings-only tracking*.

On the one hand, a challenge is the high degree of nonlinearity in the estimation process caused by the nonlinear relation of angular measurements to the Cartesian state. On the other hand, passive sensors cannot provide direct target location measurements, so bearings-only tracking suffers from poor target trajectory estimation accuracy due to marginal observability from sensor measurements. In order to achieve observability, that means to be able to estimate the complete target state, multiple passive sensor measurements must be fused. The measurements can be recorded spatially distributed by multiple dislocated sensor platforms or temporally distributed by a single, moving sensor platform. Furthermore, an extended case of bearings-only tracking is given if heterogeneous measurements from targets emitting different types of signals, are involved. With this, observability can also be achieved on a single, not necessarily moving platform.

In this work, a performance bound for complex motion models, i.e. piecewisely maneuvering targets with unknown maneuver change times, by means of bearings-only measurements from a single, moving sensor platform is derived and an efficient estimator is implemented and analyzed. Furthermore, an observability analysis is carried out for targets emitting acoustic and electromagnetic signals. Here, the different signal propagation velocities can be exploited to ensure observability on a single, not necessarily moving platform.

Based on the theoretical performance and observability analyses a distributed fusion system has been realized by means of heterogeneous sensors, which shall detect an event and localize a threat. This is performed by a microphone array to detect sound waves emitted by the threat as well as a radar detector that detects electromagnetic emissions from the threat. Since multiple platforms are involved to provide increased observability

and also redundancy against possible breakdowns, a WiFi mobile ad hoc network is used for communications. In order to keep up the network in a breakdown OLSR (optimized link state routing) routing approach is employed.

Acknowledgments

I would like to express my sincere gratitude to my supervisor Prof. Dr. Wolfgang Koch. I am very grateful for his support in the last years providing guidance and perfect research and working conditions in his department of Sensor Data and Information Fusion at Fraunhofer FKIE.

I would also like to thank Prof. Dr. Peter Martini for being the second supervisor and Prof. Dr. Rainer Manthey and Prof. Dr. Andreas Eberle from the University of Bonn for serving in the examination committee.

Special thanks go to my colleagues at Fraunhofer FKIE, namely Dr. Felix Govaers for many fruitful discussions and proofreading this thesis, Dr. Marc Oispuu who gave the first inspirations and co-authored many papers this thesis in based on, Klaus Wild for giving me the opportunity to work on highly interesting research projects, and Peter Sevenich for providing me motivation to finalize this work. Without your support, this thesis would not have been possible.

Finally, I would like to say thank you to my family and numerous friends which are too many to name them all for always believing in me and thus motivating me to continue to write this thesis!

Contents

1 Introduction

State estimation, i.e. determining the trajectory, of a maneuvering target from noisy measurements collected by a single or multiple passive sensors (e.g. passive sonar and radar) has wide civil and military applications, for example underwater surveillance, air defence, wireless communications, and self-protection of military vehicles. These passive sensors are listening to target emitted signals without emitting signals themselves which give them concealing properties. Tactical scenarios exists where the own position shall not be revealed as it would be using a radar ping, e.g. for tracking submarines with passive sonar [BH09, Li12], localizing shooters with acoustic sensors [LWGH09], interception and analysis of emitted signals in a warfare situation in order to exploit these for military actions (electronic support measures – ESM) [GC82], or tracking an aerial target by means of electro-optic image sensors like infrared sensors [Hu01]. This estimation process is widely known as *bearings-only tracking* (BOT) [LSM08] since in most cases, the measurements are line of sight (LoS) azimuth angle measurements corrupted by noise. Such measurements are also called angle-only measurements [RA03], *direction of arrival (DoA)*, or *angle of arrival (AoA)* measurements [Far99]. An alternative term for this estimation process is bearings-only *target motion analysis* (TMA or sometimes BO-TMA) which is particularly used in the submarine domain [LG78, Bec01].

As the passive sensors cannot provide direct target location measurements, BOT or TMA suffers from poor target trajectory estimation accuracy due to marginal observability from sensor measurements [LSM08]. In order to achieve observability, that means to be able to estimate the complete target state, multiple passive sensor measurements must be fused. The measurements can be recorded spatially distributed by multiple dislocated sensor platforms or temporally distributed by a single, moving sensor platform. Depending on the target's motion behavior, the platform must even "outmaneuver" the target. This is explained in [RA03] as "observer motion is one derivative higher than that of the target and one component of the motion is perpendicular to the LOS [line of sight]". See also [NA81, FG88, Bec93, JP96, LWBL16] for further reading. However, under certain circumstances, for example a circular motion target (performing a constant turn) observed by a non-maneuvering platform moving with constant velocity, observability conditions can be met [CPPJ11, CPPJ13][1]. An extended case of BOT is given if heterogeneous measurements from, for example, targets emitting acoustic and electromagnetic signals,

[1] The setting of BOT involving a circular motion target has already been treated by Gauss [Gau09] and Laplace [Lap80] in the 18/19th century while observing the trajectory of an asteroid with a telescope. Gauss, and independently Legendre [Leg06], invented the least squares method in this context [Sor70].

are involved [YNBS15]. Here, the different signal propagation velocities can be exploited to ensure observability on a single, not necessarily moving platform [HK16].

As mentioned, the performance of such a passive system depends on the spatial constellation of the sensors with strong relation to their nonlinear sensor models. Hence, a further challenge is the high degree of nonlinearity in the estimation process caused by the nonlinear relation of angular measurements to the Cartesian state as well as complex motion models considering maneuvering targets. In order to assess the best possible estimation performance in such a nonlinear setting, estimation error bounds as the *Cramér-Rao lower bound* (CRLB) have to be evaluated. These pose a lower limit on what an estimator can achieve meaning that no estimator, on average, can provide better results than given by the bound [Ker89].

Typically, one has to distinguish between *Bayesian* and *non-Bayesian* methods for state estimation. Although both approaches are eligible and practically relevant today and depending on the scenario, one has to thoroughly choose the appropriate technique, since they have their origin in different philosophical views of probability, see e.g. [Tsc14]. The classical, non-Bayesian, method is preferred in economic and social sciences as well as biology. In order to estimate a parameter or to test a hypothesis, it only uses the sample of observations. In this context, the term probability means relative frequency within a random experiment. Hence, classical statisticians are often called frequentists. Transferred to state estimation, the state is modeled as an unknown constant and it is estimated by assessing how likely the state is given all obtained measurements by means of a likelihood function [BSLK01]. An important example is the *maximum likelihood estimator* (MLE). On the other hand, the Bayesian interpretation of probability is an expression of knowledge. The difference to the classical method is that one assumes prior knowledge about the problem. By means of Bayes' rule, established by reverend Bayes in 1763 [Bay63], one can derive improved knowledge by including the observations. For a popular science perspective on the Bayesian sphere, see [McG11]. The Bayesian statistic is preferred in the technical domain and in artificial intelligence. A remarkable example is the description of the search for crashed flight MH370 using Bayesian methods [DGH+16][2]. Since fusion and tracking also lie in these domains, an outsize number of papers uses Bayesian state estimation. Here, the state is modeled as a random variable and associated with a prior density which subsumes the a priori knowledge about the state. Using Bayes' rule, a posterior density of the state can be calculated which includes the information from motion and measurement. Such an estimator is often called *filter*, its major representative is the *Kalman filter* [Kal60].

A fundamental disadvantage of many non-Bayesian state estimation methods is the computational complexity: For the vast majority of nonlinear problems, a numerical optimization algorithm has to be applied trying to find the optimal state considering the

[2] Unfortunately, despite the Bayesian approach, the airplane wreck has not been found yet. The reason for the accident that happened in March 2014 remains a puzzle.

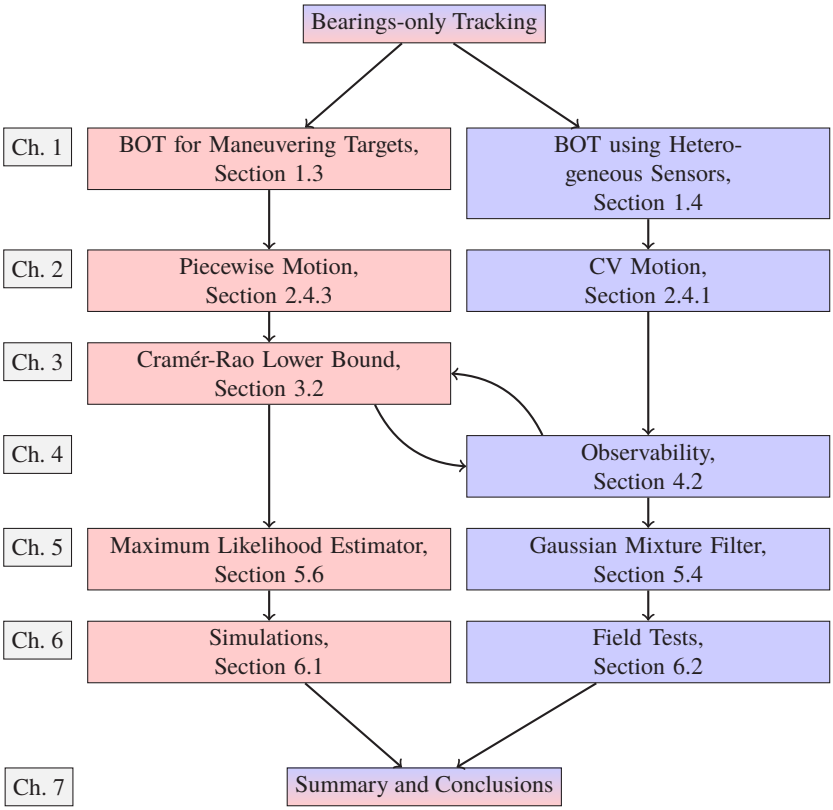

Figure 1.1: Structure of this thesis with vertical central themes differentiated by color and horizontal chapters. In each chapter, the key sections relevant to the central themes are named.

complete observation batch. Bayesian filters have successfully tackled this problem by using a recursive update scheme. Nevertheless, with the availability of higher computational power in recent times, batch calculations may undergo a renaissance. Focussing on this thesis, both schools of thinking are reflected depending on their relevance on the concrete estimation problem.

1.1 Structure of this Thesis

The structure of this thesis is illustrated in Fig. 1.1, where all key sections are addressed: There are two central themes or estimation problems, depicted as left and right path, namely *bearings-only tracking for maneuvering targets* focussing on motion models and *bearings-only tracking using heterogeneous sensors* focussing on different measurement types. The central themes form a vertical partition of this thesis, whereas the chapters form a horizontal organization and are ordered from theoretical backgrounds (performance bound, observability), via theoretical, but nuts-and-bolts estimators, to practical results.

In the following sections, Section 1.3 and Section 1.4, both central themes are introduced and motivated. Theory begins in Chapter 2, where fundamental properties of bearings-only measurements and motion models for maneuvering targets are given. Regarding the central themes, these are piecewise motion models, see Section 2.4.3, and constant velocity (CV) motion, see Section 2.4.1. The subsequent Chapter 3 introducing a performance bound, called Cramér-Rao lower bound (CRLB), is mostly related to maneuvering targets since its contribution is that the aformentioned piecewise motion models are incorporated into the bound, see Section 3.2. In contrast to the CRLB, the observability examination in Chapter 4 is for the most part related to heterogeneous tracking since new aspects of exploiting different signal propagation velocities due to heterogeneous signals are presented, see Section 4.2. However, also general observability criteria are discussed which are especially relevant in bearings-only tracking. Since observability has a strong connection to the CRLB, both nodes are connected in Fig. 1.1. In order to provide tools to realize estimation, state estimation is covered in Chapter 5. Due to its robustness for bearings-only tracking of maneuvering targets, a non-Bayesian batch maximum likelihood estimator is presented in Section 5.6. A recursive filter solution, the Gaussian mixture filter is closely examined and special aspects of Gaussian mixture weight choice are discussed, see Section 5.4 with an application to heterogeneous tracking in mind. After having illuminated the two central themes from a more theoretical perspective, the results of the application of the respective aforementioned estimators to the two estimation problems are presented in Chapter 6. A simulative approach is chosen for the maneuvering targets case along with an analysis of the CRLB, see Section 6.1. The practical side is covered by field tests involving communications and acoustic and electromagnetic sensors that have been carried out, see Section 6.2. The performance of the Gaussian mixture filter is verified under these real conditions. Finally, in Chapter 7, a summary of this thesis and further conclusions are given.

1.2 Contributions of this Thesis

Theoretical contributions This thesis makes the following theoretical contributions which are beyond the state of art:

1. Derivation of a performance bound (Cramér-Rao lower bound, CRLB) and implementation and analysis of an efficient estimator for complex motion models, i.e. piecewisely maneuvering targets with unknown maneuver change times, by means of passively measuring bearing and bearing rate, see [HO10], © 2010 Gesellschaft für Informatik, [OH10], © 2010 IEEE, [HO11a], © 2011 IEEE, and [HOK14], © 2014 IEEE. These topics are covered in Sections 2.4.3, 3.2, 5.6, and 6.1. This corresponds to the left path in Fig. 1.1.

2. Observability analysis for distributed heterogeneous passive sensors by means of exploitation of different signal propagation velocities [HK16], © 2016 IEEE: Information from acoustic and electromagnetic sensors is considered. In contrast to the case of homogeneous signals (e.g. electromagnetic radar signals) on a single platform, where the target state can only be estimated under certain circumstances (e.g. platform maneuvers), the state can always be estimated by means of exploitation of different signal speeds in a heterogeneous sensor setup.

3. Mathematically rigorous derivation of two Gaussian mixture likelihood approximation methods for bearing measurements from a general likelihood approximation approach that is linear in target state, see Section 5.5. The fact that these approximations are linear in target state allows for a linear Gaussian mixture filter to operate on the nonlinear problem of bearings-only tracking [Hör14], © 2014 IEEE. The two approximation methods are compared in simulations and with real acoustic bearing data, see Section 6.2.3 and their properties are outlined.

Practical contributions Based on the theoretical performance and observability analyses and the examined state estimation methods, a distributed fusion system which acts as a proof of concept for the protection of platforms has been built up [HGR+16], © 2016 IEEE. It has been realized by means of heterogeneous sensors, which shall detect an event and localize a threat which caused the event. This is performed by a microphone array to detect sound waves emitted by the threat and so obtain its direction (bearings-only tracking) as well as a radar detector that detects electromagnetic emissions from the threat. Since multiple platforms are involved to provide increased observability and also redundancy against possible breakdowns, a WiFi mobile or vehicular ad hoc network (MANET) is used for communications. In order to keep up the network in a breakdown of a network node, sophisticated routing approaches, namely OLSRv2 (optimized link state routing) are employed. The complex interaction of heterogeneous sensors and communications is one major practical contribution which is verified in field tests, see Sections 1.4 and 6.2. Furthermore, the Gaussian mixture filter based on likelihood approximation, discussed in Section 5.4 is applied in this context for tracking a target emitting acoustic signals.

1.3 Bearings-only Tracking for Maneuvering Targets

This section shall motivate the first central theme of this thesis, bearings-only tracking for maneuvering targets. One focus is on complex motion models incorporating target maneuvers. The derivation of the Cramér-Rao lower bound for maneuvering targets in Chapter 3 refers to this type of targets.

For stationary targets, measured bearings can be intersected to determine the range. This is known as cross bearing or triangulation and has been used since the beginnings of seafaring. In modern times, the need to obtain the range of moving targets has emerged, leading to bearings-only target motion analysis which has been a research area for nearly sixty years. Before the computational power to solve the connected optimization problem was available, submarine operators performed this task manually by means of graphical methods like Ekelund ranging [Eke58, Col94]: Ekelund's proposition to obtain a target's range was to divide the difference between target and observer speeds across the line of sight (LoS) by the difference between bearing rates. With the availability of faster computers, non-Bayesian batch methods like maximum likelihood estimators (MLE) and least squares methods have been preferred to tackle the TMA problem [NLG84]. Alternatively, Aidala et al. solved the BO-TMA problem by means of Bayesian filter approaches like extended Kalman filters (EKF) both in Cartesian and modified polar coordinates (MPC) [Aid79, AH83]. Within MP coordinates, the bearings-only measurement equation is linear, but the motion is non-linear. However, this technique shows less degradation than using Cartesian coordinates. Concluding, non-Bayesian batch methods show a better performance and robustness than Bayesian filters especially for long-range target scenarios [HAGL83, dVGM92, KBSL01]. Of course, the global optimization implies the disadvantage of a high computational burden.

Considering target motion, one class of targets, particularly marine vessels (including surface ships and submarines), preferably moves straight ahead and sometimes changes its direction, also called course, which appears to occur instantaneously: The duration of a maneuver, i.e. the length of the maneuver phase, relative to the sampling interval is low [BSF88]. A typical example of such a scenario is depicted in Fig. 1.2. This kind of motion is performed due to the heavy weight of the vessel and its consequent inertia. In this thesis, this class of targets is modeled by means of inertial motion, also known and constant velocity (CV) motion [LJ03]. A segment of CV and constant course is also called *leg*. If course and/or speed changes (more general: a maneuver is performed) are considered, an extended model, called piecewise inertial (or piecewise rectilinear motion model [JPP10]), is considered.

Another class of target is not necessarily moving inertially but is partly strongly maneuvering. Examples are aircraft, especially jets, helicopters, and unmanned aerial vehicles, which are more agile than marine vessels. Thus, aircraft often perform higher-order motion maneuvers, such as turns and speed changes, which both imply the occurrence

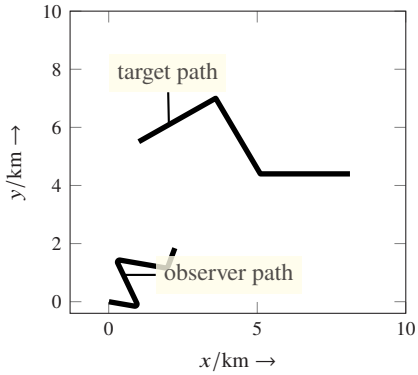

Figure 1.2: Typical scenario of bearings-only tracking for maneuvering targets: A maneuvering observer tries to localize a maneuvering target based on angular measurements.

of accelerations. These target type can be characterized by the *curvilinear motion model* [BN97] or its extension, the *piecewise curvilinear motion model* [Bec05a]. Alternatively, such motion patterns can be handled by the interacting multiple model (IMM) approach, where multiple simple motion models are weighted depending on the measurements [BSL95, KBSL01]. Furthermore, a hidden Markov model (HMM) has been applied in this context [LCT98].

Since the focus is on maneuvering targets, the detection of a maneuver is commonly a testing or decision problem [LJ02]. Based on, for example, chi-square or likelihood ratio tests, a decision is taken whether a maneuver change has taken place. However, all these approaches assume that the maneuver change times are not part of the estimation problem. In contrast to that, our approach tries to *estimate* the maneuver change times. Therefore, the target state is augmented by the maneuver change times. Furthermore, another technique in [JPP10] also assumes unknown maneuver change times as part of the estimation problem.

The CRLB for maneuvering targets has been evaluated with the limiting condition that the maneuver change times and the number of maneuvers are exactly known [RA03, RAG04]. In this thesis, the CRLB is calculated with respect to the complete target state, especially the maneuver change times modeling abrupt change. A similar investigation is done in [JPP14]. In order evaluate the performance of the investigated approaches, we will consider bearing measurements as well as additional bearing rate measurements [DW08].

1.4 Bearings-only Tracking in a Vehicular Ad hoc Network Using Heterogeneous Sensors

This example shall introduce how bearings-only tracking can be practically used in ad hoc Wi-Fi network involving multiple vehicles and multiple heterogeneous sensors [HGR+16, HK16]. A motivation and fundamental concepts are given here, whereas observability aspects, state estimation techniques, and field test results are presented in the respective chapters 4, 5, and 6.

The motivational background is that protection of personnel and platforms of armed land forces during missions gains more and more importance. A possible approach to strengthen safety is to equip military vehicles with automatic protection systems. These systems provide data which lead to automatic or semi-automatic countermeasures by triggering different kinds of effectors. Usually, these systems are self-contained and often do not provide an interface to use the data externally. Thus, they only affect a single, the own, platform. Hence, the objective of this example is to investigate how sensor data from automatic protection systems contribute to the joint protection of a military formation, e.g. convoy, patrol, or checkpoint. For that, we consider a line formation of vehicles as a tactical scenario for our field tests and fuse sensor data from their automatic protection systems by means of radio communication. These systems are mounted on different platforms in order to present an up-to-date situation overview of the formation. The formation commander shall then be able to decide whether his subordinate vehicles shall engage, hold position, or retreat. This way, he will be enabled to improve the safety of own forces and to accomplish operations successfully [PT08].

The prototypic concept of a mobile ad hoc network (MANET) including multiple, heterogeneous sensors is depicted in Fig. 1.3. Since the network nodes are able to move, one can also refer to a vehicular ad hoc network (VANET). A subset of vehicles is equipped with one or multiple sensors, whereas each vehicle carries a fusion center, and an ad hoc routing capable radio device. Only the sensors with red background have been integrated as hardware (see also Fig. 1.4), i.e., acoustic sensor (microphone array) and electronic support measures (ESM) sensor (laser/radar detector). The threat is represented by a sonic blast-shock cannon and a device emitting electromagnetic radiation in typical radar bands (radar warner trigger). These reproduce a muzzle blast as an acoustic event as well as a muzzle flash as an electromagnetic signal from a real weapon. The prototype implementation is based on Wi-Fi but can later be exchanged by another ad hoc capable military radio technologies. One vehicle is the designated formation lead, i.e. it has the formation commander on board who decides further proceedings based on the fused information. Concerning the fusion center, we propagate redundancy since each vehicle shall be able to acquire formation lead if the designated vehicle has a breakdown. That means, the measurements from all sensors are exchanged between all vehicles and each vehicle fuses the measurements locally to obtain a localization result regarding the threat.

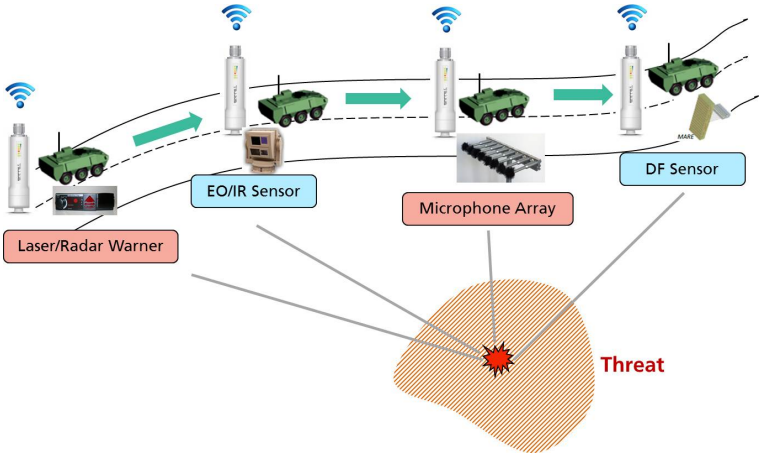

Figure 1.3: Concept for military VANET in a formation including multiple, heterogeneous sensors localizing a threat. The integration of sensors with red background is realized; the integration of sensors with blue background is planned, see also [HGR+16], © 2016 IEEE.

In order to create a link between the vehicles for data exchange, we establish a MANET. This network can also be characterized as a VANET due to the following aspects [LSK06]: Nodes are moving resulting in a possible high rate of topology changes, self-localization is performed by means of global navigation satellite system (GNSS) receivers including all their inaccuracies, and energy consumption can normally be neglected. One advantage of a MANET is that it allows spontaneous linking of nodes, i.e., dynamic entry and exit of the network at routing level. Additionally, it is able to respond to topology changes caused by vehicle motion, vehicle breakdown, or jamming. A suitable MANET routing protocol allows multi-hop transmissions via one or more relay nodes which especially becomes important in military operations where it cannot be guaranteed that every time arbitrary two nodes are in line of sight of each other. This is e.g. due to terrain or buildings. In Fig. 1.5, the layer model for our proposed MANET is depicted. At the lowest level, the data link layer, we apply IEEE 802.11 commonly known as Wi-Fi. This is prototypical to emulate the properties of future tactical radios. For the network layer, IPv4 is used. The transport protocol is UDP since TCP is only partly suitable for MANETs. Especially in a data fusion context, the focus lies on on-time transmission of the data, whereas errors, data loss, or duplication do not pose a fatal problem to the system. If a high degree of reliability is desired, it could be realized at application level. Based on UDP, optimized link state routing protocol, versions 1 and 2 (OLSRv1/v2[3]),

[3] For an implementation of OLSR, see [OLS].

Figure 1.4: Hardware for field tests. Upper left: Microphone array, radar warner, XSens, and bullet mounted on car. Upper right: Power supplies and sound card mounted inside car. Lower left: Sonic blast-shock cannon and radar warner trigger. Lower right: commercial off-the-shelf radar and laser detector "Valentine One", © 2016 IEEE.

described in RFC 3626 [CJ03] and RFC 7181 [CDJH14] is used for MANET routing. Finally, at application layer, the exchanging of user data is performed. Furthermore, the fusion center operates here where all incoming information is collected and combined to provide a tactical situation overview.

The applied routing protocol must be able to determine the network topology and choose suitable relay nodes for multi-hop transmission paths. Such a unicast MANET routing protocol is OLSRv2 [BFK+15], the successor of OLSRv1 which is well-established in the tactical and civil context. The following features are in particular advantageous for the scenario in Fig. 1.3:

- Link state routing: The state of a local link is broadcast throughout the complete network by means of HELLO and topology control (TC) messages. Hence, each node has a global knowledge of the network topology and thus of the current nodes. Thus, one always knows whether the fusion center is up and, if necessary, can redirect the traffic to an alternative fusion center.

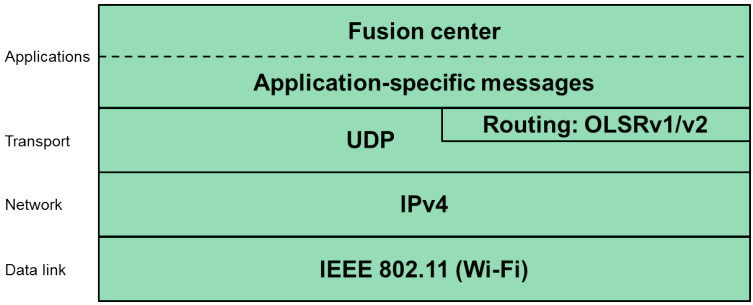

Figure 1.5: Layer model for proposed MANET, © 2016 IEEE.

- Pro-active routing: Routes are pre-calculated and therefore they are available without delay, e.g. caused by route finding. This means the data to be fused is at the fusion center on time without avoidable delay affecting the currentness of the situation picture.
- The extensible packet format described in RFC 5444 [CDDA09] allows transmission of additional data, e.g. routing metrics. This helps ensuring a stable quality of the network.
- Link quality and link speed aware routing metric. The directional airtime metric [RB13] assesses the links based on their quality in terms of the estimated number of retransmissions needed and the current data rate of the link. This way, links at low rates creating bottlenecks are automatically avoided so that the data to be fused is transmitted to the fusion center as fast as possible.

2 Measurement and Motion Models

This chapter deals with fundamental models required for state estimation, namely measurement and motion models. Beginning with the Gaussian density in Section 2.2, which is the base for all following models, we examine bearings-only and bearing rate measurements in Section 2.3 which are the essence of this thesis. The motion model part in Section 2.4 begins with a simple, widely used model, namely the constant velocity model. Since this thesis focuses on maneuvering targets, models which can deal with this type of motion are presented. These include piecewise motion models, where motion segments are concatenated in order to represent maneuvers.

2.1 Probability Density Function

The *probability density function* (PDF), often simply called *density*, of a d-dimensional (continuous) random vector $\mathbf{x}$ is an integrable, non-negative function $p : \mathbb{R}^d \to [0, \infty)$. It is used to describe the probability for the event that $\mathbf{x}$ takes values in the d-dimensional set D as follows:

$$\Pr(\mathbf{x} \in D) = \int_D p(\mathbf{u}) \, \mathrm{d}\mathbf{u} \,. \tag{2.1}$$

One often also uses $\mathbf{x}$ instead of $\mathbf{u}$ as the integration variable, which makes the terms easier to read. A PDF has the property that its integral over $\mathbb{R}^d$ equals one representing the certain event that $\mathbf{x}$ is in $\mathbb{R}^d$. The *expected value* or *mean* of a random vector $\mathbf{x}$ with respect to its PDF p is defined as

$$\hat{\mathbf{x}} = \mathrm{E}\{\mathbf{x}\} = \int_{\mathbb{R}^d} \mathbf{x} \, p(\mathbf{x}) \, \mathrm{d}\mathbf{x} \,. \tag{2.2}$$

Furthermore, the covariance matrix of a random vector $\mathbf{x}$ with respect to p describing its uncertainty is given by

$$\mathrm{Cov}\{\mathbf{x}\} = \mathrm{E}\left\{(\mathbf{x} - \hat{\mathbf{x}})(\mathbf{x} - \hat{\mathbf{x}})^{\mathrm{T}}\right\} \,. \tag{2.3}$$

2.2 Gaussian Distribution

One of the most important density in state estimation and filtering and thus the central density employed in this thesis is the *Gaussian* or *normal* distribution. Its multivariate

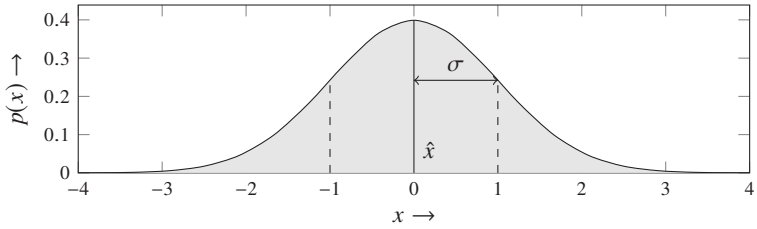

Figure 2.1: Visualization of a univariate Gaussian density with $\hat{x} = 0$ and $\sigma = 1$.

probability density function, also called Gaussian density in the following, with respect to a d-dimensional random vector $\mathbf{x}$ is defined as

$$p(\mathbf{x}) = \mathcal{N}(\mathbf{x}; \hat{\mathbf{x}}, \mathbf{P}) = \frac{1}{\sqrt{(2\pi)^d \det \mathbf{P}}} e^{-\frac{1}{2}(\mathbf{x}-\hat{\mathbf{x}})^{\mathrm{T}} \mathbf{P}^{-1} (\mathbf{x}-\hat{\mathbf{x}})} \tag{2.4}$$

with mean and covariance in vector and matrix form, respectively, according to (2.2) and (2.3) given by

$$\hat{\mathbf{x}} = \mathrm{E}\{\mathbf{x}\} = \int_{\mathbb{R}^d} \mathbf{x}\, \mathcal{N}(\mathbf{x}; \hat{\mathbf{x}}, \mathbf{P})\, \mathrm{d}\mathbf{x}\,, \tag{2.5a}$$

$$\mathbf{P} = \mathrm{Cov}\{\mathbf{x}\} = \mathrm{E}\left\{(\mathbf{x} - \hat{\mathbf{x}})(\mathbf{x} - \hat{\mathbf{x}})^{\mathrm{T}}\right\}. \tag{2.5b}$$

Here, the covariance matrix $\mathbf{P}$ is symmetric and positive semi-definite and its shape is $d \times d$. Positive semi-definiteness is also expressed by the term $\mathbf{P} \geq 0$. This is a shortcut for the fact that positive semi-definiteness is defined as $\mathbf{a}^{\mathrm{T}}\mathbf{P}\mathbf{a} \geq 0$ for all $\mathbf{a}$. The factor $\sqrt{(2\pi)^d \det \mathbf{P}}$ in (2.4) is used for normalization and therefore ensures that the integral of the density is equal to one. If a random vector $\mathbf{x}$ is Gaussian distributed with mean $\hat{\mathbf{x}}$ and covariance matrix $\mathbf{P}$, i.e. $p(\mathbf{x}) = \mathcal{N}(\mathbf{x}; \hat{\mathbf{x}}, \mathbf{P})$, then we also write the term $\mathbf{x} \sim \mathcal{N}(\hat{\mathbf{x}}, \mathbf{P})$.

The univariate (one-dimensional) Gaussian density is given by

$$p(x) = \mathcal{N}(x; \hat{x}, \sigma) = \frac{1}{\sigma\sqrt{2\pi}} e^{-\frac{(x-\hat{x})^2}{2\sigma^2}} \tag{2.6}$$

with mean $\hat{x}$ and standard deviation σ, which is also denoted as variance σ^2. It is depicted in Fig. 2.1. Furthermore, Fig. 2.2 shows the multivariate Gaussian density (2.4) for $d = 2$.

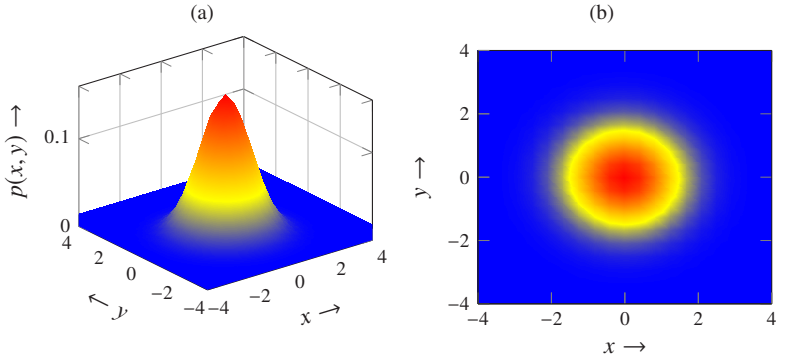

Figure 2.2: Visualization of a multivariate Gaussian density from different perspectives: (a) side view and (b) top view.

2.2.1 Product Formula for Gaussians

Key to the derivation of many state estimation methods is the solution of the product of two Gaussians. For matrices and vectors with compatible dimensions, the following holds:

$$\mathcal{N}(\mathbf{z};\mathbf{H}\mathbf{x},\mathbf{R})\,\mathcal{N}(\mathbf{x};\hat{\mathbf{x}},\mathbf{P}) = \mathcal{N}(\mathbf{z};\mathbf{H}\hat{\mathbf{x}},\mathbf{S})\,\mathcal{N}(\mathbf{x};\mathbf{y},\mathbf{Y}) \tag{2.7}$$

with

$$\begin{aligned} \mathbf{S} &= \mathbf{R} + \mathbf{H}\mathbf{P}\mathbf{H}^{\mathrm{T}} \\ \mathbf{y} &= \hat{\mathbf{x}} + \mathbf{K}(\mathbf{z} - \mathbf{H}\hat{\mathbf{x}}) \\ \mathbf{Y}^{-1} &= \mathbf{P}^{-1} + \mathbf{H}^{\mathrm{T}}\mathbf{R}^{-1}\mathbf{H} \\ \mathbf{K} &= \mathbf{P}\mathbf{H}^{\mathrm{T}}\mathbf{S}^{-1}\,. \end{aligned} \tag{2.8}$$

A formal proof as well as alternative representations can be found in [Koc14].

2.3 Measurement Models

A measurement model is a technique to relate a measured quantity taken by a sensor to an internal state one is interested in. The measurements can be observed directly, but the state cannot. Measurements are error-prone due to the limited resolving capabilities of a sensor, so that measurement noise is attached to the model to take these perturbations into account. The process to systematically derive a state, named $\mathbf{x}_k$, from noise corrupted measurements $\{\mathbf{z}_0,\ldots,\mathbf{z}_k\}$ is called *state estimation* and is further outlined in Chapter 5.

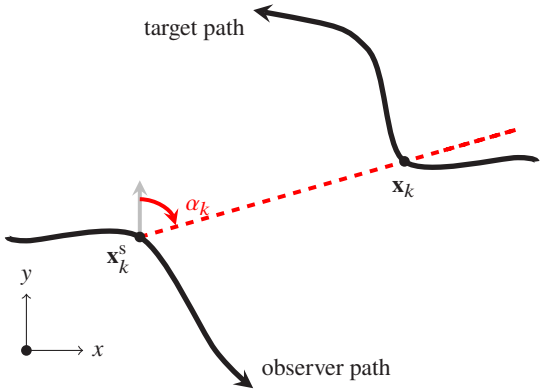

Figure 2.3: Geometry for an bearings-only tracking (BOT) scenario with maneuvering target and maneuvering observer. The angle α_k is the true target line-of-sight azimuth, © 2014 IEEE.

In general, the (nonlinear) measurement model equation with additive noise $\boldsymbol{\nu}_k$ is given by

$$\mathbf{z}_k = \mathbf{h}(\mathbf{x}_k) + \boldsymbol{\nu}_k \,, \tag{2.9}$$

where $\mathbf{z}_k$ is the measurement received at the sensor a time t_k and $\mathbf{h}(\cdot)$ is an arbitrary function mapping the state to the measurement. The measurement noise is assumed to be white and Gaussian distributed with zero mean and a sensor-specific covariance matrix $\mathbf{R}_k$, i.e. $\boldsymbol{\nu}_k \sim \mathcal{N}(\mathbf{0}, \mathbf{R}_k)$.

An important special case is a linear measurement equation

$$\mathbf{z}_k = \mathbf{H}_k \mathbf{x}_k + \boldsymbol{\nu}_k \,, \tag{2.10}$$

which differs from the nonlinear case by using a linear measurement function $\mathbf{H}_k \mathbf{x}_k$ replacing the general transformation $\mathbf{h}(\cdot)$. It should be clear that linear models are easier to handle than nonlinear ones. In particular, state estimation problems with linear models can be solved in an optimal way, see e.g. the Kalman filter in Chapter 5 and [BSLK01], which is not the case for nonlinear problems. However, most state estimation problems are nonlinear and this thesis will focus on an important type of nonlinear measurements, namely bearings-only measurements.

2.3.1 Bearings-only Measurements

Line of sight angular measurements are also called bearings-only measurements as outlined in Chapter 1. The angle can be measured in various ways, for example in the

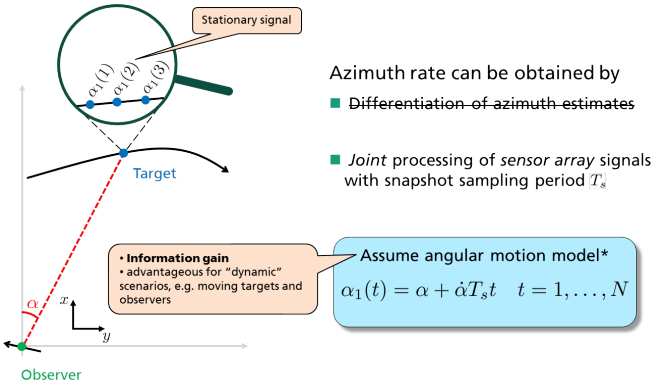

Figure 2.4: Illustration of obtaining bearing rate by an angular motion model. Taken from conference presentation of [HO10].

mathematical sense. If the reference direction is true north, and this is the way we deal with angles throughout this thesis, we also refer to the term *azimuth*. According to the general nonlinear measurement model (2.9) and illustrated in Fig. 2.3, the bearings-only measurement equation including a noise corrupted azimuth measurement is given by

$$\mathbf{z}_k = \alpha(\mathbf{x}_k) + v_k \,. \tag{2.11}$$

Here, $\alpha(\cdot)$ is the (noise free) measurement function obtaining the true azimuth described by

$$\mathbf{h}(\mathbf{x}_k) = \alpha(\mathbf{x}_k) = \alpha_k = \arctan \frac{\Delta x_k}{\Delta y_k} \,, \tag{2.12}$$

and v_k is assumed to be white and Gaussian distributed measurement noise with zero mean and standard deviation σ_α. We assume that target state $\mathbf{x}_k$ and sensor state $\mathbf{x}_k^{\mathrm{s}}$ comprise at least the respective position components, i.e., $\mathbf{x}_k = [x_k, y_k, \ldots]^{\mathrm{T}}$ and $\mathbf{x}_k^{\mathrm{s}} = [x_k^{\mathrm{s}}, y_k^{\mathrm{s}}, \ldots]^{\mathrm{T}}$. Then, $\Delta x_k = x_k - x_k^{\mathrm{s}}$ and $\Delta y_k = y_k - y_k^{\mathrm{s}}$ are the corresponding distance vectors between target and sensor position.

2.3.2 Bearing Rate Measurements

A further measurement quantity discussed in this thesis is *bearing rate* or *azimuth rate* characterizing the rate as measured line of sight angle changes, see also [HO10]. Certainly, simple differentiation of bearing measurements will not lead to any additional information about target kinematics. Thus, the bearing rate will typically be obtained by joint processing of sensor array signals. Several estimation approaches have been

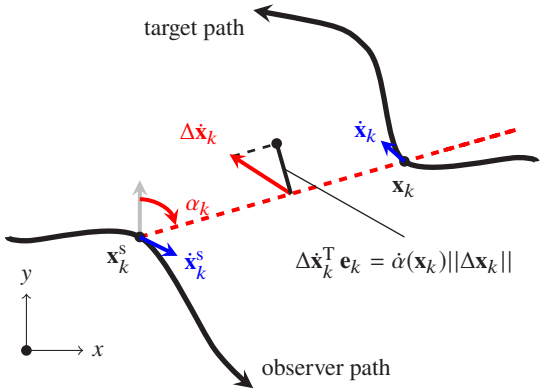

Figure 2.5: Geometry for bearing and bearing rate tracking scenario with maneuvering target and maneuvering observer, © 2014 IEEE.

proposed: E.g., a subspace-based approach including an initialization technique has been established in [MBS05]. Furthermore, a maximum likelihood approach, e.g., for linear array geometries to obtain azimuth angles and azimuth rate has been presented by Wigren and Eriksson [WE95]. They mention that this approach can be also applied for planar arrays to capture additional elevation angles and the corresponding rate. The key idea of all these approaches is to use a direction finding approach with an *embedded angular motion model*, see Fig. 2.4. This way, stationary assumptions on the target signals are avoided.

By defining

$$\Delta\dot{\mathbf{x}}_k = \begin{bmatrix} \Delta\dot{x}_k \\ \Delta\dot{y}_k \end{bmatrix} = \dot{\mathbf{x}}_k - \dot{\mathbf{x}}_k^s \tag{2.13}$$

as difference velocity between sensor and target, and $r_k^2 = ||\Delta\mathbf{x}_k||^2 = \Delta x_k^2 + \Delta y_k^2$ as squared distance (range) between sensor and target, we obtain

$$\mathbf{h}(\mathbf{x}_k) = \dot{\alpha}(\mathbf{x}_k) = \frac{\Delta\dot{x}_k\Delta y_k - \Delta\dot{y}_k\Delta x_k}{r_k^2} = \frac{\Delta\dot{\mathbf{x}}_k^T\mathbf{e}_k}{r_k}\,. \tag{2.14}$$

Note that (2.14) can be derived from (2.12) by using the notation $\mathbf{x}_k = \mathbf{x}(t_k)$ and

$$\dot{\alpha}(\mathbf{x}_k) = \frac{\partial\alpha(\mathbf{x}_k)}{\partial t_k} = \left.\frac{\partial\alpha(\mathbf{x}(t))}{\partial t}\right|_{t=t_k}, \tag{2.15}$$

where the latter form of the derivative is the mathematical exact one. However, the former one will be used throughout this thesis due to readability. Referring again to (2.14), we assume that target and sensor state at least contain position and velocity, thus $\mathbf{x}_k = [x_k, y_k, \dot{x}_k, \dot{y}_k, \ldots]^{\mathrm{T}}$ and $\mathbf{x}_k^{\mathrm{s}} = [x_k^{\mathrm{s}}, y_k^{\mathrm{s}}, \dot{x}_k^{\mathrm{s}}, \dot{y}_k^{\mathrm{s}}, \ldots]^{\mathrm{T}}$. In (2.14), $\mathbf{e}_k$, obtained by $\mathbf{e}_k = [\Delta y_k, -\Delta x_k]^{\mathrm{T}}/r_k$, is a unit vector orthogonal to the vector $\Delta\mathbf{x}_k$. Hence, the inner product $\Delta\dot{\mathbf{x}}_k^{\mathrm{T}}\mathbf{e}_k$ in (2.14) is a scalar projection of $\Delta\dot{\mathbf{x}}_k$ in the direction of $\mathbf{e}_k$, i.e. in the direction orthogonal to $\Delta\mathbf{x}_k$, see Fig. 2.5. Finally, the equation for noise corrupted bearing rate measurements is given by

$$\mathbf{z}_k = \dot{\alpha}(\mathbf{x}_k) + \nu_k \tag{2.16}$$

where we assume that ν_k is white and Gaussian distributed measurement noise with zero mean and standard deviation $\sigma_{\dot{\alpha}}$.

2.4 Motion Models

A motion or system model describes a target's future (or past) behavior by state prediction (or retrodiction). It consists of a deterministic part representing the transition of the state according to the physical model and, optionally, a stochastic part subsuming any occurring disturbances. The stochastic part is also referred to as *process* or *system noise* and is due to the fact that no model can be considered perfectly appropriate. However, especially when only selective disturbances, e.g. in terms of target maneuvers, occur as it is the case for ships, the state trajectory is often modeled deterministically [Aid79, NLG84, NG97].

2.4.1 Constant Velocity Motion

The state of a target moving with constant velocity, which is also called inertially moving target, at time t_k is described by the following Cartesian state vector

$$\mathbf{x}(t_k) = \mathbf{x}_k = [x_k, y_k, \dot{x}, \dot{y}]^{\mathrm{T}} \,. \tag{2.17}$$

Since the target velocities are assumed constant, the time index k is omitted there. Using the aforementioned Cartesian state vector, a deterministic equation describing a linear state transition from the state at some reference time t_{r} to the state at time t_k can be expressed by

$$\mathbf{x}_k = \boldsymbol{\Phi}(t_k, t_{\mathrm{r}})\mathbf{x}_{\mathrm{r}} \,. \tag{2.18}$$

The state at time t_r is written shortly as $\mathbf{x}_\mathrm{r} = \mathbf{x}(t_\mathrm{r})$. The corresponding state transition matrix $\mathbf{\Phi}(t_k, t_\mathrm{r})$ for the constant velocity motion case is given by

$$\mathbf{\Phi}(t_k, t_\mathrm{r}) = \begin{bmatrix} \mathbf{I}_2 & (t_k - t_\mathrm{r})\,\mathbf{I}_2 \\ \mathbf{0} & \mathbf{I}_2 \end{bmatrix}. \tag{2.19}$$

Usually in Bayesian tracking approaches (see Chapter 5), the state transition is expressed by the usage of process noise which models the stochastic perturbations due to e.g. small velocity changes. However, in this case, the model is not deterministic any more. Since for Bayesian tracking, the state is commonly predicted to the following time scan, the linear motion equation is usually given by

$$\mathbf{x}_{k+1} = \underbrace{\mathbf{F}_k}_{=\mathbf{\Phi}(t_{k+1}, t_k)} \mathbf{x}_k + \mathbf{w}_k \tag{2.20}$$

with state transition matrix $\mathbf{F}_k$ and white process noise $\mathbf{w}_k$ which is assumed to be Gaussian distributed with zero mean and covariance matrix $\mathbf{Q}_k$. In the literature, this model is referred to as *(nearly) constant-velocity motion model* (CV) model [LJ03].

There are different approaches to define the process noise. We will highlight two of them here: The first option is to assume the acceleration as white noise. This leads to the following process noise covariance matrix $\mathbf{Q}_k$ [BSLK01]:

$$\mathbf{Q}_k = q_k^2 \begin{bmatrix} T^3/3\,\mathbf{I}_2 & T^2/2\,\mathbf{I}_2 \\ T^2/2\,\mathbf{I}_2 & T\,\mathbf{I}_2 \end{bmatrix}, \tag{2.21}$$

where $T = t_{k+1} - t_k$ is the sampling time and the factor q_k affects the process noise level. This model is often referred to as continuous white noise acceleration model (CWNA). In [BSLK01], there is also a guideline on how to reasonably choose the process noise intensity "fudge" factor q_k.

If the acceleration is assumed to be constant during a sampling period $[t_k, t_{k+1}]$, we obtain the discrete white noise acceleration model (DWNA), see e.g. [BSLK01, LJ03], with $\mathbf{Q}_k$ given by

$$\mathbf{Q}_k = q_k^2 \begin{bmatrix} T^4/4\,\mathbf{I}_2 & T^3/2\,\mathbf{I}_2 \\ T^3/2\,\mathbf{I}_2 & T^2\,\mathbf{I}_2 \end{bmatrix}. \tag{2.22}$$

However, this model has several weaknesses: If the sampling period is long, i.e. T is big, the assumption of a constant acceleration is at least questionable. Furthermore, $\mathbf{Q}_k$ is a singular matrix which will be problematic as soon as its inverse shall be used, which is, for example, the case when a special performance bound shall be calculated,

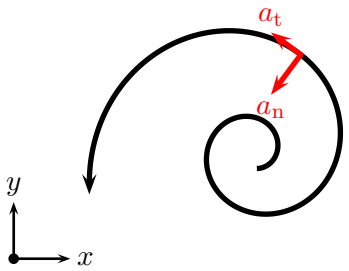

Figure 2.6: Spiral-shaped curvilinear motion trajectory. Tangential and normal acceleration a_t and a_n are simultaneously active, © 2014 IEEE.

see [TMN98]. In fact, this bound is not covered in this thesis. Nevertheless, the CWNA model will be the preferred one for Bayesian state estimation in this work .

2.4.2 Deterministic Curvilinear Motion

Consider a target moving deterministically along a trajectory with speed v_k, heading φ_k, constant tangential acceleration a_t, as well as constant normal acceleration a_n according to [BN97]. See Fig. 2.6 for an example with both tangential and normal acceleration unequal to zero which results in a spiral-shaped trajectory. The state of such a *curvilinearly* moving target can be completely described by position and velocity components given by

$$\begin{bmatrix} \dot{x}_k \\ \dot{y}_k \end{bmatrix} = v_k \begin{bmatrix} \sin\varphi_k \\ \cos\varphi_k \end{bmatrix}, \tag{2.23}$$

as well as acceleration components a_t and a_n. The special cases of inertial motion ($a_\mathrm{t} = a_\mathrm{n} = 0$, see also Subsection 2.4.1), straight-line acceleration ($a_\mathrm{t} \neq 0$, $a_\mathrm{n} = 0$), and circular motion ($a_\mathrm{t} = 0$, $a_\mathrm{n} \neq 0$) are included in this model. Note that in (2.23) the heading angle φ_k is defined with respect to the north. All target parameters are comprised in the parameter vector

$$\mathbf{x}_k = [x_k, y_k, v_k, \varphi_k, a_\mathrm{t}, a_\mathrm{n}]^\mathrm{T} . \tag{2.24}$$

In contrast to the inertial motion case from the previous subsection, where a Cartesian state leads to a linear motion model, the consideration of polar velocity and acceleration components is preferred here. The advantages are constant tangential and normal accelerations and thus easy conversion from speed (along-track velocity) to tangential acceleration. The drawback of such modeling is the non-linearity of the motion equation.

Using polar velocities and accelerations, a mathematical model of the target motion can be specified by the non-linear differential equation

$$\dot{\mathbf{x}}_k = \begin{bmatrix} 0 & 0 & \sin\varphi_k & 0 & 0 & 0 \\ 0 & 0 & \cos\varphi_k & 0 & 0 & 0 \\ 0 & 0 & 0 & 0 & 1 & 0 \\ 0 & 0 & 0 & 0 & 0 & v_k^{-1} \\ 0 & 0 & 0 & 0 & 0 & 0 \\ 0 & 0 & 0 & 0 & 0 & 0 \end{bmatrix} \mathbf{x}_k \,. \tag{2.25}$$

An approximate solution of the curvilinear motion equation with the form $\mathbf{x}_k = \mathbf{\Phi}(t_k, t_\mathrm{r})\,\mathbf{x}_\mathrm{r}$ can be found in [BN97]. However, an exact solution of the initial value problem (2.25) with $\mathbf{x}_\mathrm{r}$ as initial value is needed in order to calculate the CRLB (see also Subsection 3.2.2). The solution is given by the non-linear motion equation

$$\mathbf{x}_k = \mathbf{f}\,(\mathbf{x}_\mathrm{r}; t_k, t_\mathrm{r}) \tag{2.26}$$

which describes the temporal transition of the target state from any reference time t_r to time t_k. In order to provide a solution of the curvilinear motion equation, we define

$$c_\mathrm{a} = \frac{1}{4a_\mathrm{t}^2 + a_\mathrm{n}^2} \tag{2.27a}$$

$$S(t) = (2a_\mathrm{t} \sin\varphi(t) - a_\mathrm{n} \cos\varphi(t))\, v^2(t) \tag{2.27b}$$

$$T(t) = (2a_\mathrm{t} \cos\varphi(t) + a_\mathrm{n} \sin\varphi(t))\, v^2(t) \tag{2.27c}$$

$$\Delta t_k = t_k - t_\mathrm{r} \tag{2.27d}$$

$$\Delta S_k = S(t_k) - S(t_\mathrm{r}) \tag{2.27e}$$

$$\Delta T_k = T(t_k) - T(t_\mathrm{r})\,. \tag{2.27f}$$

With this, the components of $\mathbf{f}(\mathbf{x}_\mathrm{r}; t_k, t_\mathrm{r})$ are specified by

$$x_k = \begin{cases} x_\mathrm{r} + c_\mathrm{a}\Delta S_k & \text{for } a_\mathrm{t} \neq 0 \text{ or } a_\mathrm{n} \neq 0 \\ x_\mathrm{r} + v_\mathrm{r} \sin\varphi_\mathrm{r}\Delta t_k & \text{for } a_\mathrm{t} = 0 \text{ and } a_\mathrm{n} = 0 \end{cases} \tag{2.28a}$$

$$y_k = \begin{cases} y_\mathrm{r} + c_\mathrm{a}\Delta T_k & \text{for } a_\mathrm{t} \neq 0 \text{ or } a_\mathrm{n} \neq 0 \\ y_\mathrm{r} + v_\mathrm{r} \cos\varphi_\mathrm{r}\Delta t_k & \text{for } a_\mathrm{t} = 0 \text{ and } a_\mathrm{n} = 0 \end{cases} \tag{2.28b}$$

$$v_k = v_\mathrm{r} + a_\mathrm{t}\Delta t_k\,, \tag{2.28c}$$

$$\varphi_k = \begin{cases} \varphi_\mathrm{r} + \frac{a_\mathrm{n}}{a_\mathrm{t}} \ln\left|1 + \frac{a_\mathrm{t}}{v_\mathrm{r}}\Delta t_k\right| & \text{for } a_\mathrm{t} \neq 0 \\ \varphi_\mathrm{r} + \frac{a_\mathrm{n}}{v_\mathrm{r}}\Delta t_k & \text{for } a_\mathrm{t} = 0 \end{cases}. \tag{2.28d}$$

2.4.3 Piecewise Deterministic Motion Models

For maneuvering targets, piecewise motion models are introduced in the following two subsections. A piecewise motion consists of several maneuver segments where in each segment, the target performs either inertial motion or curvilinear motion. Thus, these models are called piecewise inertial motion model and piecewise curvilinear motion model, respectively. The second, more general, model established by Becker [Bec05a] has also been used in our former publication [OH10]. The model using inertial motion can be seen as special case of the piecewise curvilinear motion model.

For each model, the maneuver segments are concatenated by *maneuver change points* where the constant parameters in a segment abruptly change. This has the effect that the state is not continuous over time. For the piecewise inertial motion presented in Subsection 2.4.4, the segment parameters are the Cartesian velocities $\dot{x}$ and $\dot{y}$, whereas for the piecewise curvilinear motion discussed in Subsection 2.4.5, these parameters are the tangential and normal accelerations a_t and a_n. The time when a maneuver change takes place is called *maneuver change time* and is part of the target state. More precisely, the target state is modeled in such a way that all past segment parameters and maneuver change times are contained. This leads to a non-constant dimension of the target state: With each maneuver change, the state dimension increases by the number of segment parameters as well as the maneuver change time for the new segment.

2.4.4 Piecewise Deterministic Inertial Motion

For piecewise inertial motion, the target state is expressed by a Cartesian vector with constant velocities and maneuver change times per segment. In Fig. 2.7 an example

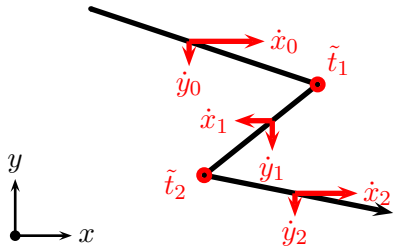

Figure 2.7: Piecewise inertial motion trajectory with $M = 3$ maneuver segments (legs). In each segment, inertial motion with different Cartesian velocities is performed. The maneuver change times $\tilde{t}_1$ and $\tilde{t}_2$ concatenate the maneuver segments, © 2014 IEEE.

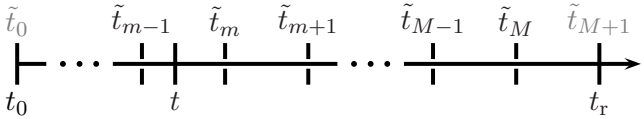

Figure 2.8: Relative displacements of time t_k compared with the maneuver change times, and the reference time t_r, © 2014 IEEE.

trajectory with three maneuver segments is depicted. The target state for M maneuver change times is given by

$$\mathbf{x}_k = \left[x_k, y_k, \mathbf{v}^\mathrm{T}, \tilde{\mathbf{t}}^\mathrm{T}\right]^\mathrm{T} \in \mathbb{R}^{(4+3M)\times 1}, \tag{2.29}$$

where the $\mathbf{v}$ comprises the Cartesian velocities. Thus,

$$\mathbf{v} = [\dot{x}_0, \dot{y}_0, \dot{x}_1, \dot{y}_1, \ldots, \dot{x}_M, \dot{y}_M]^\mathrm{T} \in \mathbb{R}^{2(M+1)\times 1}. \tag{2.30}$$

The vector $\tilde{\mathbf{t}}$ consists of the maneuver change times, so one has

$$\tilde{\mathbf{t}} = [\tilde{t}_1, \ldots, \tilde{t}_M]^\mathrm{T} \in \mathbb{R}^{M\times 1}. \tag{2.31}$$

Parameters $\dot{x}_m$ and $\dot{y}_m$ denote the Cartesian velocities in the interval $[\tilde{t}_m, \tilde{t}_{m+1}]$ for $m = 0, \ldots, M$ if we consider two notional maneuver change times $\tilde{t}_0$ and $\tilde{t}_{M+1}$ such that $\tilde{t}_0 = t_0$ and $\tilde{t}_{M+1} = t_k$. Note that we define the components of maneuver segment $m-1$ to be active at maneuver change time $\tilde{t}_m$.

Based on the inertial motion model discussed in Subsection 2.4.1, we have chosen Cartesian velocities since they lead to a linear motion equation. This has the effect that the state dimension increases by two elements with each maneuver change point.

The target state with respect to the M maneuver change times $\tilde{t}_1, \ldots, \tilde{t}_M$ can be expressed by

$$\mathbf{x}_k = \begin{cases} \boldsymbol{\Phi}(t_k, \tilde{t}_1)\mathbf{x}_1 & \text{for } t_0 \le t_k \le \tilde{t}_1 \\ \vdots & \vdots \\ \boldsymbol{\Phi}(t_k, \tilde{t}_m)\mathbf{x}_m & \text{for } \tilde{t}_{m-1} \le t_k \le \tilde{t}_m \\ \vdots & \vdots \\ \boldsymbol{\Phi}(t_k, \tilde{t}_M)\mathbf{x}_M & \text{for } \tilde{t}_{M-1} \le t_k \le \tilde{t}_M \\ \boldsymbol{\Phi}(t_k, t_\mathrm{r})\mathbf{x}_\mathrm{r} & \text{for } \tilde{t}_M \le t_k \le t_\mathrm{r} \end{cases} \tag{2.32}$$

with $\mathbf{x}_m = \mathbf{x}(\tilde{t}_m)$. For $\tilde{t}_{m-1} \le t_k, \tau \le \tilde{t}_m$, $m = 1, \ldots, M$, i.e., t_k and τ are in the same maneuver segment, the state transition matrix $\boldsymbol{\Phi}(t_k, \tau) \in \mathbb{R}^{(4+3M)\times(4+3M)}$ is defined element by element by

$$[\boldsymbol{\Phi}(t_k, \tau)]_{i,j} = \begin{cases} 1 & \text{for } i = j \\ t_k - \tau & \text{for } i = 1,\ j = 2m+1 \\ t_k - \tau & \text{for } i = 2,\ j = 2m+2 \\ 0 & \text{else} \end{cases}. \tag{2.33}$$

Fig. 2.8 shows typical relative displacements for time t_k, the maneuver change times, and the reference time. Hence, the state at time t_k is related to the reference state at time t_r as follows:

$$\mathbf{x}_k = \underbrace{\boldsymbol{\Phi}(t_k, \tilde{t}_m) \cdots \boldsymbol{\Phi}(\tilde{t}_{M-1}, \tilde{t}_M)\boldsymbol{\Phi}(\tilde{t}_M, t_\mathrm{r})}_{=\boldsymbol{\Phi}(t_k, t_\mathrm{r})} \mathbf{x}_\mathrm{r} \tag{2.34}$$

for $t_k \le \tilde{t}_m \le \tilde{t}_M \le t_\mathrm{r}$. Moreover, the cumulative state transition matrix $\boldsymbol{\Phi}(t_k, t_\mathrm{r})$ from time t_r to t_k, which is the product of the individual state transition matrices in the above equation, can be expressed by

$$\boldsymbol{\Phi}(t_k, t_\mathrm{r}) = \left[\begin{array}{c|c|c|c} \mathbf{I}_2 & \mathbf{0}_{2\times(m-1)} & \Delta T_m & \mathbf{0}_{2\times M} \\ \hline \mathbf{0}_{(2+3M)\times 2} & \multicolumn{3}{c}{\mathbf{I}_{2+3M}} \end{array}\right] \tag{2.35}$$

with

$$\Delta T_m = \begin{bmatrix} (t_k - \tilde{t}_m)\mathbf{I}_2 & \ldots & (\tilde{t}_{M-1} - \tilde{t}_M)\mathbf{I}_2 & (\tilde{t}_M - t_\mathrm{r})\mathbf{I}_2 \end{bmatrix}, \tag{2.36}$$

where $\Delta T_m \in \mathbb{R}^{2\times(2(M+1)-(m-1))}$. For the simple case $M = 0$ (no maneuver change), we obtain $\boldsymbol{\Phi}(t_k, t_\mathrm{r})$ from (2.19) in Subsection 2.4.1.

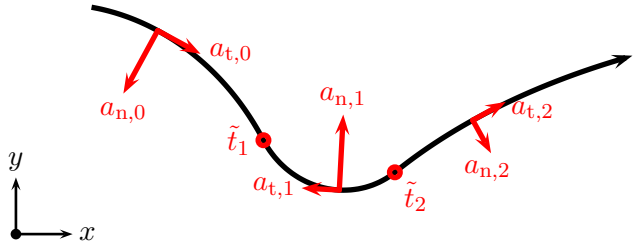

Figure 2.9: Piecewise curvilinear motion trajectory with $M = 3$ maneuver segments. In each segment, curvilinear motion with different tangential and normal accelerations is performed. The maneuver change times $\tilde{t}_1$ and $\tilde{t}_2$ concatenate the maneuver segments, © 2014 IEEE.

2.4.5 Piecewise Deterministic Curvilinear Motion

In the case of piecewise curvilinear motion, the target state is given by a state vector consisting of constant tangential and normal accelerations and maneuver change times. See Fig. 2.9 for an example trajectory. So, the state for M maneuver change points is specified by

$$\mathbf{x}_k = \left[x_k, y_k, v_k, \varphi_k, \mathbf{a}^{\mathrm{T}}, \tilde{\mathbf{t}}^{\mathrm{T}}\right]^{\mathrm{T}} \in \mathbb{R}^{(6+3M)\times 1} . \tag{2.37}$$

For the acceleration components for each maneuver segment we have

$$\mathbf{a} = \left[a_{\mathrm{t},0}, a_{\mathrm{n},0}, \ldots, a_{\mathrm{t},M}, a_{\mathrm{n},M}\right]^{\mathrm{T}} \in \mathbb{R}^{2(M+1)\times 1} \tag{2.38}$$

and for the maneuver change times

$$\tilde{\mathbf{t}} = [\tilde{t}_1, \ldots, \tilde{t}_M]^{\mathrm{T}} \in \mathbb{R}^{M\times 1} . \tag{2.39}$$

Obviously, the dimension of the target state increases by three components with each maneuver change point, since two acceleration components and the maneuver change time are added to the state with each maneuver change. The parameter $\tilde{t}_m$ is the m-th maneuver change time and $a_{\mathrm{t},m}$ and $a_{\mathrm{n},m}$ denote the tangential and normal acceleration in the time interval $[\tilde{t}_m, \tilde{t}_{m+1}]$ for $m = 0, \ldots, M$ with $\tilde{t}_0 = t_0$ and $\tilde{t}_{M+1} = t_{\mathrm{r}}$. Similar to the previous subsection, it is defined that the components of maneuver segment $m-1$ are active at maneuver change time $\tilde{t}_m$.

Since the reference state is commonly the current target state, the target state for M maneuver change points at the times $\tilde{t}_1, \ldots, \tilde{t}_M$ in the interval $[t_0, t_\mathrm{r}]$ is given by

$$\mathbf{x}_k = \begin{cases} \mathbf{f}_0\left(\mathbf{x}_1; t, \tilde{t}_1\right) & \text{for } t_0 \leq t_k \leq \tilde{t}_1 \\ \vdots & \vdots \\ \mathbf{f}_{m-1}\left(\mathbf{x}(\tilde{t}_m); t_k, \tilde{t}_m\right) & \text{for } \tilde{t}_{m-1} \leq t_k \leq \tilde{t}_m \\ \vdots & \vdots \\ \mathbf{f}_{M-1}\left(\mathbf{x}(\tilde{t}_M); t_k, \tilde{t}_M\right) & \text{for } \tilde{t}_{M-1} \leq t_k \leq \tilde{t}_M \\ \mathbf{f}_M\left(\mathbf{x}_\mathrm{r}; t_k, t_\mathrm{r}\right) & \text{for } \tilde{t}_M \leq t_k \leq t_\mathrm{r} \end{cases} . \tag{2.40}$$

For $\tilde{t}_{m-1} \leq t_k, \tau \leq \tilde{t}_m$, i.e., t_k and τ are both in the maneuver segment $m-1$, $\mathbf{f}_{m-1} : \mathbb{R}^{(6+3M)\times 1} \to \mathbb{R}^{(6+3M)\times 1}$ is defined by the motion function (2.26) according to

$$\mathbf{f}_{m-1}\left(\mathbf{x}(\tau); t_k, \tau\right) = \left.\mathbf{f}\left(\mathbf{x}(\tau); t_k, \tau\right)\right|_{\substack{a_\mathrm{t}=a_{\mathrm{t},m-1} \\ a_\mathrm{n}=a_{\mathrm{n},m-1}}} . \tag{2.41}$$

This means, we have to replace a_t by $a_{\mathrm{t},m-1}$ and a_n by $a_{\mathrm{n},m-1}$ in (2.28). Fig. 2.8 shows typical relative displacements for time t_k, the maneuver change times, and the reference time. Altogether, we obtain for the relation of the target state at some arbitrary time t_k to the reference state

$$\mathbf{x}_k = \mathbf{f}_{m-1}\left(\mathbf{f}_m\left(\cdots \mathbf{f}_M\left(\mathbf{x}_\mathrm{r}; \tilde{t}_M, t_\mathrm{r}\right); \cdots\right); t_k, \tilde{t}_m\right) \tag{2.42}$$

with $\tilde{t}_{m-1} \leq t_k \leq \tilde{t}_m \leq \tilde{t}_M \leq t_\mathrm{r}$.

2.5 Summary of the Chapter

In this chapter, we have introduced or recapped fundamental concepts used in this thesis such as the Gaussian density and measurement and motion models. Bearings-only or angle-only measurements are essential in this thesis since both central themes base on them. Furthermore, we sketched the basics of bearing rate measurements which are used as additional measurements to evaluate the performance of the state estimator, see Chapter 6.

Regarding motion models, we have presented a simple but widespread model considering only constant velocity. In this context, we discussed the usage of process noise which is on the one hand featured for Bayesian approaches, but on the other hand often avoided for non-Bayesian methods due to its non-deterministic nature. Furthermore, a more complex motion model incorporating accelerations called curvilinear motion model has been introduced. To model maneuver changes, segments of basic motion can be concatenated in a piecewise manner. In this context, two types of piecewise motion have been intro-

duced and investigated: The first one is piecewise inertial motion, where targets move in segments of constant velocity and heading. The second one is piecewise curvilinear motion, where targets move in segments of constant tangential and normal acceleration. These models will be employed in the performance bound derivation in the following Chapter 3.

3 Performance Bound for Bearings-only Tracking of Maneuvering Targets

A performance bound shall help to gauge the maximum achievable performance for an estimation problem. The most widespread bound is the Cramér-Rao lower bound (CRLB) which is named after the pioneering papers of Cramér [Cra46] and Rao [Rao45] who both derived the inequality (3.3) later entitled Cramér-Rao inequality. Nevertheless, for special problems, other, to some extent tighter bounds exist as, for example, the Bhattacharyya [Bha48], Bobrovsky-Zakai [BZ75], Weiss-Weinstein [WW88], or Barankin [Bar49] lower bounds. Also refer to [RN05] for a comparison. These bounds are not part of this thesis as we concentrate on the CRLB. Thus, the CRLB is derived in a general manner in Section 3.1. Subsequently, it is shown in Section 3.2 how the piecewise motion models can be incorporated into the bound and finally in Section 3.3 how also passive measurement models are considered. So, the result of this chapter will be a CRLB for tracking problems involving highly maneuvering targets under passive measurements. This is also the main contribution of the own paper [HOK14].

3.1 Cramér-Rao Lower Bound

In order to judge an estimation problem it is important to know the maximum mean estimation accuracy, i.e. the best mean performance, that can be attained given all available measurements up to a reference time t_k. Hence, the Cramér-Rao lower bound (CRLB) provides a lower bound on the mean-square estimation error achievable for any unbiased estimator and its parameter dependencies reveal characteristic features of the estimation problem. That means, no matter what estimator is used, none, on average, can do better than what the CRLB specifies [Ker89]. Thus, it serves as a general and powerful benchmark for the performance of an estimator.

Consider the following nonlinear estimation problem with a deterministic motion model and a measurement model with additive white Gaussian noise

$$\mathbf{x}_k = \mathbf{f}_{k-1}(\mathbf{x}_{k-1}) \tag{3.1a}$$

$$\mathbf{z}_k = \mathbf{h}_k(\mathbf{x}_k) + \boldsymbol{\nu}_k \,. \tag{3.1b}$$

The noise term $\boldsymbol{\nu}_k$ is zero mean and has a covariance matrix denoted by $\mathbf{R}_k$. An important equation is the *likelihood* function $p(\mathbf{z}_k|\mathbf{x}_k)$, which describes how likely the

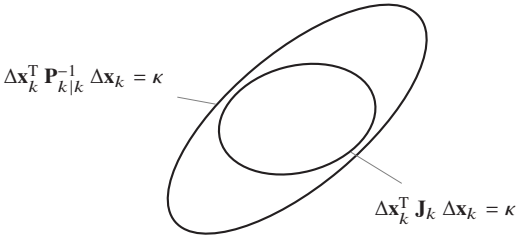

Figure 3.1: Visualization of the Cramér-Rao inequality by concentration ellipses.

state is given the measurements and therefore serves as a measure of the evidence from the data [BSLK01]. For the examined Gaussian case it is given by

$$p(\mathbf{z}_k|\mathbf{x}_k) = \mathcal{N}(\mathbf{z}_k; \mathbf{h}_k(\mathbf{x}_k), \mathbf{R}_k)\,. \tag{3.2}$$

This Gaussian case is already a special case, but we will not consider more general cases with non-additive or non-Gaussian noise in this thesis, see [RAG04] for details. Furthermore, also a bound for non-deterministic, i.e. stochastic state dynamics, exists which is referred to as *posterior* CRLB first formulated by Van Trees [VT68] and refined by Tichavský et al. [TMN98, ŠKT01]. This bound is not covered in this work either.

Let $\hat{\mathbf{x}}_{k|k}$ be an unbiased estimate of the d-dimensional state vector $\mathbf{x}_k$ based on the measurement sequence $\mathbf{Z}_{1:k} = \{\mathbf{z}_1, \ldots, \mathbf{z}_k\}$ (see also Section 5.6), and $\mathbf{P}_{k|k}$ the covariance matrix of $\hat{\mathbf{x}}_{k|k}$. Then the CRLB denoted by $\mathbf{J}_k^{-1}$ is given by the expected value [VT68] in the following inequality

$$\mathbf{P}_{k|k} = \mathrm{E}\left\{\left(\mathbf{x}_k - \hat{\mathbf{x}}_{k|k}\right)\left(\mathbf{x}_k - \hat{\mathbf{x}}_{k|k}\right)^{\mathrm{T}}\right\} \geq \mathbf{J}_k^{-1}\,, \tag{3.3}$$

where the inequality means that the matrix difference $\mathbf{P}_{k|k} - \mathbf{J}_k^{-1}$ is positive semidefinite. The inverse of the CRLB denoted by $\mathbf{J}_k$ is named *Fisher information matrix (FIM)*. If the estimator covariance attains the CRLB the estimator is called *efficient*.

3.1.1 Visualization of the Cramér-Rao Lower Bound

Geometrically, the covariance matrix $\mathbf{P}_{k|k}$ can be illustrated by a concentration ellipse [Sch91, Bec92]

$$\Delta\mathbf{x}_k^{\mathrm{T}}\,\mathbf{P}_{k|k}^{-1}\,\Delta\mathbf{x}_k = \kappa\,, \tag{3.4}$$

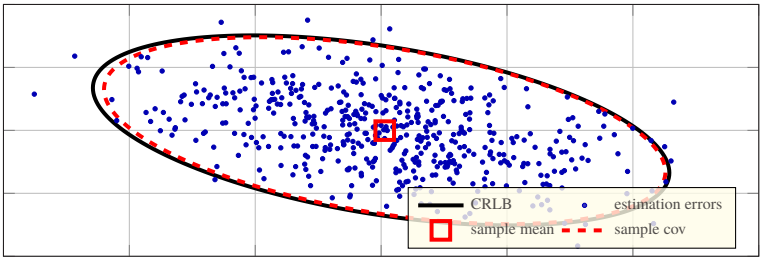

Figure 3.2: Visualization of estimation errors showing an unbiased and nearly efficient estimator since the sample covariance attains the CRLB and the sample mean is zero. Also refer to Chapter 6, © 2014 IEEE.

where $\Delta\mathbf{x}_k = \mathbf{x}_k - \hat{\mathbf{x}}_{k|k}$ denotes the estimation error and κ is a constant determining the size of the enclosed volume V with

$$V = V_d \sqrt{\det\left(\kappa\, \mathbf{P}_{k|k}\right)}, \tag{3.5}$$

where V_d is the volume of the d-dimensional unit sphere. Analogously, the CRLB can be visualized by a concentration ellipse as follows:

$$\Delta\mathbf{x}_k^{\mathrm{T}}\, \mathbf{J}_k\, \Delta\mathbf{x}_k = \kappa\,, \tag{3.6}$$

The ellipses are depicted in Fig. 3.1. One can see that the CRLB concentration ellipse (3.6) completely lies inside the covariance concentration ellipse (3.4) which is the geometric interpretation of the CR inequality $\mathbf{P}_{k|k} \geq \mathbf{J}_k^{-1}$ (3.3). The FIM defines the smallest concentration ellipse that can be achieved for any consistent estimator.

If an estimator is evaluated in several (for example hundreds of) Monte Carlo runs, the distribution of the estimates and, since it is an additive relation, equivalently the distribution of the estimate errors forming its sample covariance tends to the covariance of the estimate. If the estimator is efficient, the covariance is equal to the CRLB. If the estimator is unbiased, the mean of the estimation error is zero. Fig. 3.2 shows the distribution of estimation errors after 500 Monte Carlo runs. It turns out to be a nearly unbiased and efficient estimator for two parameters since the sample covariance is very similar to the CRLB and the sample mean is zero. This illustration is borrowed from the results in Chapter 6. Refer to that chapter for further details.

3.1.2 Derivation of the Cramér-Rao Lower Bound

In order to derive the CRLB based on all past information, we have to consider a sequence of target states: Let $\hat{\mathbf{X}}_{k|k}$ be an unbiased estimate of the target state sequence (or trajectory) $\{\mathbf{x}_0, \mathbf{x}_1, \ldots, \mathbf{x}_k\}$ identified by the stacked vector

$$\mathbf{X}_{0:k} = \left[\mathbf{x}_0^{\mathrm{T}}, \mathbf{x}_1^{\mathrm{T}}, \ldots, \mathbf{x}_k^{\mathrm{T}}\right]^{\mathrm{T}} \in \mathbb{R}^{(k+1)d} \tag{3.7}$$

based on the measurement sequence $\mathbf{Z}_{1:k}$. Then the covariance matrix of $\hat{\mathbf{X}}_{k|k}$ has a CRLB given by the following expected value:

$$\mathrm{E}\left\{\left(\mathbf{X}_{0:k} - \hat{\mathbf{X}}_{k|k}\right)\left(\mathbf{X}_{0:k} - \hat{\mathbf{X}}_{k|k}\right)^{\mathrm{T}}\right\} \geq \mathcal{J}^{-1}(\mathbf{X}_{0:k})\,. \tag{3.8}$$

In [RAG04], $\mathcal{J}$ is called *trajectory information matrix* and has shape $(k+1)d \times (k+1)d$. It is defined as [TMN98]:

$$\mathcal{J}(\mathbf{X}_{0:k}) = \mathrm{E}\left\{\left(\nabla_{\mathbf{X}_{0:k}} \log p\left(\mathbf{Z}_{1:k}|\mathbf{X}_{0:k}\right)\right)\left(\nabla_{\mathbf{X}_{0:k}} \log p\left(\mathbf{Z}_{1:k}|\mathbf{X}_{0:k}\right)\right)^{\mathrm{T}}\right\} \tag{3.9}$$

or equivalently as [VT68, BSLK01]

$$\mathcal{J}(\mathbf{X}_{0:k}) = -\mathrm{E}\left\{\nabla_{\mathbf{X}_{0:k}}\left(\nabla_{\mathbf{X}_{0:k}} \log p\left(\mathbf{Z}_{1:k}|\mathbf{X}_{0:k}\right)\right)^{\mathrm{T}}\right\}\,. \tag{3.10}$$

Here, $\nabla_{\mathbf{X}_{0:k}}$ is the first-order partial derivative operator with respect to $\mathbf{X}_{0:k}$ defined as

$$\nabla_{\mathbf{X}_{0:k}} = \left[\frac{\partial}{\partial \mathbf{x}_0}, \ldots, \frac{\partial}{\partial \mathbf{x}_k}\right]^{\mathrm{T}} \tag{3.11}$$

with dimension $(k+1)d$. Furthermore, $p\left(\mathbf{Z}_{1:k}|\mathbf{X}_{0:k}\right)$ is the trajectory likelihood function which is related to the single-state likelihood function $p(\mathbf{z}_k|\mathbf{x}_k)$ by [Tay79]

$$p\left(\mathbf{Z}_{1:k}|\mathbf{X}_{0:k}\right) = p(\mathbf{x}_0) \cdot \prod_{j=1}^{k} p(\mathbf{z}_j|\mathbf{x}_j)\,. \tag{3.12}$$

Note that the likelihood (3.12) is used in (3.9) and (3.10) instead of the joint probability distribution $p\left(\mathbf{X}_{0:k}, \mathbf{Z}_{1:k}\right)$. This is allowed due to the deterministic trajectory [RAG04] or non-random parameter [VT68] assumption. If no prior $p(\mathbf{x}_0)$ is given, we can either omit $p(\mathbf{x}_0)$ or set $p(\mathbf{x}_0) = 1$ which is algebraically equivalent. Taking the logarithm of both sides, we can express the log-likelihood as

$$\log p\left(\mathbf{Z}_{1:k}|\mathbf{X}_{0:k}\right) = \log p(\mathbf{x}_0) + \sum_{j=1}^{k} \log p(\mathbf{z}_j|\mathbf{x}_j)\,. \tag{3.13}$$

Due to the Gaussian assumptions, the likelihood $p(\mathbf{z}_k|\mathbf{x}_k)$ is given as in (3.2) and its logarithm, using the definition of a Gaussian (2.4), by

$$\log p(\mathbf{z}_k|\mathbf{x}_k) = c_k - \frac{1}{2}\left(\mathbf{z}_k - \mathbf{h}_k(\mathbf{x}_k)\right)^{\mathrm{T}} \mathbf{R}_k^{-1} \left(\mathbf{z}_k - \mathbf{h}_k(\mathbf{x}_k)\right) \tag{3.14}$$

with a constant c_k. If a prior $p(\mathbf{x}_0)$ is given, we assume that $\mathbf{x}_0$ is Gaussian distributed with mean $\boldsymbol{\mu}_0$ and covariance matrix $\mathbf{P}_0$. Hence, $p(\mathbf{x}_0) = \mathcal{N}(\mathbf{x}_0, \boldsymbol{\mu}_0, \mathbf{P}_0)$ and thus we have,

$$\frac{\partial \log p(\mathbf{x}_0)}{\partial \mathbf{x}_0} = \frac{\partial}{\partial \mathbf{x}_0}\left(c_0 - \frac{1}{2}\left(\mathbf{x}_0 - \boldsymbol{\mu}_0\right)^{\mathrm{T}} \mathbf{P}_0^{-1} \left(\mathbf{x}_0 - \boldsymbol{\mu}_0\right)\right) = -\mathbf{P}_0^{-1}\left(\mathbf{x}_0 - \boldsymbol{\mu}_0\right) . \tag{3.15}$$

Otherwise, if no prior is given, we can set $\partial \log p(\mathbf{x}_0)/\partial \mathbf{x}_0 = 0$. For $k > 0$, we have

$$\nabla_{\mathbf{X}_{0:k}} \log p\left(\mathbf{Z}_{1:k}|\mathbf{X}_{0:k}\right) = \left[\frac{\partial \log p\left(\mathbf{Z}_{1:k}|\mathbf{X}_{0:k}\right)}{\partial \mathbf{x}_1}, \ldots, \frac{\partial \log p\left(\mathbf{Z}_{1:k}|\mathbf{X}_{0:k}\right)}{\partial \mathbf{x}_k}\right]^{\mathrm{T}} . \tag{3.16}$$

Due to the sum in (3.13), the components of (3.16) are given by

$$\frac{\partial \log p\left(\mathbf{Z}_{1:k}|\mathbf{X}_{0:k}\right)}{\partial \mathbf{x}_i} = \sum_{j=1}^{k} \left(\frac{\partial \mathbf{h}_j(\mathbf{x}_j)}{\partial \mathbf{x}_i}\right)^{\mathrm{T}} \mathbf{R}_j^{-1} \left(\mathbf{z}_j - \mathbf{h}_j(\mathbf{x}_j)\right) \tag{3.17}$$

for $i = 1, \ldots, k$.

3.1.3 Computation of the Fisher Information Matrix

In [VT68, Tay79] the FIM for the state $\mathbf{x}_k$ at time t_k is given by the $d \times d$ right-lower block of $\mathcal{J}(\mathbf{X}_{0:k})$ denoted by $\mathbf{J}_k$, i.e.,

$$\mathbf{J}_k = \mathrm{E}\left\{\left(\frac{\partial \log p\left(\mathbf{Z}_{1:k}|\mathbf{X}_{0:k}\right)}{\partial \mathbf{x}_k}\right)\left(\frac{\partial \log p\left(\mathbf{Z}_{1:k}|\mathbf{X}_{0:k}\right)}{\partial \mathbf{x}_k}\right)^{\mathrm{T}}\right\} . \tag{3.18}$$

Inserting (3.17) and (3.15) into (3.18) and taking the expectation yields

$$\mathbf{J}_k = \left(\frac{\partial \mathbf{x}_0}{\partial \mathbf{x}_k}\right)^{\mathrm{T}} \mathbf{P}_0^{-1} \frac{\partial \mathbf{x}_0}{\partial \mathbf{x}_k} + \sum_{j=1}^{k} \left(\frac{\partial \mathbf{h}_j(\mathbf{x}_j)}{\partial \mathbf{x}_k}\right)^{\mathrm{T}} \mathbf{R}_j^{-1} \frac{\partial \mathbf{h}_j(\mathbf{x}_j)}{\partial \mathbf{x}_k} , \tag{3.19}$$

where the first term is zero if no prior is given. The partial derivatives in (3.19) with respect to time t_k are calculated by means of the chain rule as follows:

$$\frac{\partial \mathbf{h}_j(\mathbf{x}_j)}{\partial \mathbf{x}_k} = \frac{\partial \mathbf{h}_j(\mathbf{x}_j)}{\partial \mathbf{x}_j} \cdot \frac{\partial \mathbf{x}_j}{\partial \mathbf{x}_k} . \tag{3.20}$$

Following the deterministic state transition equation (3.1a), we define $\widetilde{\mathbf{F}}_k$ as

$$\widetilde{\mathbf{F}}_k = \frac{\partial \mathbf{f}_k(\mathbf{x}_k)}{\partial \mathbf{x}_k} = \frac{\partial \mathbf{x}_{k+1}}{\partial \mathbf{x}_k} = \left(\frac{\partial \mathbf{x}_k}{\partial \mathbf{x}_{k+1}} \right)^{-1} = \left(\widetilde{\mathbf{F}}_k^{-1} \right)^{-1} . \tag{3.21}$$

Hence, the backward state transition from time t_{k+1} to time t_k is expressed by matrix $\widetilde{\mathbf{F}}_k^{-1}$. For the state transition from an arbitrary time t_j to time t_k with $t_j \leq t_k$, we can apply the chain rule,

$$\frac{\partial \mathbf{x}_j}{\partial \mathbf{x}_k} = \frac{\partial \mathbf{x}_j}{\partial \mathbf{x}_{j+1}} \cdots \frac{\partial \mathbf{x}_{k-1}}{\partial \mathbf{x}_k} = \widetilde{\mathbf{F}}_j^{-1} \cdots \widetilde{\mathbf{F}}_{k-1}^{-1} , \tag{3.22}$$

where this decomposition is also known as continuity property [Tay79]. Subsequently, we define $\widetilde{\mathbf{\Phi}}(t_j, t_k)$ for $t_j \leq t_k$ as

$$\widetilde{\mathbf{\Phi}}(t_j, t_k) = \prod_{i=j}^{k-1} \widetilde{\mathbf{F}}_i^{-1} = \frac{\partial \mathbf{x}_j}{\partial \mathbf{x}_k} , \tag{3.23}$$

which is similar to the definition of $\mathbf{\Phi}$ in Chapter 2. Finally, by letting

$$\widetilde{\mathbf{H}}_j = \frac{\partial \mathbf{h}_j(\mathbf{x}_j)}{\partial \mathbf{x}_j} , \tag{3.24}$$

we can reformulate the FIM (3.19) as

$$\mathbf{J}_k = \sum_{j=0}^{k} \widetilde{\mathbf{\Phi}}(t_j, t_k)^{\mathrm{T}} \widetilde{\mathbf{H}}_j^{\mathrm{T}} \mathbf{R}_j^{-1} \widetilde{\mathbf{H}}_j \widetilde{\mathbf{\Phi}}(t_j, t_k) \tag{3.25}$$

by explicitly choosing $\widetilde{\mathbf{H}}_0$ and $\mathbf{R}_0$ so that $\widetilde{\mathbf{H}}_0^{\mathrm{T}} \mathbf{R}_0^{-1} \widetilde{\mathbf{H}}_0 = \mathbf{P}_0^{-1}$. The FIM will also play a role for observability aspects in Chapter 4 since it is strongly connected to the observability Gramian which can be used to figure out whether a system is observable.

If the dimensionality of the state vector remains constant – and that is important, since for piecewise motion the state vector dimension increases, see Subsection 2.4.3 – a recursive FIM update formula can easily be deduced from (3.25):

$$\mathbf{J}_k = \left(\widetilde{\mathbf{F}}_{k-1}^{-1} \right)^{\mathrm{T}} \mathbf{J}_{k-1} \widetilde{\mathbf{F}}_{k-1}^{-1} + \widetilde{\mathbf{H}}_k^{\mathrm{T}} \mathbf{R}_k^{-1} \widetilde{\mathbf{H}}_k . \tag{3.26}$$

If the state vector dimension is not constant, (3.25) has to be used to calculate the FIM. All summands have to be re-evaluated using the current state vector dimension. That means, the advantages of recursive calculation, e.g. less computational burden, do not apply.

As an alternative to (3.26), one can calculate the FIM by denoting $\mathbf{J}_k$ by the inverse of a covariance matrix of an efficient filter, $\mathbf{P}_{k|k}^{-1}$, and by applying the matrix inversion lemma

$$\mathbf{P}_{k|k}^{-1} = \left(\widetilde{\mathbf{F}}_{k-1}\mathbf{P}_{k-1|k-1}\widetilde{\mathbf{F}}_{k-1}^{\mathrm{T}}\right)^{-1} + \widetilde{\mathbf{H}}_k^{\mathrm{T}}\mathbf{R}_k^{-1}\widetilde{\mathbf{H}}_k \,, \tag{3.27}$$

which is algebraically identical to the inverse covariance update of the extended Kalman filter (EKF) if no process noise is assumed [VTB07], see also Chapter 5.

In the following Section 3.2, we will derive a CRLB for unknown maneuver change times tackling the motion part of the FIM (3.25). How to incorporate bearing, bearing rate, and range measurements into (3.25) is explained in Section 3.3.

3.2 Incorporating Piecewise Motion Models into the CRLB

In this section, details about incorporating both piecewise motion models introduced in Chapter 2 are outlined. Precisely, the calculation of the state transition matrix $\widetilde{\mathbf{\Phi}}(t_j, t_k)$ (3.23) is performed by means of applying the chain rule under the conditions of an increasing state vector dimension due to the maneuver change times. These calculations have first been established by Becker [Bec05a] for the piecewise curvilinear motion model. Here, it is extended to the piecewise inertial motion model. Also refer to the own papers [OH10, HO11b, HOK14] as well as the thesis [Ois14] for a reference on the following derivations.

3.2.1 Piecewise Deterministic Inertial Motion

In order to compute the CRLB for piecewise deterministic inertial motion introduced in Subsection 2.4.4, we recall the $(4 + 3M)$-dimensional target state (2.29) assuming M maneuver change times:

$$\mathbf{x}_k = \left[x_k, y_k, \mathbf{v}^{\mathrm{T}}, \tilde{\mathbf{t}}^{\mathrm{T}}\right]^{\mathrm{T}} \tag{3.28}$$

with position $\mathbf{r}_k = [x_k, y_k]^{\mathrm{T}}$, velocities

$$\mathbf{v} = [\dot{x}_0, \dot{y}_0, \dot{x}_1, \dot{y}_1, \ldots, \dot{x}_M, \dot{y}_M]^{\mathrm{T}} \,, \tag{3.29}$$

and maneuver change times

$$\tilde{\mathbf{t}} = [\tilde{t}_1, \ldots, \tilde{t}_M]^{\mathrm{T}} \,. \tag{3.30}$$

Due to the maneuver change times, we have to express the state transition $\widetilde{\mathbf{\Phi}}(t_j, t_k)$ from time t_i to a reference time t_k described by the Jacobian matrix $\partial \mathbf{x}_i / \partial \mathbf{x}_k$ (cf. (3.22)) with respect the maneuver change times enclosed in the vector $\tilde{\mathbf{t}}$ as well as the segment velocities in vector $\mathbf{v}$. Since we assume the reference time t_k to be the current time,

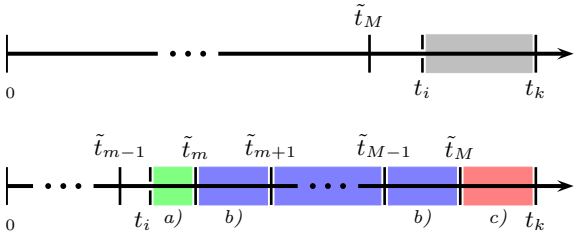

Figure 3.3: Relative displacement of time t_i and reference time t_r. Upper case: t_i and t_k lie in the same maneuver segment. Lower case: the segment containing t_i occurs before the segment containing t_k, © 2014 IEEE.

the relative displacement of t_i and t_k regarding the maneuver change times makes it necessary to distinguish between two different cases, see Fig. 3.3:

1) t_i and t_k lie in the same maneuver segment, and

2) the segment containing t_i occurs before the segment containing t_k.

Considering both cases, the structure of the $(4+3M)\times(4+3M)$ Jacobian matrix $\partial\mathbf{x}_i/\partial\mathbf{x}_k$ is given by

$$\widetilde{\mathbf{\Phi}}(t_i,t_k)=\frac{\partial\mathbf{x}_i}{\partial\mathbf{x}_k}=\left[\begin{array}{c|c|c} \dfrac{\partial\mathbf{r}_i}{\partial\mathbf{r}_k}=\mathbf{I}_2 & \dfrac{\partial\mathbf{r}_i}{\partial\mathbf{v}} & \dfrac{\partial\mathbf{r}_i}{\partial\tilde{\mathbf{t}}}=\mathbf{0} \\ \hline \dfrac{\partial\mathbf{v}}{\partial\mathbf{r}_k}=\mathbf{0} & \dfrac{\partial\mathbf{v}}{\partial\mathbf{v}}=\mathbf{I}_{2M+2} & \dfrac{\partial\mathbf{v}}{\partial\tilde{\mathbf{t}}}=\mathbf{0} \\ \hline \dfrac{\partial\tilde{\mathbf{t}}}{\partial\mathbf{r}_k}=\mathbf{0} & \dfrac{\partial\tilde{\mathbf{t}}}{\partial\mathbf{v}}=\mathbf{0} & \dfrac{\partial\tilde{\mathbf{t}}}{\partial\tilde{\mathbf{t}}}=\mathbf{I}_M \end{array}\right]. \tag{3.31}$$

Case 1) In case of $\tilde{t}_M \le t_i \le t_k$, the measurement time t_i and the reference time t_k are in the same maneuver segment. Here, no maneuver change points have to be considered. Thus,

$$\frac{\partial\mathbf{x}_i}{\partial\mathbf{x}_k}=\begin{bmatrix}\mathbf{I}_2 & \partial\mathbf{r}_i/\partial\mathbf{v} & \partial\mathbf{r}_i/\partial\tilde{\mathbf{t}} \\ \mathbf{0} & \mathbf{I}_{2M+2} & \mathbf{0} \\ \mathbf{0} & \mathbf{0} & \mathbf{I}_M\end{bmatrix}. \tag{3.32}$$

In the above matrix, we use appropriately dimensioned zero block matrices. The only non-zero or non-identity block matrix is the Jacobian matrix $\partial \mathbf{r}_i / \partial \mathbf{v}$ given by

$$\frac{\partial \mathbf{r}_i}{\partial \mathbf{v}} = \Bigg[\mathbf{0}_{2\times 2M} \qquad \underbrace{\frac{\partial \mathbf{r}_i}{\partial \dot{x}_M} \quad \frac{\partial \mathbf{r}_i}{\partial \dot{y}_M}}_{=(t_i - t_k)\mathbf{I}_2, \text{ see Appendix A.1.}} \Bigg] \in \mathbb{R}^{2\times(2M+2)} . \tag{3.33}$$

For the special case of $M = 0$ we obtain

$$\frac{\partial \mathbf{x}_i}{\partial \mathbf{x}_k} = \mathbf{\Phi}(t_i, t_k) . \tag{3.34}$$

So, this Jacobian matrix is equal to the state transition matrix for inertial motion (2.19).

For Case 2 we assume that $t_i \le \tilde{t}_m \le \tilde{t}_{m+1} \le \tilde{t}_M \le t_k$. That means, we consider several maneuver change times, see also Fig. 3.3. By applying the chain rule similar to (3.22), the Jacobian matrix can be written as

$$\frac{\partial \mathbf{x}_i}{\partial \mathbf{x}_k} = \underbrace{\frac{\partial \mathbf{x}_i}{\partial \mathbf{x}_m}}_{2a)} \underbrace{\frac{\partial \mathbf{x}_m}{\partial \mathbf{x}_{m+1}} \cdots \frac{\partial \mathbf{x}_{M-1}}{\partial \mathbf{x}_M}}_{2b)} \underbrace{\frac{\partial \mathbf{x}_M}{\partial \mathbf{x}_k}}_{2c)} . \tag{3.35}$$

It can be recognized that the above equation contains three qualitatively different classes of matrices which will be handled in the subsequent cases 2a), 2b), and 2c).

Case 2a) $\partial \mathbf{x}_i / \partial \mathbf{x}_m$ is the Jacobian matrix describing the transition from t_i to the first maneuver change time $\tilde{t}_m$. It has the following form

$$\frac{\partial \mathbf{x}_i}{\partial \mathbf{x}_m} = \begin{bmatrix} \mathbf{I}_2 & \partial \mathbf{r}_i / \partial \mathbf{v} & \partial \mathbf{r}_i / \partial \tilde{\mathbf{t}} \\ \mathbf{0} & \mathbf{I}_{2M+2} & \mathbf{0} \\ \mathbf{0} & \mathbf{0} & \mathbf{I}_M \end{bmatrix} \tag{3.36}$$

with appropriately dimensioned zero block matrices. The Jacobian matrix $\partial \mathbf{r}_i / \partial \mathbf{v}$ is obtained by

$$\frac{\partial \mathbf{r}_i}{\partial \mathbf{v}} = \Bigg[\mathbf{0} \ \dots \ \mathbf{0} \quad \underbrace{\frac{\partial \mathbf{r}_i}{\partial \dot{x}_{m-1}} \quad \frac{\partial \mathbf{r}_i}{\partial \dot{y}_{m-1}}}_{=(t_i - \tilde{t}_m)\mathbf{I}_2} \quad \mathbf{0} \ \dots \ \mathbf{0} \Bigg] \in \mathbb{R}^{2\times(2M+2)} , \tag{3.37}$$

where $\mathbf{0} \in \mathbb{R}^{2\times 2}$. For $\partial \mathbf{r}_i / \partial \tilde{\mathbf{t}}$ we have

$$\frac{\partial \mathbf{r}_i}{\partial \tilde{\mathbf{t}}} = \begin{bmatrix} \mathbf{0} & \dots & \mathbf{0} & \dfrac{\partial \mathbf{r}_i}{\partial \tilde{t}_m} & \mathbf{0} & \dots & \mathbf{0} \end{bmatrix} \in \mathbb{R}^{2\times M} \tag{3.38}$$

with $\mathbf{0} \in \mathbb{R}^{2\times 1}$. Here, $\partial \mathbf{r}_i / \partial \tilde{t}_m = -[\dot{x}_{m-1}, \dot{y}_{m-1}]^{\mathrm{T}}$ holds, see Appendix A.1.

Case 2b) $\partial \mathbf{x}_m / \partial \mathbf{x}_{m+1}$ is the Jacobian matrix describing the transition from maneuver change time $\tilde{t}_m$ to the following maneuver change time $\tilde{t}_{m+1}$. It can be written as

$$\frac{\partial \mathbf{x}_m}{\partial \mathbf{x}_{m+1}} = \begin{bmatrix} \mathbf{I}_2 & \partial \mathbf{r}_m / \partial \mathbf{v} & \partial \mathbf{r}_m / \partial \tilde{\mathbf{t}} \\ \mathbf{0} & \mathbf{I}_{2M+2} & \mathbf{0} \\ \mathbf{0} & \mathbf{0} & \mathbf{I}_M \end{bmatrix} \tag{3.39}$$

with appropriately dimensioned zero block matrices where $\partial \mathbf{r}_m / \partial \mathbf{v}$ is denoted as

$$\frac{\partial \mathbf{r}_m}{\partial \mathbf{v}} = \begin{bmatrix} \mathbf{0} & \dots & \mathbf{0} & \underbrace{\dfrac{\partial \mathbf{r}_m}{\partial \dot{x}_m} \quad \dfrac{\partial \mathbf{r}_m}{\partial \dot{y}_m}}_{=(\tilde{t}_m - \tilde{t}_{m+1})\mathbf{I}_2} & \mathbf{0} & \dots & \mathbf{0} \end{bmatrix} \in \mathbb{R}^{2\times(2M+2)} \tag{3.40}$$

with $\mathbf{0} \in \mathbb{R}^{2\times 2}$. The Jacobian matrix $\partial \mathbf{r}_m / \partial \tilde{\mathbf{t}}$ is given by

$$\frac{\partial \mathbf{r}_m}{\partial \tilde{\mathbf{t}}} = \begin{bmatrix} \mathbf{0} & \dots & \mathbf{0} & \dfrac{\partial \mathbf{r}_m}{\partial \tilde{t}_m} & \dfrac{\partial \mathbf{r}_m}{\partial \tilde{t}_{m+1}} & \mathbf{0} & \dots & \mathbf{0} \end{bmatrix} \in \mathbb{R}^{2\times M}, \tag{3.41}$$

where $\mathbf{0} \in \mathbb{R}^{2\times 1}$. Here, $\partial \mathbf{r}_m / \partial \tilde{t}_m = -\partial \mathbf{r}_m / \partial \tilde{t}_{m+1} = [\dot{x}_m, \dot{y}_m]^{\mathrm{T}}$ holds.

Case 2c) Finally, $\partial \mathbf{x}_M / \partial \mathbf{x}_k$ is the Jacobian matrix describing the transition from the last maneuver change time $\tilde{t}_M$ to the reference time t_k. It is given by

$$\frac{\partial \mathbf{x}_M}{\partial \mathbf{x}_k} = \begin{bmatrix} \mathbf{I}_2 & \partial \mathbf{r}_M / \partial \mathbf{v} & \partial \mathbf{r}_M / \partial \tilde{\mathbf{t}} \\ \mathbf{0} & \mathbf{I}_{2M+2} & \mathbf{0} \\ \mathbf{0} & \mathbf{0} & \mathbf{I}_M \end{bmatrix} \tag{3.42}$$

with appropriately dimensioned zero block matrices. The Jacobian matrix $\partial \mathbf{r}_M / \partial \mathbf{v}$ is given by

$$\frac{\partial \mathbf{r}_M}{\partial \mathbf{v}} = \begin{bmatrix} \mathbf{0}_{2\times 2M} & \underbrace{\dfrac{\partial \mathbf{r}_M}{\partial \dot{x}_M} \quad \dfrac{\partial \mathbf{r}_M}{\partial \dot{y}_M}}_{=(\tilde{t}_M - t_k)\mathbf{I}_2} \end{bmatrix} \in \mathbb{R}^{2\times(2M+2)}. \tag{3.43}$$

Furthermore, for $\partial \mathbf{r}_M / \partial \tilde{\mathbf{t}}$ we have

$$\frac{\partial \mathbf{r}_M}{\partial \tilde{\mathbf{t}}} = \left[\mathbf{0}_{2\times 1} \ \dots \ \mathbf{0}_{2\times 1} \quad \frac{\partial \mathbf{r}_M}{\partial \tilde{t}_M} \right] \in \mathbb{R}^{2\times M} , \tag{3.44}$$

where $\partial \mathbf{r}_M / \partial \tilde{t}_M = [\dot{x}_M, \dot{y}_M]^{\mathrm{T}}$.

3.2.2 Piecewise Deterministic Curvilinear Motion

Here, we recall the target state for piecewise deterministic curvilinear motion (2.37) from Subsection 2.4.5 considering M maneuver change times:

$$\mathbf{x}_k = \left[x_k, y_k, v_k, \varphi_k, \mathbf{a}^{\mathrm{T}}, \tilde{\mathbf{t}}^{\mathrm{T}} \right]^{\mathrm{T}} \in \mathbb{R}^{(6+3M)\times 1} \tag{3.45}$$

with accelerations

$$\mathbf{a} = \left[a_{\mathrm{t},0}, a_{\mathrm{n},0}, \dots, a_{\mathrm{t},M}, a_{\mathrm{n},M} \right]^{\mathrm{T}} \tag{3.46}$$

and maneuver change times

$$\tilde{\mathbf{t}} = [\tilde{t}_1, \dots, \tilde{t}_M]^{\mathrm{T}} . \tag{3.47}$$

Analogous to the previous subsection, the Jacobian matrix $\partial \mathbf{x}_i / \partial \mathbf{x}_k$ has to be calculated with respect to several target maneuver change times in order to compute the CRLB. We define $\mathbf{y}_k$ as vector comprising the Cartesian position and polar velocity components of the curvilinear motion state $\mathbf{x}_k$

$$\mathbf{y}_k = [x_k, y_k, v_k, \varphi_k]^{\mathrm{T}} . \tag{3.48}$$

Since here, we also assume the reference time t_k to be the current time, the relative displacement of t_i and t_k regarding the maneuver changes make it necessary to distinguish between two different cases also here (cf. Subsection 3.2.1), see Fig. 3.3:

1) t_i and t_k are in the same maneuver segment, and
2) the segment containing t_i lies before the segment containing t_k.

For both cases, the $(6+3M)\times(6+3M)$ Jacobian matrix $\partial \mathbf{x}_i / \partial \mathbf{x}_k$ has the following form

$$\widetilde{\mathbf{\Phi}}(t_i, t_k) = \frac{\partial \mathbf{x}_i}{\partial \mathbf{x}_k} = \left[\begin{array}{c|c|c} \dfrac{\partial \mathbf{y}_i}{\partial \mathbf{y}_k} = \mathbf{I}_4 & \dfrac{\partial \mathbf{y}_i}{\partial \mathbf{a}} & \dfrac{\partial \mathbf{y}_i}{\partial \tilde{\mathbf{t}}} = \mathbf{0} \\ \hline \dfrac{\partial \mathbf{a}}{\partial \mathbf{y}_k} = \mathbf{0} & \dfrac{\partial \mathbf{a}}{\partial \mathbf{a}} = \mathbf{I}_{2M+2} & \dfrac{\partial \mathbf{a}}{\partial \tilde{\mathbf{t}}} = \mathbf{0} \\ \hline \dfrac{\partial \tilde{\mathbf{t}}}{\partial \mathbf{y}_k} = \mathbf{0} & \dfrac{\partial \tilde{\mathbf{t}}}{\partial \mathbf{a}} = \mathbf{0} & \dfrac{\partial \tilde{\mathbf{t}}}{\partial \tilde{\mathbf{t}}} = \mathbf{I}_M \end{array} \right] . \tag{3.49}$$

Case 1) If $\tilde{t}_M \leq t_i \leq t_k$, which means the measurement time t_i and the reference time t_k are in the same maneuver segment, no maneuver changes have to be considered. Thus,

$$\frac{\partial \mathbf{x}_i}{\partial \mathbf{x}_k} = \begin{bmatrix} \mathbf{I}_4 & \partial \mathbf{y}_i / \partial \mathbf{a} & \partial \mathbf{y}_i / \partial \tilde{\mathbf{t}} \\ \mathbf{0} & \mathbf{I}_{2M+2} & \mathbf{0} \\ \mathbf{0} & \mathbf{0} & \mathbf{I}_M \end{bmatrix} \tag{3.50}$$

with appropriately dimensioned zero block matrices. The partial derivative $\partial \mathbf{y}_i / \partial \mathbf{a}$ is obtained by

$$\frac{\partial \mathbf{y}_i}{\partial \mathbf{a}} = \begin{bmatrix} \mathbf{0}_{4\times 2M} & \dfrac{\partial \mathbf{y}_i}{\partial a_{\mathrm{t},M}} & \dfrac{\partial \mathbf{y}_i}{\partial a_{\mathrm{n},M}} \end{bmatrix} \in \mathbb{R}^{4\times(2M+2)}. \tag{3.51}$$

See Appendix A.2 for the partial derivatives $\partial \mathbf{y}_i / \partial \mathbf{y}_k$, $\partial \mathbf{y}_i / \partial a_{\mathrm{t},M}$, and $\partial \mathbf{y}_i / \partial a_{\mathrm{n},M}$. These derivations are calculated by replacing t with t_i, a_{t} with $a_{\mathrm{t},M}$, and a_{n} with $a_{\mathrm{n},M}$ in the equations given there.

For Case 2 we assume that $t_i \leq \tilde{t}_m \leq \tilde{t}_{m+1} \leq \tilde{t}_M \leq t_k$. Hence, we consider several maneuver changes, see Fig. 3.3. Analogously to Subsection 3.2.1 we have three qualitatively different classes of matrices recalling (3.35):

$$\frac{\partial \mathbf{x}_i}{\partial \mathbf{x}_k} = \underbrace{\frac{\partial \mathbf{x}_i}{\partial \mathbf{x}_m}}_{a)} \underbrace{\frac{\partial \mathbf{x}_m}{\partial \mathbf{x}_{m+1}} \cdots \frac{\partial \mathbf{x}_{M-1}}{\partial \mathbf{x}_M}}_{b)} \underbrace{\frac{\partial \mathbf{x}_M}{\partial \mathbf{x}_k}}_{c)}. \tag{3.52}$$

Case 2a) $\partial \mathbf{x}_i / \partial \mathbf{x}_m$ is the Jacobian matrix describing the transition from t_i to the first maneuver change time $\tilde{t}_m$. It has the same form as matrix (3.49) and is given by

$$\frac{\partial \mathbf{x}_i}{\partial \mathbf{x}_m} = \begin{bmatrix} \mathbf{I}_4 & \partial \mathbf{y}_i / \partial \mathbf{a} & \partial \mathbf{y}_i / \partial \tilde{\mathbf{t}} \\ \mathbf{0} & \mathbf{I}_{2M+2} & \mathbf{0} \\ \mathbf{0} & \mathbf{0} & \mathbf{I}_M \end{bmatrix} \tag{3.53}$$

with appropriately dimensioned zero block matrices. For the Jacobian matrix $\partial \mathbf{y}_i / \partial \mathbf{a}$ we have

$$\frac{\partial \mathbf{y}_i}{\partial \mathbf{a}} = \begin{bmatrix} \mathbf{0} \ \dots \ \mathbf{0} & \dfrac{\partial \mathbf{y}_i}{\partial a_{\mathrm{t},m-1}} & \dfrac{\partial \mathbf{y}_i}{\partial a_{\mathrm{n},m-1}} & \mathbf{0} \ \dots \ \mathbf{0} \end{bmatrix} \in \mathbb{R}^{4\times(2M+2)} \tag{3.54}$$

with $\mathbf{0} \in \mathbb{R}^{4\times 2}$. Furthermore, $\partial \mathbf{y}_i / \partial \tilde{\mathbf{t}}$ can be expressed as

$$\frac{\partial \mathbf{y}_i}{\partial \tilde{\mathbf{t}}} = \begin{bmatrix} \mathbf{0} \ \dots \ \mathbf{0} & \dfrac{\partial \mathbf{y}_i}{\partial \tilde{t}_m} & \mathbf{0} \ \dots \ \mathbf{0} \end{bmatrix} \in \mathbb{R}^{4\times M}, \tag{3.55}$$

where $\mathbf{0} \in \mathbb{R}^{4\times 1}$. The above partial derivatives are given in Appendix A.2. In order to perform these derivations, one has to replace $\mathbf{y}_k$ by $\mathbf{y}_m$, t_k by $\tilde{t}_m$, t by t_i, a_t by $a_{\mathrm{t},m-1}$, and a_n by $a_{\mathrm{n},m-1}$.

Case 2b) $\partial \mathbf{x}_m / \partial \mathbf{x}_{m+1}$ is the Jacobian matrix describing the transition from maneuver change time $\tilde{t}_m$ to the following maneuver change time $\tilde{t}_{m+1}$. It can be written as

$$\frac{\partial \mathbf{x}_m}{\partial \mathbf{x}_{m+1}} = \begin{bmatrix} \mathbf{I}_4 & \partial \mathbf{y}_m / \partial \mathbf{a} & \partial \mathbf{y}_m / \partial \tilde{\mathbf{t}} \\ \mathbf{0} & \mathbf{I}_{2M+2} & \mathbf{0} \\ \mathbf{0} & \mathbf{0} & \mathbf{I}_M \end{bmatrix} \tag{3.56}$$

with appropriately dimensioned zero block matrices. The partial derivative of $\partial \mathbf{y}_m / \partial \mathbf{a} \in \mathbb{R}^{4\times(2M+2)}$ is given by

$$\frac{\partial \mathbf{y}_m}{\partial \mathbf{a}} = \begin{bmatrix} \mathbf{0} & \dots & \mathbf{0} & \dfrac{\partial \mathbf{y}_m}{\partial a_{\mathrm{t},m}} & \dfrac{\partial \mathbf{y}_m}{\partial a_{\mathrm{n},m}} & \mathbf{0} & \dots & \mathbf{0} \end{bmatrix} \tag{3.57}$$

with $\mathbf{0} \in \mathbb{R}^{4\times 2}$. For $\partial \mathbf{y}_m / \partial \tilde{\mathbf{t}} \in \mathbb{R}^{4\times M}$ we have

$$\frac{\partial \mathbf{y}_m}{\partial \tilde{\mathbf{t}}} = \begin{bmatrix} \mathbf{0} & \dots & \mathbf{0} & \dfrac{\partial \mathbf{y}_m}{\partial \tilde{t}_m} & \dfrac{\partial \mathbf{y}_m}{\partial \tilde{t}_{m+1}} & \mathbf{0} & \dots & \mathbf{0} \end{bmatrix} \tag{3.58}$$

with $\mathbf{0} \in \mathbb{R}^{4\times 1}$. Also here, Appendix A.2 contains the above partial derivatives. The current replacement rules are: substitute $\mathbf{y}_k$ by $\mathbf{y}_{m+1}$, t_k by $\tilde{t}_{m+1}$, t by $\tilde{t}_m$, a_t by $a_{\mathrm{t},m}$, and a_n by $a_{\mathrm{n},m}$.

Case 2c) Finally, $\partial \mathbf{x}_M / \partial \mathbf{x}_k$ is the Jacobian matrix describing the transition from the last maneuver change time $\tilde{t}_M$ to the reference time t_k. It is given by

$$\frac{\partial \mathbf{x}_M}{\partial \mathbf{x}_k} = \begin{bmatrix} \mathbf{I}_4 & \partial \mathbf{y}_M / \partial \mathbf{a} & \partial \mathbf{y}_M / \partial \tilde{\mathbf{t}} \\ \mathbf{0} & \mathbf{I}_{2M+2} & \mathbf{0} \\ \mathbf{0} & \mathbf{0} & \mathbf{I}_M \end{bmatrix} \tag{3.59}$$

with appropriately dimensioned zero block matrices. Here, the partial derivative $\partial \mathbf{y}_M / \partial \mathbf{a}$ is denoted as

$$\frac{\partial \mathbf{y}_M}{\partial \mathbf{a}} = \begin{bmatrix} \mathbf{0}_{4\times 2M} & \dfrac{\partial \mathbf{y}_M}{\partial a_{\mathrm{t},M}} & \dfrac{\partial \mathbf{y}_M}{\partial a_{\mathrm{n},M}} \end{bmatrix} \in \mathbb{R}^{4\times(2M+2)}. \tag{3.60}$$

For $\partial \mathbf{y}_M / \partial \tilde{\mathbf{t}}$ we have

$$\frac{\partial \mathbf{y}_M}{\partial \tilde{\mathbf{t}}} = \begin{bmatrix} \mathbf{0}_{4\times 1} & \dots & \mathbf{0}_{4\times 1} & \dfrac{\partial \mathbf{y}_M}{\partial \tilde{t}_M} \end{bmatrix} \in \mathbb{R}^{4\times M} . \tag{3.61}$$

When performing the above partial derivatives using Appendix A.2, one has to substitute t by $\tilde{t}_M$, a_t by $a_{\mathrm{t},M}$, and a_n by $a_{\mathrm{n},M}$.

3.3 Incorporating Measurements into the CRLB

We recall the measurement functions for bearing (2.12) and bearing rate measurements (2.14),

$$\alpha(\mathbf{x}_k) = \arctan \frac{\Delta x_k}{\Delta y_k} \tag{3.62a}$$

$$\dot{\alpha}(\mathbf{x}_k) = \frac{\Delta \dot{x}_k \Delta y_k - \Delta \dot{y}_k \Delta x_k}{\Delta x_k^2 + \Delta y_k^2} , \tag{3.62b}$$

where Δ denotes the respective state component's difference from the target to the observer, and define a range measurement function as follows:

$$\rho(\mathbf{x}_k) = \sqrt{\Delta x_k^2 + \Delta y_k^2} . \tag{3.63}$$

Recapping the FIM equation (3.25)

$$\mathbf{J}_k = \sum_{j=0}^{k} \widetilde{\mathbf{\Phi}}(t_j, t_k)^\mathrm{T} \widetilde{\mathbf{H}}_j^\mathrm{T} \mathbf{R}_j^{-1} \widetilde{\mathbf{H}}_j \widetilde{\mathbf{\Phi}}(t_j, t_k) , \tag{3.64}$$

the measurement matrix $\widetilde{\mathbf{H}}_j$ (3.24) is given by the derivative of the measurement function $\mathbf{h}(\cdot)$ including all three measurement types with respect to $\mathbf{x}_j$:

$$\left[\frac{\partial \alpha(\mathbf{x}_j)}{\partial \mathbf{x}_j}, \frac{\partial \dot{\alpha}(\mathbf{x}_j)}{\partial \mathbf{x}_j}, \frac{\partial \rho(\mathbf{x}_j)}{\partial \mathbf{x}_j} \right]^\mathrm{T} , \tag{3.65}$$

where

$$\mathbf{h}(\mathbf{x}_j) = \left[\alpha(\mathbf{x}_j), \dot{\alpha}(\mathbf{x}_j), \rho(\mathbf{x}_j) \right]^\mathrm{T} . \tag{3.66}$$

Note that the partial derivatives of the measurement functions are outlined in Appendix A.3.

We further assume that the measurement errors are uncorrelated leading to a measurement covariance matrix $\mathbf{R} = \mathrm{diag}\left(\sigma_\alpha^2, \sigma_{\dot{\alpha}}^2, \sigma_\rho^2\right)$ with the individual measurement

variances on its diagonal. With this, the inverse covariance matrix is given by $\mathbf{R}^{-1} = \operatorname{diag}\left(\sigma_\alpha^{-2}, \sigma_{\dot\alpha}^{-2}, \sigma_\rho^{-2}\right)$. Due to the diagonal structure of $\mathbf{R}$, we can write

$$\widetilde{\mathbf{H}}_j^{\mathrm{T}} \mathbf{R}^{-1} \widetilde{\mathbf{H}}_j = \mathbf{D}_j^{\alpha} + \mathbf{D}_j^{\dot\alpha} + \mathbf{D}_j^{\rho} \tag{3.67}$$

with

$$\mathbf{D}_j^{\alpha} = \frac{1}{\sigma_\alpha^2} \left(\frac{\partial \alpha(\mathbf{x}_j)}{\partial \mathbf{x}_j} \right)^{\mathrm{T}} \frac{\partial \alpha(\mathbf{x}_j)}{\partial \mathbf{x}_j} \tag{3.68}$$

and $\mathbf{D}_j^{\dot\alpha}$ and $\mathbf{D}_j^{\rho}$ defined analogously.

Due to the sum in (3.67), the FIMs for the measurement types can be calculated independently and added up to an overall FIM. This also holds for arbitrary combinations of the measurement types leading to

$$\mathbf{J}_k = \begin{cases} \mathbf{J}_\alpha(\mathbf{x}_k) & \text{for bearings-only (BO)} \\ \mathbf{J}_\alpha(\mathbf{x}_k) + \mathbf{J}_{\dot\alpha}(\mathbf{x}_k) & \text{for bearing and bearing rate (B-BR)} \\ \mathbf{J}_\alpha(\mathbf{x}_k) + \mathbf{J}_\rho(\mathbf{x}_k) & \text{for bearing and range (BR)} \end{cases}, \tag{3.69}$$

which will be the three cases investigated in a simulation study in Section 6.1.

Finally, the resulting FIM incorporating the complex piecewise motion models as well as nonlinear bearing, bearing rate, and range measurements follows the following scheme according to (3.20) and (3.25)

$$\mathbf{J}_\psi(\mathbf{x}_k) = \frac{1}{\sigma_\psi^2} \sum_{j=1}^{k} \left(\frac{\partial \psi(\mathbf{x}_j)}{\partial \mathbf{x}_j} \frac{\partial \mathbf{x}_j}{\partial \mathbf{x}_k} \right)^{\mathrm{T}} \underbrace{\frac{\partial \psi(\mathbf{x}_j)}{\partial \mathbf{x}_j}}_{\text{see also Appendix A.3}} \underbrace{\frac{\partial \mathbf{x}_j}{\partial \mathbf{x}_k}}_{\text{see Section 3.2}} \tag{3.70}$$

for $\psi = \{\alpha, \dot\alpha, \rho\}$. Note that the applicability of the recursive FIM update formula (3.26) is not possible at this time, but remains an open question. This is since the state vector dimension increases with each maneuver change and thus the FIM dimension increases, too.

3.4 Summary of the Chapter

This chapter reflects the central theme of bearings-only tracking of maneuvering targets. A performance bound involving the piecewise motion models introduced in Chapter 2 is needed. For this reason, the Cramér-Rao lower bound (CRLB) which is the best achievable error performance that can be attained for any estimator has been derived, initially in a general manner. It has been mentioned and illustrated that an estimator

is called efficient if it attains the CRLB. Based on this, the CRLB has been derived in a rigorous manner for the piecewise motion models. The challenge has been the non-constant dimensionality of the state vector since it increases with the number of maneuver segments. The resulting formula for the CRLB (3.70) gives information about the maximum achievable performance of all segment velocities or accelerations as well as maneuver change times which is the main result of this chapter and a fundamental contribution of this thesis.

4 Observability in Heterogeneous Bearings-Only Tracking

This chapter introduces the concept of observability. It means that a state can be determined from measurements, see for example [Che99]. Especially for bearings-only tracking an analysis of observability is inevitable since angular measurements do not provide any range information. In this context, only if the measurements are provided spatially distributed by multiple dislocated sensor platforms or temporally distributed by a single, moving sensor platform, observability can be ensured. In Fig. 4.1, an illustration of the problem is given: If observer and target are both moving with constant velocity, an infinite number of compatible target trajectories is possible based on the given bearings-only measurements meaning the target is not observable. If the observer is performing a maneuver, only one target trajectory is possible which means the target is observable.

Nevertheless, when focussing on heterogeneous sensors, different signal propagation velocities can be exploited. For example, electronic and acoustic sensors can be used in conjunction to localize objects emitting electromagnetic waves and sound, see also the practical example in Section 1.4 and the results in Chapter 6. Thus, this chapter serves as the theoretical foundation for this example and is based on the own work [HK16], which has been inspired by [YNBS15]: They present a tracking method for heterogeneous bearings-only tracking, but no observability analysis.

Fundamental observability criteria are recapped in Section 4.1 for linear continuous-time systems as well as linear and nonlinear discrete-time systems. This section serves as educational introduction into observability in order to understand the following analysis. Nonlinear continuous-time systems are omitted, but can be studied for example in [KET73, BZ83]. Also the strong connection to the Cramér-Rao lower bound is pointed out, see also [Far99, Jau07] meaning that a non-invertible FIM is equivalent to non-observability which is very easy to see after having defined the observability Gramian.

In order to complete this chapter, these insights are applied in Section 4.2 for a heterogeneous passive sensor setup involving electromagnetic detection and acoustic bearing sensors. The observability is studied, even for the case that the signals are not emitted simultaneously. It is shown that observability can be established and target maneuvers are not necessary. Finally, a numerical analysis of the Cramér-Rao lower bound is performed to verify the results.

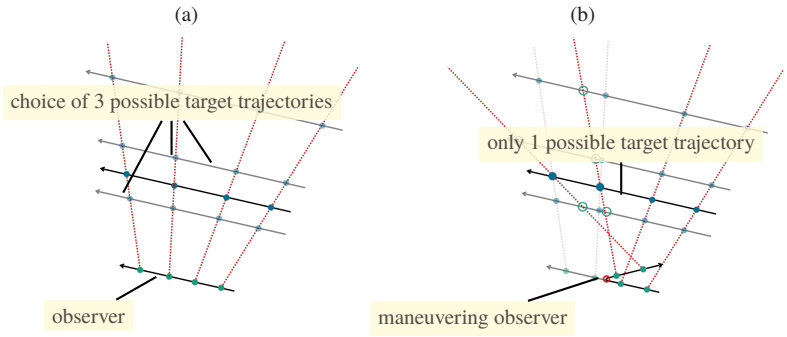

Figure 4.1: Observability for bearings-only tracking with moving observer and target. (a) No observability: If observer and target are both moving with constant velocity, an infinite number of compatible target trajectories is possible based on the given bearings-only measurements, three of them are depicted. (b) If the observer is performing a maneuver, only one target trajectory is possible.

4.1 Observability Criteria

In this section, we will recall the basics of several observability criteria in continuous-time as well as discrete-time systems which are strongly connected.

4.1.1 Linear Continuous-time Systems

Consider the noise-free, input-free, continuous-time linear system

$$\dot{\mathbf{x}}(t) = \mathbf{A}\mathbf{x}(t), \quad \mathbf{x}(t_0) = \mathbf{x}_0 \tag{4.1a}$$

$$\mathbf{z}(t) = \mathbf{H}(t)\mathbf{x}(t) \tag{4.1b}$$

with state $\mathbf{x}(t) \in \mathbb{R}^n$, measurement $\mathbf{z}(t) \in \mathbb{R}^p$, system matrix $\mathbf{A} \in \mathbb{R}^{n\times n}$, and measurement matrix $\mathbf{H}(t) \in \mathbb{R}^{p\times n}$. We call the system *observable* on $[t_0, t_1]$ if any initial state $\mathbf{x}(t_0) = \mathbf{x}_0$ can be uniquely determined from $\mathbf{z}(t)$ on $[t_0, t_1]$ [Che99]. The knowledge of $\mathbf{x}(t_0)$ is sufficient to determine $\mathbf{x}$ at any time t. Solving the differential equation (4.1a) yields

$$\mathbf{x}(t) = e^{\mathbf{A}(t-t_0)}\mathbf{x}(t_0) = \mathbf{\Phi}(t, t_0)\mathbf{x}(t_0)\,. \tag{4.2}$$

with state transition matrix $\mathbf{\Phi}(t, t_0)$, as defined in Chapter 2. Furthermore, define a matrix $\mathbf{M}(t) \in \mathbb{R}^{p\times n}$ as [Son96]

$$\mathbf{M}(t) = \mathbf{H}(t)\mathbf{\Phi}(t, t_0)\,. \tag{4.3}$$

Especially, a relation between $\mathbf{z}(t)$ and $\mathbf{x}(t_0)$ is then given by

$$\mathbf{z}(t) = \mathbf{M}(t)\mathbf{x}(t_0)\,. \tag{4.4}$$

Observability Gramian It can be proven [Che99, JP96] that system (4.1a)-(4.1b) is observable on $[t_0, t_1]$ if and only if the observability Gramian

$$\begin{aligned}\mathbf{B}(t_1, t_0) &= \int_{t_0}^{t_1} \mathbf{M}(t)^{\mathrm{T}}\mathbf{M}(t)\,\mathrm{d}t \\ &= \int_{t_0}^{t_1} \mathbf{\Phi}(t, t_0)^{\mathrm{T}}\mathbf{H}(t)^{\mathrm{T}}\mathbf{H}(t)\mathbf{\Phi}(t, t_0)\,\mathrm{d}t\end{aligned} \tag{4.5}$$

is positive definite for any $t_1 > t_0$. This equation is used by Becker [Bec93] as well as Jauffret and Pillon [JP96]. If $\mathbf{M}(t)$ is identified as matrix-valued function, the observability Gramian is formed by the inner product of functions over the domain $[t_0, t_1]$. In order that $\mathbf{B}(t_1, t_0)$ is positive definite, the following must hold:

$$\forall \boldsymbol{\xi} \neq \mathbf{0} : \; \boldsymbol{\xi}^{\mathrm{T}}\mathbf{B}(t_1, t_0)\boldsymbol{\xi} > 0\,. \tag{4.6}$$

In [JP96], an equivalent expression is formulated:

$$\forall \boldsymbol{\xi} \neq \mathbf{0} : \; \int_{t_0}^{t_1} ||\mathbf{M}(t)\boldsymbol{\xi}||^2\,\mathrm{d}t > 0\,. \tag{4.7}$$

To let this integral be greater than zero, it is sufficient that there is one $t \in [t_0, t_1]$ for which $\mathbf{M}(t)\boldsymbol{\xi}$ is non-zero (for all $\boldsymbol{\xi} \neq \mathbf{0}$). This leads directly to the following Theorem [Bec93, JP96]:

Theorem 1 *System* (4.1a)-(4.1b) *is observable on* $[t_0, t_1]$ *if and only if for any n-dimensional vector* $\boldsymbol{\xi} \neq \mathbf{0}$*, there exists some* $t \in [t_0, t_1]$ *such that*

$$\mathbf{M}(t)\boldsymbol{\xi} \neq \mathbf{0}\,. \tag{4.8}$$

Note that Theorem 1 makes a statement on observability on the complete interval $[t_0, t_1]$. If observability is established at time t_m with $t_0 < t_\mathrm{m} < t_1$, e.g. by an observer maneuver, this criterion is not suitable: It would result in non-observability which is correct considering the complete interval $[t_0, t_1]$.

An equivalent formulation of the theorem is its contrapose [JP96]:

Theorem 2 *System* (4.1a)-(4.1b) *is observable on* $[t_0, t_1]$ *if and only if the following statement holds:*

$$\{\forall t \in [t_0, t_1] : \mathbf{M}(t)\boldsymbol{\xi} = \mathbf{0},\ \boldsymbol{\xi} = const.\} \Rightarrow \{\boldsymbol{\xi} = \mathbf{0}\} \tag{4.9}$$

Note that $\boldsymbol{\xi}$ must be constant for any t, i.e. it must not depend on t. In other words, Theorem 2 means that the system is observable if and only if the columns in $\mathbf{M}(\cdot)$ are linearly independent over $[t_0, t_1]$ [Kai80]. If only stationary targets are considered, $\boldsymbol{\Phi}(t, t_0) = \mathbf{I}_n$ Thus, $\boldsymbol{\Phi}$ can, as well as the time t, be omitted in above theorems.

Observability Matrix Consider a time-invariant system, i.e. $\mathbf{H}(t) = \mathbf{H} = \text{const.}$ in (4.1b). Then, an alternative approach to observability is the following: Remember that we want to uniquely determine $\mathbf{x}(t_0)$ from all the measurements $\mathbf{z}(t)$ on $[t_0, t_1]$. For continuous-time systems, we can apply a technique which involves repeatedly taking the derivatives of the measurement equation (4.1b), which corresponds to a time shift in the discrete-time domain (see Subsection 4.1.2):

$$\begin{aligned}
\mathbf{z}(t_0) &= \mathbf{H}\mathbf{x}(t_0) \\
\dot{\mathbf{z}}(t_0) &= \mathbf{H}\dot{\mathbf{x}}(t_0) = \mathbf{H}\mathbf{A}\mathbf{x}(t_0) \\
\ddot{\mathbf{z}}(t_0) &= \mathbf{H}\ddot{\mathbf{x}}(t_0) = \mathbf{H}\mathbf{A}^2\mathbf{x}(t_0) \\
&\vdots \\
\mathbf{z}^{(n-1)}(t_0) &= \mathbf{H}\mathbf{x}^{(n-1)}(t_0) = \mathbf{H}\mathbf{A}^{n-1}\mathbf{x}(t_0)
\end{aligned} \quad . \tag{4.10}$$

The aforementioned equations can be transformed to matrix form as

$$\mathcal{Z}(t_0) = O_n \mathbf{x}(t_0) \tag{4.11}$$

with

$$\mathcal{Z}(t) = \begin{bmatrix} \mathbf{z}(t) \\ \dot{\mathbf{z}}(t) \\ \ddot{\mathbf{z}}(t) \\ \vdots \\ \mathbf{z}^{(n-1)}(t) \end{bmatrix} \text{ and } O_n = \begin{bmatrix} \mathbf{H} \\ \mathbf{H}\mathbf{A} \\ \mathbf{H}\mathbf{A}^2 \\ \vdots \\ \mathbf{H}\mathbf{A}^{n-1} \end{bmatrix} . \tag{4.12}$$

Here, $O_n \in \mathbb{R}^{(np)\times n}$ is called *continuous-time observability matrix* . Since

$$\mathbf{x}(t_0) = \left(O_n^{\mathrm{T}} O_n\right)^{-1} O_n^{\mathrm{T}} \mathcal{Z}(t_0)\,, \tag{4.13}$$

we conclude that $\mathbf{x}(t_0)$ can be uniquely determined from measurements $\mathbf{z}(t_0)$ if and only if $O_n^{\mathrm{T}} O_n$ has full rank, i.e. $\operatorname{rank} O_n = n$. This statement is equivalent to Theorem 1 [Che99] using the observability Gramian. The smallest number ν that satisfies $\operatorname{rank} O_\nu = \operatorname{rank} O_{\nu+1}$ is called *observability index* [Che99].

4.1.2 Linear Discrete-time Systems

In contrast to the previous subsection, consider now the following discrete-time, noise-free, input-free linear system:

$$\mathbf{x}(t_k) = \mathbf{x}_k = \mathbf{\Phi}(t_k, t_{k-1})\mathbf{x}_{k-1} \tag{4.14a}$$

$$\mathbf{z}(t_k) = \mathbf{z}_k = \mathbf{H}(t_k)\mathbf{x}_k \tag{4.14b}$$

with $\mathbf{x}_k \in \mathbb{R}^n$, $\mathbf{z}_k \in \mathbb{R}^p$, $\mathbf{\Phi} \in \mathbb{R}^{n\times n}$, and $\mathbf{H} \in \mathbb{R}^{p\times n}$. Based on Brogan [Bro74], Le Cadre and Jauffret [LCJ97] use this discrete-time formulation for their observability analysis of a bearings-only TMA setting, whereas Goshen-Meskin and Bar-Itzhack [GMBI92] use it more generally to point out the connection between observability and estimability.

Observability Matrix Following [Che99, LCJ97, GMBI92] we can, analogous to Subsection 4.1.1, formulate an equation:

$$\mathbf{Z}_k = O_k \mathbf{x}_0 \tag{4.15}$$

with $\mathbf{Z}_k^{\mathrm{T}} = \left[\mathbf{z}_0^{\mathrm{T}}, \ldots, \mathbf{z}_k^{\mathrm{T}}\right]$ and the $(k+1)p \times n$-dimensional discrete-time observability matrix

$$O_k = \begin{bmatrix} \mathbf{M}(t_0) \\ \mathbf{M}(t_1) \\ \vdots \\ \mathbf{M}(t_k) \end{bmatrix} = \begin{bmatrix} \mathbf{H}(t_0) \\ \mathbf{H}(t_1)\mathbf{\Phi}(t_1, t_0) \\ \vdots \\ \mathbf{H}(t_k)\mathbf{\Phi}(t_k, t_0) \end{bmatrix}, \tag{4.16}$$

which corresponds to stacking matrices $\mathbf{M}(\cdot)$ (4.3) evaluated at discrete time scans. The difference to the procedure in Subsection 4.1.1 is that we perform time shifts here which correspond to the repeated differentiation in the continuous-time domain. Also here, $\mathbf{x}_0$ can be uniquely determined from $\mathbf{Z}_k$ if and only if $\operatorname{rank} O_k = n$, where n is the state dimension and $k \geq n$. In this case, the aforementioned discrete-time linear system is observable. The observability index is defined exactly as in Subsection 4.1.1, i.e. it is the smallest number ν for which $\operatorname{rank} O_\nu = \operatorname{rank} O_{\nu+1}$. In other words, it answers the question how many measurements are at least needed to ensure observability.

Observability Gramian Also for the discrete-time case, an observability Gramian can be found [GMBI92, Che99] given by

$$\begin{aligned}\mathbf{B}_k &= \sum_{j=0}^{k} \mathbf{M}(t_j)^{\mathrm{T}}\mathbf{M}(t_j) \\ &= \sum_{j=0}^{k} \mathbf{\Phi}(t_j,t_0)^{\mathrm{T}}\mathbf{H}(t_j)^{\mathrm{T}}\mathbf{H}(t_j)\mathbf{\Phi}(t_j,t_0)\,,\end{aligned} \tag{4.17}$$

which obviously is the discretized version of (4.5). Further examination reveals that the Gramian can be constructed from the discrete-time observability matrix as standard matrix inner product by

$$\mathbf{B}_k = O_k^{\mathrm{T}} O_k\,, \tag{4.18}$$

cf. to functional inner product (4.5).

Connection to the Cramér-Rao Lower Bound To elucidate the connection to the CRLB, consider the linear measurement equation (4.14b) and substitute the following noisy measurement equation

$$\mathbf{z}_k^* = \mathbf{H}(t_k)\mathbf{x}_k + \mathbf{v}_k\,. \tag{4.19}$$

Here, $\mathbf{v}_k$ is white measurement noise which is assumed to be Gaussian distributed with zero mean and covariance matrix $\mathbf{R}_k$. According to the derivations in Chapter 3, the FIM at time t_0 based on the information up to time t_k, denoted by $\mathbf{J}_{0|k}$, is given by

$$\mathbf{J}_{0|k} = \sum_{j=0}^{k} \mathbf{\Phi}(t_j,t_0)^{\mathrm{T}}\mathbf{H}(t_j)^{\mathrm{T}}\mathbf{R}_j^{-1}\mathbf{H}(t_j)\mathbf{\Phi}(t_j,t_0)\,. \tag{4.20}$$

Comparing (4.20) to (4.5), we can recognize that the FIM equals the observability Gramian besides the measurement noise covariance $\mathbf{R}_k$. One can easily prove that if $\mathbf{B}_k$ is positive definite, then $\mathbf{J}_{0|k}$ is also positive definite and vice versa. Thus, the CRLB can be used for an observability analysis. However, the noise-free FIM a.k.a. observability Gramian is preferable since no noise has to be considered. A formal proof of the link between FIM invertibility and observability is presented by Jauffret [Jau07].

4.1.3 Nonlinear Discrete-time systems

Now consider the discrete-time, noise-free, input-free nonlinear system:

$$\begin{aligned}\mathbf{x}_k &= \mathbf{f}(\mathbf{x}_{k-1}) \\ \mathbf{z}_k &= \mathbf{h}(\mathbf{x}_k)\end{aligned} \tag{4.21}$$

with state $\mathbf{x}_k \in \mathbb{R}^n$, measurement $\mathbf{z}_k \in \mathbb{R}^p$, state transition function $\mathbf{f} : \mathbb{R}^n \to \mathbb{R}^n$, and measurement function $\mathbf{h} : \mathbb{R}^n \to \mathbb{R}^p$.

Observability matrix Similar to the linear observability matrix (4.16), we define an observability map $\mathcal{H}_k : \mathbb{R}^n \to \mathbb{R}^{p(k+1)}$ as

$$\mathcal{H}_k(\mathbf{x}) = \begin{bmatrix} \mathbf{h}(\mathbf{x}) \\ \mathbf{h}(\mathbf{f}(\mathbf{x})) \\ \mathbf{h}(\mathbf{f}(\mathbf{f}(\mathbf{x}))) \\ \vdots \\ \mathbf{h}(\mathbf{f}^k(\mathbf{x})) \end{bmatrix}, \tag{4.22}$$

so that $\mathbf{Z}_k = \mathcal{H}_k(\mathbf{x}_0)$. We can then say that system (4.21) satisfies the observability rank condition at $\mathbf{x}_0$ if the rank of map $\mathcal{H}_k$ equals n [Son84, SG92]. Since the rank of a nonlinear mapping at $\mathbf{x}_0$ is defined as the rank of its Jacobian at $\mathbf{x}_0$, we form the derivative of $\mathcal{H}_k$ by applying the chain rule,

$$\frac{\partial \mathcal{H}_k}{\partial \mathbf{x}}(\mathbf{x}_0) = \begin{bmatrix} \frac{\partial \mathbf{h}}{\partial \mathbf{x}}(\mathbf{x}_0) \\ \frac{\partial \mathbf{h}}{\partial \mathbf{x}}(\mathbf{x}_1)\frac{\partial \mathbf{f}}{\partial \mathbf{x}}(\mathbf{x}_0) \\ \vdots \\ \frac{\partial \mathbf{h}}{\partial \mathbf{x}}(\mathbf{x}_k)\frac{\partial \mathbf{f}}{\partial \mathbf{x}}(\mathbf{x}_{k-1}) \cdots \frac{\partial \mathbf{f}}{\partial \mathbf{x}}(\mathbf{x}_0) \end{bmatrix}. \tag{4.23}$$

Furthermore, (4.23) can also be expressed by

$$\widetilde{O}_k = \frac{\partial \mathcal{H}_k}{\partial \mathbf{x}}(\mathbf{x}_0) = \begin{bmatrix} \widetilde{\mathbf{H}}(t_0) \\ \widetilde{\mathbf{H}}(t_1)\widetilde{\mathbf{\Phi}}(t_1, t_0) \\ \vdots \\ \widetilde{\mathbf{H}}(t_k)\widetilde{\mathbf{\Phi}}(t_k, t_0) \end{bmatrix}, \tag{4.24}$$

where

$$\widetilde{\mathbf{H}}(t_i) = \frac{\partial \mathbf{h}}{\partial \mathbf{x}}(\mathbf{x}_i) \tag{4.25}$$

and

$$\widetilde{\mathbf{\Phi}}(t_j, t_i) = \prod_{\ell=i}^{j-1} \frac{\partial \mathbf{f}}{\partial \mathbf{x}}(\mathbf{x}_\ell) \tag{4.26}$$

with $i, j = 0, \ldots, k$. Thus, $\widetilde{O}_k$ is the linearized equivalent to the linear observability matrix (4.16), see also [Fit72], and is denoted as nonlinear observability matrix. System (4.21) satisfies the observability rank condition at $\mathbf{x}_0$ if rank $\widetilde{O}_k = n$.

Observability Gramian Analoguous to the linear case, an observability Gramian can be found by

$$\begin{aligned}\widetilde{\mathbf{B}}_k &= \widetilde{O}_k^{\mathrm{T}} \widetilde{O}_k \\ &= \sum_{j=0}^{k} \widetilde{\mathbf{\Phi}}(t_j, t_0)^{\mathrm{T}} \widetilde{\mathbf{H}}(t_j)^{\mathrm{T}} \widetilde{\mathbf{H}}(t_j) \widetilde{\mathbf{\Phi}}(t_j, t_0)\,.\end{aligned} \tag{4.27}$$

Local Observability

In contrast to the linear case, satisfying the observability rank condition does not necessarily imply observability [HK77] meaning $\mathbf{h}$ is a one to one mapping from $\mathbb{R}^n$ to $\mathbf{h}(\mathbb{R}^n)$. Fitts [Fit72] presents some conditions on $\mathcal{H}_k$ for which fulfilling the observability rank condition and observability are equivalent. However, checking for these conditions seems to be cumbersome. Hence, we stick to the local observability approach used by Hermann and Krener [HK77] as well as Nijmeijer [Nij82]. First, we have to introduce the term indistinguishability as follows: A pair of points $\mathbf{x}$ and $\bar{\mathbf{x}}$ is said to be indistinguishable if they realize the same output, i.e. $\mathbf{h}(\mathbf{f}^k(\mathbf{x})) = \mathbf{h}(\mathbf{f}^k(\bar{\mathbf{x}}))$ for all $k \in \mathbb{N}_0$ [Nij82]. Let $I(\mathbf{x})$ be the set of indistinguishable points of $\mathbf{x}$. Then, a system is observable at $\mathbf{x}$ if $I(\mathbf{x}) = \{\mathbf{x}\}$ and it is observable if $I(\mathbf{x}) = \{\mathbf{x}\}$ for all $\mathbf{x} \in \mathbb{R}^n$. That means, a system is observable if for any point, the only indistinguishable point is the point itself.

We define a system to be locally observable at $\mathbf{x}$ if there exists a neighborhood U of $\mathbf{x}$ such that for any $\bar{\mathbf{x}} \in U$, $\mathbf{h}(\mathbf{f}^k(\mathbf{x})) = \mathbf{h}(\mathbf{f}^k(\bar{\mathbf{x}}))$ for $k = 0, \ldots, n$ implies $\mathbf{x} = \bar{\mathbf{x}}$. The system is locally observable if the aforementioned condition holds for each $\mathbf{x} \in \mathbb{R}^n$ [Nij82][1]. Intuitively, local observability means that one can instantaneously distinguish each point from its neighbor. The advantage of local observability is that it leads to a simple algebraic test which is the main statement of this subsection: If system (4.21) satisfies the observability rank condition, i.e. rank $\widetilde{O}_k = n$, then the system is locally observable [Nij82].

Further insights on local (and global) observability for nonlinear systems are also given in [DM85, BM88]. An analysis of the extended Kalman filter (EKF) as a state observer (which is the noise-free version of a filter) for non-linear systems is performed in [SG92, RGYU99, SS85]. These papers reveal further properties of nonlinear observability and also a strong connection to the EKF, cf. with the connection of CRLB and EKF in Chapter 3.

[1] Note that the terms are not unique: Nijmeijer [Nij82] defines this as strongly locally observable, whereas Hermann and Krener [HK77] use the term locally weakly observable. To keep things simple, we will stick to locally observable here.

Connection to the Cramér-Rao Lower Bound Altering the nonlinear measurement equation from (4.21) with a white noise term $\mathbf{v}_k$ which is Gaussian distributed, has zero mean and covariance matrix $\mathbf{R}_k$, i.e.

$$\mathbf{z}_k^* = \mathbf{h}(\mathbf{x}_k) + \mathbf{v}_k \,, \tag{4.28}$$

and using the definition of the FIM (3.18), leads to a FIM for time t_0 based on the information up to time t_k as follows:

$$\mathbf{J}_{0|k} = \sum_{j=0}^{k} \widetilde{\mathbf{\Phi}}(t_j, t_0)^{\mathrm{T}} \widetilde{\mathbf{H}}(t_j)^{\mathrm{T}} \mathbf{R}_j^{-1} \widetilde{\mathbf{H}}(t_j) \widetilde{\mathbf{\Phi}}(t_j, t_0) \,, \tag{4.29}$$

which is structurally equivalent to the FIM for the linear case (4.20). Here, $\widetilde{\mathbf{H}}$ and $\widetilde{\mathbf{\Phi}}$ are the partial derivatives of $\mathbf{h}$ and $\mathbf{f}$, respectively, as given in (4.25) and (4.26). Analogous to the linear case, the observability Gramian (4.27) is the noise-free variant of the FIM[2].

4.2 Observability Analysis Exploiting Different Signal Propagation Velocities

The previous section 4.1 has provided a toolbox of observability criteria for linear and nonlinear discrete-time problems. This section deals with applying these approaches to practical scenarios involving acoustic bearing and electromagnetic detection sensors so that different signal propagation velocities are exploited. We consider two cases: First, the electromagnetic and the acoustic signal are emitted simultaneously and secondly, there is a certain time, denoted as *emission delay*, between the emission of the electromagnetic and the acoustic signal.

4.2.1 Acoustic and Electromagnetic Signal Emitted Simultaneously

Assume a stationary observer with an acoustic bearing and an electromagnetic detection sensor at coordinates $[x^{\mathrm{o}}, y^{\mathrm{o}}]$, see Fig. 4.2 for an illustration. Furthermore, the target moves with constant speed along a deterministic trajectory $\mathbf{x}_k = [x(t_k), y(t_k), \dot{x}, \dot{y}]^{\mathrm{T}}$ with CV state transition matrix (cf. (2.19))

$$\mathbf{\Phi}(t_k, t_{k-1}) = \begin{bmatrix} \mathbf{I}_2 & (t_k - t_{k-1})\mathbf{I}_2 \\ \mathbf{0}_2 & \mathbf{I}_2 \end{bmatrix} . \tag{4.30}$$

[2] Also note the structural equivalence of the FIM to the covariance update step of the extended Kalman filter (EKF) [RAG04] and the connection between EKF and nonlinear local observability pointed out by Song and Grizzle [SG92].

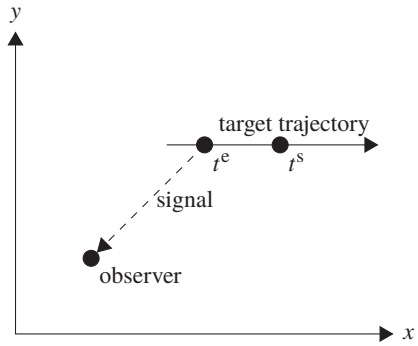

Figure 4.2: Schematic scenario for the case acoustic and electromagnetic signal emitted simultaneously: An acoustic and an electromagnetic signal are emitted from the moving target at time t^e. The electromagnetic signal is received by the stationary observer at time t^e and the acoustic signal at time t^s, © 2016 IEEE.

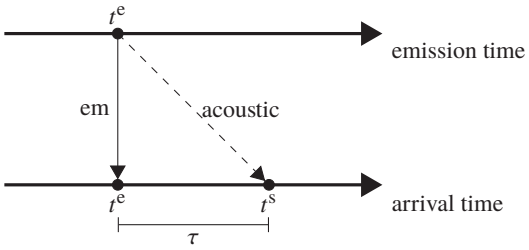

Figure 4.3: Time line illustration for the case acoustic and electromagnetic signal emitted simultaneously: An acoustic and an electromagnetic (em) signal are emitted from the moving target at time t^e. The electromagnetic signal is received by the stationary observer at time t^e and the acoustic signal at time t^s, © 2016 IEEE.

At time t^e the target emits an acoustic and an electromagnetic signal which is received at the observer at times t^s and t^e, respectively. This is depicted in Fig. 4.3. We ignore the electromagnetic signal speed (see also [YNBS15]) which is the speed of light, so that emission time of the electromagnetic signal equals its arrival time. On the other hand, the acoustic signal speed must be considered: It is denoted by c. Without loss of generality, we assume that $[x^o, y^o] = [0, 0]$ in order to simplify calculations.

Since the target has constant speed,

$$\begin{bmatrix} x(t_k) \\ y(t_k) \end{bmatrix} = \begin{bmatrix} x_0 \\ y_0 \end{bmatrix} + \begin{bmatrix} \dot{x} \\ \dot{y} \end{bmatrix} t_k \tag{4.31}$$

holds with $x_0 = x(t_0)$ and $y_0 = y(t_0)$. Therefore, it is sufficient to estimate the target state vector $\mathbf{x}_0 = [x_0, y_0, \dot{x}, \dot{y}]^{\mathrm{T}}$. A measurement batch $\mathbf{z}_k = [\alpha(t_k), \tau(t_k)]^{\mathrm{T}}$ consists of an acoustic bearing $\alpha(t_k)$ and a time difference of arrival (TDoA) measurement $\tau(t_k)$ between the arrival times of the electromagnetic and the acoustic signal:

The acoustic bearing at time t^{s} is given by

$$\alpha(t^{\mathrm{s}}) = \arctan \frac{x(t^{\mathrm{e}}) - x^{\mathrm{o}}(t^{\mathrm{s}})}{y(t^{\mathrm{e}}) - y^{\mathrm{o}}(t^{\mathrm{s}})}, \tag{4.32}$$

which simplifies to

$$\alpha(t^{\mathrm{s}}) = \arctan \frac{x(t^{\mathrm{e}})}{y(t^{\mathrm{e}})} \tag{4.33}$$

due to the assumption of a stationary observer at $[0, 0]$.

The time difference between acoustic signal emission time t^{e} and its arrival time t^{s}, which is also the measurement equation for the TDoA measurements, is given by

$$\tau(t^{\mathrm{s}}) = t^{\mathrm{s}} - t^{\mathrm{e}} = \frac{r(t^{\mathrm{e}})}{c} \tag{4.34}$$

with $r(t^{\mathrm{e}})$ denoting the distance between observer and target at time t^{e}, i.e.

$$r(t^{\mathrm{e}}) = \sqrt{x(t^{\mathrm{e}})^2 + y(t^{\mathrm{e}})^2} = \sqrt{(x_0 + \dot{x}t^{\mathrm{e}})^2 + (y_0 + \dot{y}t^{\mathrm{e}})^2}\,. \tag{4.35}$$

In terms of the acoustic signal arrival time t^{s}, we have

$$\begin{bmatrix} x(t^{\mathrm{e}}) \\ y(t^{\mathrm{e}}) \end{bmatrix} = \begin{bmatrix} x_0 \\ y_0 \end{bmatrix} + \begin{bmatrix} \dot{x} \\ \dot{y} \end{bmatrix} t^{\mathrm{s}} - \begin{bmatrix} \dot{x} \\ \dot{y} \end{bmatrix} \frac{r(t^{\mathrm{e}})}{c}\,. \tag{4.36}$$

In order to form the nonlinear observability matrix according to (4.24), we have to calculate the partial derivatives of α with respect to $\mathbf{x}_0$ leading to

$$\frac{\partial \alpha}{\partial \mathbf{x}_0} = \left[\frac{\partial \alpha}{\partial x_0}, \frac{\partial \alpha}{\partial y_0}, \frac{\partial \alpha}{\partial \dot{x}}, \frac{\partial \alpha}{\partial \dot{y}} \right], \tag{4.37}$$

where

$$\begin{aligned} \frac{\partial \alpha}{\partial x_0}(t^{\mathrm{e}}) &= \frac{y(t^{\mathrm{e}})}{r(t^{\mathrm{e}})^2} & \frac{\partial \alpha}{\partial y_0}(t^{\mathrm{e}}) &= -\frac{x(t^{\mathrm{e}})}{r(t^{\mathrm{e}})^2} \\ \frac{\partial \alpha}{\partial \dot{x}}(t^{\mathrm{e}}) &= \frac{y(t^{\mathrm{e}})t^{\mathrm{e}}}{r(t^{\mathrm{e}})^2} & \frac{\partial \alpha}{\partial \dot{y}}(t^{\mathrm{e}}) &= -\frac{x(t^{\mathrm{e}})t^{\mathrm{e}}}{r(t^{\mathrm{e}})^2} \end{aligned} . \tag{4.38}$$

with

The partial derivatives of the TDoA measurement equation (4.34) are expressed via the partial derivatives of r since τ is proportional to r yielding

$$\frac{\partial \tau}{\partial \mathbf{x}_0} = \frac{1}{c}\left[\frac{\partial r}{\partial x_0}, \frac{\partial r}{\partial y_0}, \frac{\partial r}{\partial \dot{x}}, \frac{\partial r}{\partial \dot{y}}\right], \tag{4.39}$$

where

$$\begin{aligned} \frac{\partial r}{\partial x_0}(t^{\mathrm{e}}) &= \frac{x(t^{\mathrm{e}})}{r(t^{\mathrm{e}})} & \frac{\partial r}{\partial y_0}(t^{\mathrm{e}}) &= \frac{y(t^{\mathrm{e}})}{r(t^{\mathrm{e}})} \\ \frac{\partial r}{\partial \dot{x}}(t^{\mathrm{e}}) &= \frac{x(t^{\mathrm{e}})t^{\mathrm{e}}}{r(t^{\mathrm{e}})} & \frac{\partial r}{\partial \dot{y}}(t^{\mathrm{e}}) &= \frac{y(t^{\mathrm{e}})t^{\mathrm{e}}}{r(t^{\mathrm{e}})} \end{aligned} . \tag{4.40}$$

Assume two signal emissions at times t_0^{e} and t_1^{e} and thus two measurement batches, $[\alpha(t_0^{\mathrm{e}}), \tau(t_0^{\mathrm{e}})]$ and $[\alpha(t_1^{\mathrm{e}}), \tau(t_1^{\mathrm{e}})]$. We then create the following observability matrix:

$$\widetilde{O}_1 = \begin{bmatrix} \widetilde{\mathbf{H}}(t_0^{\mathrm{e}}) \\ \widetilde{\mathbf{H}}(t_1^{\mathrm{e}})\widetilde{\mathbf{\Phi}}(t_1^{\mathrm{e}}, t_0^{\mathrm{e}}) \end{bmatrix} \tag{4.41}$$

with

$$\widetilde{\mathbf{H}} = \begin{bmatrix} \partial \alpha / \partial \mathbf{x}_0 \\ \partial \tau / \partial \mathbf{x}_0 \end{bmatrix} \in \mathbb{R}^{2\times 4} . \tag{4.42}$$

With this, the observability matrix can also be expressed as

$$\widetilde{O}_1 = \begin{bmatrix} \frac{\partial \alpha_0}{\partial x_0} & \frac{\partial \alpha_0}{\partial y_0} & \frac{\partial \alpha_0}{\partial \dot{x}} & \frac{\partial \alpha_0}{\partial \dot{y}} \\ \frac{\partial \tau_0}{\partial x_0} & \frac{\partial \tau_0}{\partial y_0} & \frac{\partial \tau_0}{\partial \dot{x}} & \frac{\partial \tau_0}{\partial \dot{y}} \\ \frac{\partial \alpha_1}{\partial x_0} & \frac{\partial \alpha_1}{\partial y_0} & \frac{\partial \alpha_1}{\partial x_0}\Delta t + \frac{\partial \alpha_1}{\partial \dot{x}} & \frac{\partial \alpha_1}{\partial y_0}\Delta t + \frac{\partial \alpha_1}{\partial \dot{y}} \\ \frac{\partial \tau_1}{\partial x_0} & \frac{\partial \tau_1}{\partial y_0} & \frac{\partial \tau_1}{\partial x_0}\Delta t + \frac{\partial \tau_1}{\partial \dot{x}} & \frac{\partial \tau_1}{\partial y_0}\Delta t + \frac{\partial \tau_1}{\partial \dot{y}} \end{bmatrix}, \tag{4.43}$$

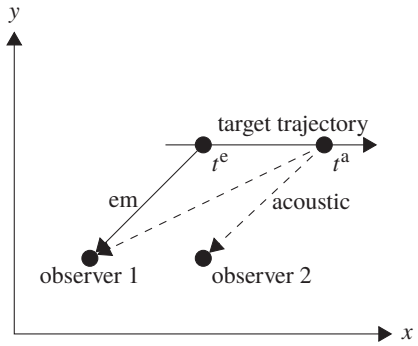

Figure 4.4: Schematic scenario for the case acoustic and electromagnetic signal emitted with emission delay: An electromagnetic signal (em) is emitted from the moving target at time t^{e} and an acoustic signal at time t^{a}. Observer 1 carries an electromagnetic detection sensor as well as an acoustic bearing sensor, whereas observer 2 only has an acoustic bearing sensor, © 2016 IEEE.

where $\alpha_j = \alpha(t_j^{\mathrm{e}})$, $\tau_j = \tau(t_j^{\mathrm{e}})\,(j = 0, 1)$, and $\Delta t = t_1^{\mathrm{e}} - t_0^{\mathrm{e}}$. Using (4.38) and (4.40), we can identify $\widetilde{O}_1$ as matrix made up of the following four 2×2 submatrices:

$$\widetilde{O}_1 = \begin{bmatrix} \mathbf{A}_0 & \mathbf{A}_0 t_0^{\mathrm{e}} \\ \mathbf{A}_1 & \mathbf{A}_1 \Delta t + \mathbf{A}_1 t_1^{\mathrm{e}} \end{bmatrix}. \tag{4.44}$$

Since the lower left and lower right block of $\widetilde{O}_1$ commute, the determinant is given by

$$\det \widetilde{O}_1 = \det \left[\mathbf{A}_0 \left(\mathbf{A}_1 \Delta t + \mathbf{A}_1 t_1^{\mathrm{e}} \right) - \mathbf{A}_0 t_0^{\mathrm{e}} \mathbf{A}_1 \right] = 4\Delta t^2 \det(\mathbf{A}_0) \det(\mathbf{A}_1) \tag{4.45}$$

The target state $\mathbf{x}_0$ is locally observable given two measurement batches iff $\widetilde{O}_1$ has full rank 4, i.e. its determinant is non-zero. This is the case iff $t_1^{\mathrm{e}} \neq t_0^{\mathrm{e}}$ and $\det \mathbf{A}_j = \frac{1}{cr(t_j^{\mathrm{e}})} \neq 0\,(j = 0, 1)$, which is always the case.

4.2.2 Acoustic and Electromagnetic Signal Emitted with Emission Delay

Now, assume two stationary observers at positions $[x^{\mathrm{o}}, y^{\mathrm{o}}] = [0, 0]$ and $[x^{\mathrm{s}}, y^{\mathrm{s}}]$, respectively. The first observer carries an acoustic bearing as well as an electromagnetic detection sensor. Furthermore, the second observer is only equipped with a acoustic bearing sensor. As in Subsection 4.2.1, the target travels with constant speed along a

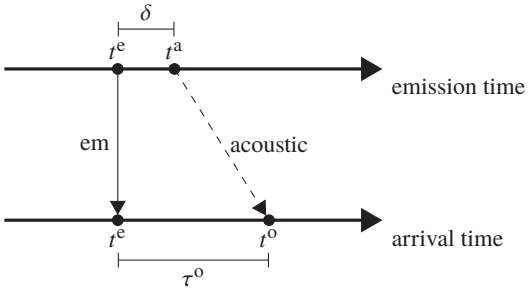

Figure 4.5: Time line illustration for the case acoustic and electromagnetic signal emitted with emission delay at observer 1: An electromagnetic signal (em) is emitted from the moving target at time t^{e} and an acoustic signal at time t^{a} with emission delay δ. The electromagnetic signal is received by the stationary observer at time t^{e} and the acoustic signal at time t^{o}, © 2016 IEEE.

deterministic trajectory so that the respective formulae also apply here. An illustration is given in Fig. 4.4.

We assume that the electromagnetic signal is emitted by the target at time t^{e} and the acoustic signal at time t^{a} with time difference $t^{\mathrm{a}} - t^{\mathrm{e}} = \delta$, denoted as emission delay. The acoustic signal is received by observer 1 located at $[0, 0]$ at time t^{o} and by observer 2 with coordinates $[x^{\mathrm{s}}, y^{\mathrm{s}}]$ at time t^{s}, see Fig. 4.5. Furthermore, the electromagnetic signal is received by observer 1 at time t^{e}. Hence, t^{a} (or equivalently δ) is unknown[3] and must be estimated. Note that we assume a constant delay δ.

The augmented target state to be estimated is then given by

$$\mathbf{x}_0^* = [x_0, y_0, \dot{x}, \dot{y}, \delta]^{\mathrm{T}} = [\mathbf{x}_0, \delta]^{\mathrm{T}} \ . \tag{4.46}$$

For the measurement equations for the acoustic bearings at the respective observers, we obtain

$$\alpha^{\mathrm{o}}(t^{\mathrm{e}}) = \arctan \frac{x_0 + \dot{x} t^{\mathrm{a}}}{y_0 + \dot{y} t^{\mathrm{a}}} \tag{4.47}$$

regarding observer 1 and

$$\alpha^{\mathrm{s}}(t^{\mathrm{e}}) = \arctan \frac{x_0 + \dot{x} t^{\mathrm{a}} - x^{\mathrm{s}}}{y_0 + \dot{y} t^{\mathrm{a}} - y^{\mathrm{s}}} \tag{4.48}$$

[3] However, we make extensive use of t^{a} in the following. Simply see it as an abbreviation for $t^{\mathrm{e}} + \delta$.

for observer 2. Furthermore, r (cf. (4.35)) can be expressed by

$$r(t^{\mathrm{e}}) = \sqrt{(x_0 + \dot{x}t^{\mathrm{a}})^2 + (y_0 + \dot{y}t^{\mathrm{a}})^2}\,. \tag{4.49}$$

Similarly, s is given by

$$s(t^{\mathrm{e}}) = \sqrt{(x_0 + \dot{x}t^{\mathrm{a}} - x^{\mathrm{s}})^2 + (y_0 + \dot{y}t^{\mathrm{a}} - y^{\mathrm{s}})^2}\,. \tag{4.50}$$

The partial derivatives of α^{o} and α^{s} are analogous to the equations in (4.38): For $\partial\alpha^{\mathrm{o}}/\partial\mathbf{x}_0$, replace t^{e} by t^{a}. For $\partial\alpha^{\mathrm{s}}/\partial\mathbf{x}_0$, replace $x(t^{\mathrm{e}})$ and $y(t^{\mathrm{e}})$ by $x(t^{\mathrm{a}}) - x^{\mathrm{s}}$ and $y(t^{\mathrm{a}}) - y^{\mathrm{s}}$, respectively, and $r(t^{\mathrm{e}})$ by $s(t^{\mathrm{a}})$. Additionally, the partial derivative of α^{o} with respect to the delay δ is given by

$$\frac{\partial\alpha^{\mathrm{o}}}{\partial\delta}(t^{\mathrm{e}}) = \frac{\dot{x}y(t^{\mathrm{a}}) - \dot{y}x(t^{\mathrm{a}})}{r(t^{\mathrm{a}})^2}\,, \tag{4.51}$$

In order to calculate $\partial\alpha^{\mathrm{s}}/\partial\delta$, replace $x(t^{\mathrm{a}})$ and $y(t^{\mathrm{a}})$ by $x(t^{\mathrm{a}}) - x^{\mathrm{s}}$ and $y(t^{\mathrm{a}}) - y^{\mathrm{s}}$ and r by s.

Regarding the TDoA measurements, we define τ^{o} as the time difference of the arrival of the electromagnetic signal to the audio signal at the first observer and τ^{s} as the time difference of arrival of the electromagnetic signal at the first observer to the audio signal at the second observer, see Fig. 4.5:

$$\tau^{\mathrm{o}}(t^{\mathrm{e}}) = t^{\mathrm{o}} - t^{\mathrm{e}} = \frac{r(t^{\mathrm{a}})}{c} + \delta \tag{4.52}$$

$$\tau^{\mathrm{s}}(t^{\mathrm{e}}) = t^{\mathrm{s}} - t^{\mathrm{e}} = \frac{s(t^{\mathrm{a}})}{c} + \delta\,. \tag{4.53}$$

A complete measurement $\mathbf{z}_k$ batch is then composed of the quadruple

$$\left[\alpha^{\mathrm{o}}(t_k), \alpha^{\mathrm{s}}(t_k), \tau^{\mathrm{o}}(t_k), \tau^{\mathrm{s}}(t_k)\right]^{\mathrm{T}}\,. \tag{4.54}$$

Analogous to (4.40), the partial derivative of τ^{o} with respect to $\mathbf{x}_0$ is given by

$$\frac{\partial\tau^{\mathrm{o}}}{\partial\mathbf{x}_0^*} = \frac{1}{c}\left[\frac{\partial r}{\partial x_0}, \frac{\partial r}{\partial y_0}, \frac{\partial r}{\partial\dot{x}}, \frac{\partial r}{\partial\dot{y}}, \frac{\partial r}{\partial\delta} + c\right] \tag{4.55}$$

and the partial derivative of τ^{s} by

$$\frac{\partial\tau^{\mathrm{s}}}{\partial\mathbf{x}_0^*} = \frac{1}{c}\left[\frac{\partial s}{\partial x_0}, \frac{\partial s}{\partial y_0}, \frac{\partial s}{\partial\dot{x}}, \frac{\partial s}{\partial\dot{y}}, \frac{\partial s}{\partial\delta} + c\right]\,. \tag{4.56}$$

We can express $\partial\tau^{\mathrm{o}}/\partial\mathbf{x}_0$ by replacing t^{e} by t^{a} in (4.40). For $\partial\tau^{\mathrm{s}}/\partial\mathbf{x}_0$, replace t^{e} by t^{a}, $x(t^{\mathrm{e}})$ and $y(t^{\mathrm{e}})$ by $x(t^{\mathrm{a}})-x^{\mathrm{s}}$ and $y(t^{\mathrm{a}})-y^{\mathrm{s}}$, respectively, and $r(t^{\mathrm{e}})$ by $s(t^{\mathrm{a}})$. The remaining partial derivatives with respect to δ are then obtained by

$$\frac{\partial r}{\partial \delta}(t^{\mathrm{e}}) = \frac{\dot{x}x(t^{\mathrm{a}}) + \dot{y}y(t^{\mathrm{a}})}{r(t^{\mathrm{a}})} \tag{4.57}$$

$$\frac{\partial s}{\partial \delta}(t^{\mathrm{e}}) = \frac{\dot{x}(x(t^{\mathrm{a}}) - x^{\mathrm{s}}) + \dot{y}(y(t^{\mathrm{a}}) - y^{\mathrm{s}})}{s(t^{\mathrm{a}})}\,. \tag{4.58}$$

Finally, we can formulate the measurement matrix $\widetilde{\mathbf{H}}^*$ as

$$\widetilde{\mathbf{H}}^* = \begin{bmatrix} \partial\alpha^{\mathrm{o}}/\partial\mathbf{x}_0^* \\ \partial\alpha^{\mathrm{s}}/\partial\mathbf{x}_0^* \\ \partial\tau^{\mathrm{o}}/\partial\mathbf{x}_0^* \\ \partial\tau^{\mathrm{s}}/\partial\mathbf{x}_0^* \end{bmatrix} \in \mathbb{R}^{4\times 5}\,. \tag{4.59}$$

Since the 4×5 matrix cannot have a full rank of 5, we have to add a further measurement batch. For this purpose, assume the electromagnetic signal emission times t_0^{e} and t_1^{e}, which are also the arrival times of the electromagnetic signal, and the (unknown) acoustic signal emission times t_0^{a} and t_1^{a}. Here, $\delta = t_0^{\mathrm{a}} - t_0^{\mathrm{e}} = t_1^{\mathrm{a}} - t_1^{\mathrm{e}}$ is constant. Hence, this leads to the following observability matrix:

$$\widetilde{O}_1^* = \begin{bmatrix} \widetilde{\mathbf{H}}^*(t_0^{\mathrm{e}}) \\ \widetilde{\mathbf{H}}^*(t_1^{\mathrm{e}})\widetilde{\mathbf{\Phi}}^*(t_1^{\mathrm{e}}, t_0^{\mathrm{e}}) \end{bmatrix} \tag{4.60}$$

with state transition matrix

$$\widetilde{\mathbf{\Phi}}^*(t_k, t_{k-1}) = \begin{bmatrix} \widetilde{\mathbf{\Phi}}(t_k, t_{k-1}) & \mathbf{0} \\ \mathbf{0} & 1 \end{bmatrix}. \tag{4.61}$$

One can show that the 8×5 observability matrix $\widetilde{O}_1^*$ has at least rank 5, so that the target state $\mathbf{x}_0^*$ is locally observable with two measurement batches. One can even prove that the first six rows of $\widetilde{O}_1^*$ have rank 5 given $t_0^{\mathrm{e}} \neq t_1^{\mathrm{e}}$ and $[x^{\mathrm{s}}, y^{\mathrm{s}}] \neq [0,0]$. This means, to achieve local observability, it is sufficient to take a full measurement batch of acoustic bearings and TDoA measurements and additional acoustic measurements regarding both observers. However, a constant emission delay δ has to be ensured. In case of a non-constant delay, it must be added to the target state so that its size will increase by one with each measurement batch.

$\det \mathbf{J}$	0	1.8248×10^{-24}	8.1610×10^{-8}
CRLB pos	∞	7.0886×10^{4} m	504.5711 m
CRLB vel	∞	639.3733 m/s	2.1420 m/s
Cond pos	1.0628×10^{5}	6.9909×10^{4}	15.9675
Cond vel	∞	6.0270	3.5094
	$k = 0$	$k = 1$	$k = 100$

Table 4.1: CRLB for acoustic and electromagnetic signal emitted simultaneously, © 2016 IEEE.

$\det \mathbf{J}$	0	1.1926×10^{-18}	0.0019
CRLB pos	∞	387.7655 m	94.1605 m
CRLB vel	∞	361.3013 m/s	0.9085 m/s
CLRB delay	∞	0.9804 s	0.1952 s
Cond pos	2.8699	2.9187	8.9031
Cond vel	∞	6.5198	3.7166
	$k = 0$	$k = 1$	$k = 100$

Table 4.2: CRLB for acoustic and electromagnetic signal emitted with emission delay, © 2016 IEEE.

4.3 Numerical Cramér-Rao Analysis

In order to verify the results of the observability study, we perform a numerical Cramér-Rao analysis. For that, we assume observer 1 carrying an acoustic and a detection sensor at $[x^{\mathrm{o}}, y^{\mathrm{o}}] = [0\,\mathrm{m}, 0\,\mathrm{m}]$ and observer 2 equipped with an acoustic sensor only at $[x^{\mathrm{s}}, y^{\mathrm{s}}] = [200\,\mathrm{m}, 0\,\mathrm{m}]$. The initial target state is $\mathbf{x}_0^* = [200\,\mathrm{m}, 200\,\mathrm{m}, 3\,\mathrm{m/s}, 0\,\mathrm{m/s}, 0.5\,\mathrm{s}]^{\mathrm{T}}$, see Fig. 4.4. The bearing standard deviation is assumed to be $\sigma_\alpha = 1°$, and the TDoA detection standard deviation $\sigma_\tau = 1\,\mathrm{s}$. This way, the measurement covariance matrix corresponds to the identity matrix. Furthermore, we assume that $t_0^{\mathrm{e}} = 1\,\mathrm{s}$ and $t_1^{\mathrm{e}} = 2\,\mathrm{s}$ and the speed of sound $c = 340\,\mathrm{m/s}$.

The results for the presented cases of acoustic and electromagnetic signal emitted simultaneously and with emission delay are shown in Tables 4.1 and 4.2. The results are exhibited after one measurement batch ($k = 0$), two measurement batches ($k = 1$), and at the end of the simulation ($k = 100$). The CRLB for position and speed is calculated by $\sqrt{\mathbf{C}_{1,1} + \mathbf{C}_{2,2}}$ and $\sqrt{\mathbf{C}_{3,3} + \mathbf{C}_{4,4}}$, respectively with $\mathbf{C} = \mathbf{J}^{-1}$. The indices denote the

particular line and column of the matrix. Furthermore, κ is the matrix condition number given by

$$\kappa = |\lambda_{\max}(\mathbf{J})/\lambda_{\min}(\mathbf{J})|\,, \tag{4.62}$$

where $\lambda_{\max}(\mathbf{J})$ and $\lambda_{\min}(\mathbf{J})$ represent the maximum and minimum eigenvalues of $\mathbf{J}$, respectively. The matrix condition number indicates whether a matrix is nearly singular. One has a well-conditioned matrix if the value is near one.

In both cases, the results show no observability for the first time step since the CRLB is infinity. As pointed out by the observability analyses, observability is only achieved in the second time step when two measurement batches are available. This clearly verifies the results from Section 4.2. Of course, using only one observer, see Table 4.1, the accuracy at time step $k = 1$ is low compared to the case where two observers are active, see Table 4.2.

4.4 Summary of the Chapter

This chapter is embedded into the central theme of heterogeneous bearings-only tracking. Its first objective has been to recapitulate observability criteria for different types of systems, i.e. linear continuous-time, linear discrete-time, and nonlinear discrete-time systems. These share the same general result: A system is observable if and only if the observability Gramian is positive definite or equivalently has full rank. Naturally, this leads to the practical bearings-only observability criteria, where an observer must outmaneuver a target. Another important insight is that the observability Gramian is strongly connected to the Cramér-Rao lower bound as it is algebraically equal to the CRLB without noise. This means that from a non-invertible FIM, we can directly conclude non-observability. Returning to heterogeneous bearings-only tracking, we have applied the observability findings in a setting including heterogeneous sensors, namely passive acoustic and electromagnetic sensors. It has been shown that the combination of different measurement types achieves observability even on a single platform and a moving target due to the exploitation of different signal propagation velocities. This is another main result of this thesis. Additionally, it shows the advantages of heterogeneous bearings-only tracking.

5 State Estimation for Bearings-only Tracking

State estimation is needed when the internal state of a system at time t_k, denoted by $\mathbf{x}(t_k) = \mathbf{x}_k$, shall be retrieved, but can only observed by measurements of the state, denoted by the set $\mathcal{Z}^k = \{\mathbf{z}_0, \mathbf{z}_1, \ldots, \mathbf{z}_k\}$, which comprises all measurements $\mathbf{z}_i$ until time t_k. This chapter is clearly based on the previous chapters, since observability, as pointed out in Chapter 4, is a requirement for state estimation, since without the state being observable, it cannot be estimated uniquely. Additionally, the Cramér-Rao lower bound, discussed in Chapter 3 indicates the maximum performance an estimator can achieve given the scenario with target-observer geometry and the measurement errors.

In Fig. 5.1 an overview over different kinds of estimators is given as hierachical tree structure. Of courese, this illustration is not exhaustive, since the estimator "zoo" contains many more variations. The colors in this figure are alike to the colors in Fig. 1.1 representing the two central themes of this thesis. This means that red indicates being part of the central theme of bearings-only tracking for maneuvering targets and blue indicates being part of the central theme of bearings-only tracking for heterogeneous sensors. Furthermore, green and gray mean that this entity is explained in this thesis for educational reasons or rather is solely mentioned for informational purposes.

Generally, estimators can be partitioned into non-Bayesian and Baysian estimators and. Non-Bayesian estimators usually take the form of batch methods, i.e. all measurements are considered at all time scans in order to minimize a certain optimization function. The most common estimator of this type is maximum likelihood estimator (MLE) explained in Section 5.6 particularly for the problem of bearings-only tracking of maneuvering targets.

On the other hand, Bayesian estimators always take the recursive filter form, i.e. the state is updated step-by-step with each observation based on the information from the previous time scan. This is also dictated by the Bayes' theorem, see (5.1). Hence, all Bayesian filters comprise of two steps: *Prediction* and *filtering*. The prediction step predicts the state at the previous time scan to the current time using the motion model and the filtering step updates the predicted state by the current observation using the mesurement model. A general form of such a filter is shown in Section 5.1.1.

Depending on the structure of the measurement and the motion equation, one can differentiate between linear and nonlinear filters. Hence, if the measurement and motion

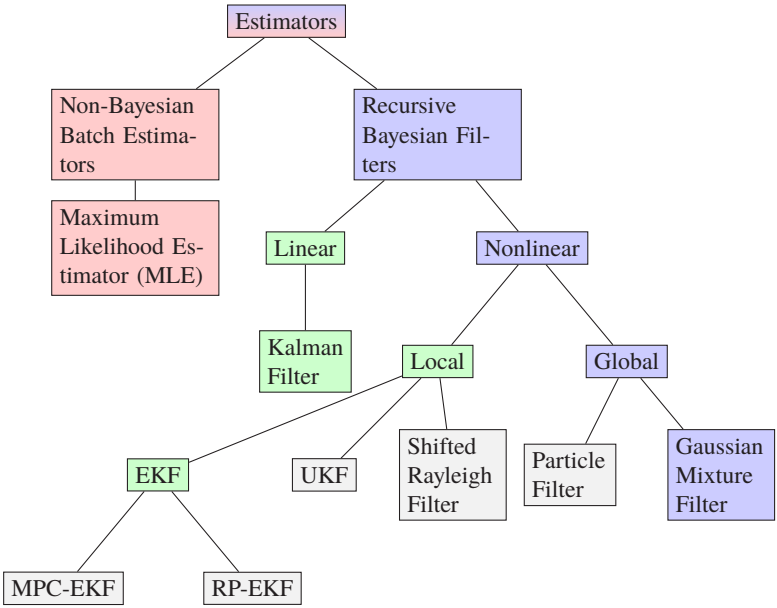

Figure 5.1: Overview (not exhaustive) over non-Bayesian batch estimators and recursive Bayesian filters. Red: Estimators covered for bearings-only maneuvering target tracking. Blue: Filters used in the domain of heterogeneous tracking. Green: Filters explained in this thesis. Gray: Filters mentioned, but not handled in this thesis.

model are both linear, one can stick to the linear branch, otherwise one has to choose a nonlinear filter. The optimal filter for linear models and zero mean and Gaussian noise[1] is the Kalman filter, named after Rudolf Kalman [Kal60], which is a closed-form solution. In case of a nonlinear state transition or measurement equation, there is generally no analytical solution to the Bayesian filtering and prediction equations. Thus, one has to use approximate techniques for Bayesian state estimation. In [SDŠ11], Straka et al. distinguish between local and global state estimation methods especially in the domain of bearings-only tracking. Additionally, Daum [Dau05] provides an interesting overview paper over different classes of nonlinear filtering algorithms with a slightly different and more fine-grained classification than Straka. However, Straka's approach seems to be reasonable to be absorbed in this thesis.

[1] which is assumed throughout this thesis

Following [SDŠ11], local state estimation methods try to approximate the first to moments of the densities, i.e. mean and covariance, and therefore provide estimates which are valid only locally. They have an identical structure to the Kalman filter and include:

- Extended Kalman filter (EKF) [Jaz70, BSLK01] with its special variations for bearings-only tracking using modified polar coordinates (MPC-EKF) [AH83] and using a bank of EKFs conditioned on specific ranges [Pea95, Kro98]. See also Subsection 5.3.2.
- Unscented Kalman filter (UKF) [JUDW95, JU04, LJ08],
- Shifted Rayleigh filter (SRF), a moment matching filter designed specifically for bearings-only tracking [CVY07, ACV07].

On the other hand, global state estimation methods provide estimates which are valid in almost the whole state space. This is achieved by trying to approximate the densities on the whole. Examples are

- Sequential Monte-Carlo methods like particle filters (PF) [GSS93, DdFG01, AMGC02, GGB$^+$02],
- Gaussian sum (or Gaussian mixture) methods [SA71, TPH99, ME06, ALS07, Mušo09, Hub15], which are featured in this thesis for the cental theme of bearings-only tracking with heterogeneous sensors. See also Section 5.4.

Comparisons between different methods as EKF, pseudomeasurement filter, and PF for bearings-only tracking is for example given in [LKBSM02], The pseudomeasurement filter is special form of linearization based on coordinate transformation. However, this results in non-Gaussian noise and subsequently in biased estimates [AN82]. Furthermore, different forms of EKFs are compared in [AR00] including a Cartesian EKF, the pseudomeasurement filter, a modified gain EKF [SS85], an MPC-EKF, and a RP-EKF. The results of both investigations reveal that the EKF shows the worst performance, especially when the initial estimate error is high.

5.1 Bayesian State Estimation

The foundation for Bayesian state estimation is the Bayes' theorem:

$$p(x|z) = \frac{p(z|x)p(x)}{p(z)} = \frac{p(z|x)p(x)}{\int_U p(z|x)p(x)\,\mathrm{d}x}\,, \tag{5.1}$$

which has been described by Reverend Bayes in his original manuscript from 1763 [Bay63]. Here, the *prior* density $p(x)$ reflects an initial degree of belief, which may be subjective. Combining this with the evidence from the data, the PDF of the observation $\mathbf{z}$ conditioned on the state or likelihood $p(z|x)$ (which is also vital for the CRLB, see Chapter 3), results

in the posterior density $p(x|z)$ [BSLK01]. This makes a statement on the probability density of x given the observation z.

5.1.1 General Bayesian Estimator

Based on Bayes' theorem (5.1), Bayesian state estimation, also named general Bayesian filter [Hau05], is the following iterative update scheme to calculate a density $p\left(\mathbf{x}_\ell \middle| \mathcal{Z}^k\right)$. This density incorporates the complete knowledge of the target state $\mathbf{x}_\ell$ at time t_ℓ conditioned on all available measurements $\mathcal{Z}^k$. Depending on the time t_ℓ at which target state estimates $\mathbf{x}_\ell$ are needed, the related density iteration process is referred to as *prediction* ($t_\ell > t_k$), *filtering* ($t_\ell = t_k$), or *retrodiction* ($t_\ell < t_k$) (also called smoothing [Sär13]). Retrodiction exceeds the scope of this thesis and is therefore not discussed here. See for example [Gov13, Koc14] for further information.

Prediction To obtain the prediction (or prior) density $p\left(\mathbf{x}_k \middle| \mathcal{Z}^{k-1}\right)$, the previous filtering density $p\left(\mathbf{x}_{k-1} \middle| \mathcal{Z}^{k-1}\right)$ has to be combined with the transition density $p(\mathbf{x}_k|\mathbf{x}_{k-1})$ representing a first-order Markovian evolution model, commonly the motion model of the target of interest, see also Chapter 2. This results in the *Chapman-Kolmogorov* [Pap84] equation as follows:

$$p\left(\mathbf{x}_k \middle| \mathcal{Z}^{k-1}\right) = \int_{\mathbb{R}^d} \underbrace{p(\mathbf{x}_k|\mathbf{x}_{k-1})}_{\text{evolution model}} \underbrace{p\left(\mathbf{x}_{k-1} \middle| \mathcal{Z}^{k-1}\right)}_{\text{previous filtering}} \mathrm{d}\mathbf{x}_{k-1} \,. \tag{5.2}$$

Filtering Using Bayes' theorem, the likelihood function $p(\mathbf{z}_k|\mathbf{x}_k)$ representing the sensor model with respect to the current measurement $\mathbf{z}_k$, as well as the prediction density $p\left(\mathbf{x}_k \middle| \mathcal{Z}^{k-1}\right)$ from the previous step, the filtering (or posterior) density $p\left(\mathbf{x}_k \middle| \mathcal{Z}^k\right)$ is given by

$$p\left(\mathbf{x}_k \middle| \mathcal{Z}^k\right) = \frac{\overbrace{p(\mathbf{z}_k|\mathbf{x}_k)}^{\text{sensor model}} \overbrace{p\left(\mathbf{x}_k \middle| \mathcal{Z}^{k-1}\right)}^{\text{prediction}}}{\int_{\mathbb{R}^d} p(\mathbf{z}_k|\mathbf{x}_k) p\left(\mathbf{x}_k \middle| \mathcal{Z}^{k-1}\right) \mathrm{d}\mathbf{x}_k} \,. \tag{5.3}$$

Since the denominator is constant, the filtering equation is commonly expressed by

$$p\left(\mathbf{x}_k \middle| \mathcal{Z}^k\right) = c_k \; p(\mathbf{z}_k|\mathbf{x}_k) \; p\left(\mathbf{x}_k \middle| \mathcal{Z}^{k-1}\right) \tag{5.4}$$

with

$$c_k = \frac{1}{\int_{\mathbb{R}^d} p(\mathbf{z}_k|\mathbf{x}_k) p\left(\mathbf{x}_k \middle| \mathcal{Z}^{k-1}\right) \mathrm{d}\mathbf{x}_k} \,. \tag{5.5}$$

Generally, the aforementioned Bayesian prediction and filtering equations cannot be solved analytically. If both measurement and motion model are linear and Gaussian densities are assumed, an analytic solution, called *Kalman filter*, can be derived. This is outlined in the next section. On the other hand, for nonlinear models, there are various non-analytic, approximative approaches discussed in Section 5.3.

5.2 Linear Bayesian State Estimation

Assume a pure linear state transition and measurement model

$$\begin{aligned} \mathbf{x}_k &= \mathbf{F}_{k-1}\mathbf{x}_{k-1} + \mathbf{w}_k \\ \mathbf{z}_k &= \mathbf{H}_k\mathbf{x}_k + \boldsymbol{\nu}_k \end{aligned} \tag{5.6}$$

with state transition matrix $\mathbf{F}_k$ and process noise $\mathbf{w}_k$, cf. (2.20), as well as measurement matrix $\mathbf{H}_k$ with measurement noise $\boldsymbol{\nu}_k$. The noise parts are assumed to be Gaussian distributed with zero mean. Therefore, the transition density $p(\mathbf{x}_k|\mathbf{x}_{k-1})$ and the likelihood $p(\mathbf{z}_k|\mathbf{x}_k)$ can be expressed by the Gaussians

$$p(\mathbf{x}_k|\mathbf{x}_{k-1}) = \mathcal{N}(\mathbf{x}_k; \mathbf{F}_{k-1}\mathbf{x}_{k-1}, \mathbf{Q}_k) \tag{5.7}$$

with process noise covariance matrix $\mathbf{Q}_k$ and

$$p(\mathbf{z}_k|\mathbf{x}_k) = \mathcal{N}(\mathbf{z}_k; \mathbf{H}_k\mathbf{x}_k, \mathbf{R}_k) \,, \tag{5.8}$$

where $\mathbf{R}_k$ is the measurement noise covariance matrix.

5.2.1 Kalman Filter

Due to the aforementioned linear and Gaussian system, one receives the following Gaussian prediction and filtering densities by inserting (5.7) and (5.8) into (5.2) and (5.3), respectively, and applying the well-known product formula for Gaussians, see Subsection 2.2.1:

$$\begin{aligned} p\left(\mathbf{x}_k \middle| \mathcal{Z}^{k-1}\right) &= \mathcal{N}(\mathbf{x}_k; \hat{\mathbf{x}}_{k|k-1}, \mathbf{P}_{k|k-1}) \\ p\left(\mathbf{x}_k \middle| \mathcal{Z}^{k}\right) &= \mathcal{N}(\mathbf{x}_k; \hat{\mathbf{x}}_{k|k}, \mathbf{P}_{k|k}) \,. \end{aligned} \tag{5.9}$$

Prediction The predicted state $\hat{\mathbf{x}}_{k|k-1}$ and its corresponding covariance $\mathbf{P}_{k|k-1}$ are calculated by

$$\begin{aligned} \hat{\mathbf{x}}_{k|k-1} &= \mathbf{F}_{k-1}\hat{\mathbf{x}}_{k-1|k-1} \\ \mathbf{P}_{k|k-1} &= \mathbf{F}_{k-1}\mathbf{P}_{k-1|k-1}\mathbf{F}_{k-1}^{\mathrm{T}} + \mathbf{Q}_k \,. \end{aligned} \tag{5.10}$$

Filtering For the estimated state $\hat{\mathbf{x}}_{k|k}$ and covariance $\mathbf{P}_{k|k}$, we have

$$\begin{aligned} \hat{\mathbf{x}}_{k|k} &= \hat{\mathbf{x}}_{k|k-1} + \mathbf{K}_k(\mathbf{z}_k - \underbrace{\mathbf{H}_k\hat{\mathbf{x}}_{k|k-1}}_{=\hat{\mathbf{z}}_{k|k-1}}) \\ \mathbf{P}_{k|k} &= \mathbf{P}_{k|k-1} - \mathbf{K}_k\mathbf{H}_k\mathbf{P}_{k|k-1} \end{aligned} \tag{5.11}$$

with gain matrix

$$\mathbf{K}_k = \mathbf{P}_{k|k-1}\mathbf{H}_k^{\mathrm{T}}\left(\mathbf{R}_k + \mathbf{H}_k\mathbf{P}_{k|k-1}\mathbf{H}_k^{\mathrm{T}}\right)^{-1} . \tag{5.12}$$

This step is also called *corrector* step since it corrects the predictions with the information from the current measurement.

This iterative update scheme is called *Kalman filter*, named after the pioneering work of R. E. Kalman [Kal60]. For further reading and more detailed discussions, also refer to [Sor70, May82]. Under the presented linear and Gaussian assumptions, the Kalman filter is the optimal estimator in the MMSE (minimum mean square error) sense [BSLK01].

5.3 Nonlinear Bayesian State Estimation

Consider the following nonlinear state transition and measurement equation:

$$\begin{aligned} \mathbf{x}_k &= \mathbf{f}_{k-1}(\mathbf{x}_{k-1}) + \mathbf{w}_k \\ \mathbf{z}_k &= \mathbf{h}_k(\mathbf{x}_k) + \boldsymbol{\nu}_k \,, \end{aligned} \tag{5.13}$$

where $\mathbf{f}_k(\cdot)$ and $\mathbf{h}_k(\cdot)$ represent a nonlinear state transition and a nonlinear measurement function, respectively, see also Chapter 2. As for the linear case, the noise terms $\mathbf{w}_k$ and $\boldsymbol{\nu}_k$ are assumed to be Gaussian distributed with zero mean and covariance matrices $\mathbf{Q}_k$ and $\mathbf{R}_k$, respectively. This leads to the transition density $p(\mathbf{x}_k|\mathbf{x}_{k-1})$ and likelihood $p(\mathbf{z}_k|\mathbf{x}_k)$ as follows:

$$p(\mathbf{x}_k|\mathbf{x}_{k-1}) = \mathcal{N}(\mathbf{x}_k; \mathbf{f}_{k-1}(\mathbf{x}_{k-1}), \mathbf{Q}_k) \tag{5.14a}$$

$$p(\mathbf{z}_k|\mathbf{x}_k) = \mathcal{N}(\mathbf{z}_k; \mathbf{h}_k(\mathbf{x}_k), \mathbf{R}_k) \,. \tag{5.14b}$$

5.3.1 Generic Local Filter

Since local state estimation methods have an identical structure to the Kalman filter described in Subsection 5.2.1, one can formulate a generic local filter as a special case of the general Bayesian estimator from Subsection 5.1.1 targeting only the first two moments according to [SDŠ11]:

Prediction The predicted state estimate and covariance are given by the relations

$$\begin{aligned}\hat{\mathbf{x}}_{k|k-1} &= \mathrm{E}\left\{\mathbf{f}_{k-1}(\mathbf{x}_{k-1}) \,\middle|\, \mathcal{Z}^{k-1}\right\} \\ \mathbf{P}_{k|k-1} &= \mathrm{E}\left\{(\mathbf{f}_{k-1}(\mathbf{x}_{k-1}) - \hat{\mathbf{x}}_{k|k-1})(\mathbf{f}_{k-1}(\mathbf{x}_{k-1}) - \hat{\mathbf{x}}_{k|k-1})^{\mathrm{T}} \,\middle|\, \mathcal{Z}^{k-1}\right\} .\end{aligned} \tag{5.15}$$

Filtering The predicted state estimate is updated with respect to the current measurement $\mathbf{z}_k$ according to

$$\begin{aligned}\hat{\mathbf{x}}_{k|k} &= \hat{\mathbf{x}}_{k|k-1} + \mathbf{K}_k(\mathbf{z}_k - \hat{\mathbf{z}}_{k|k-1}) \\ \mathbf{P}_{k|k} &= \mathbf{P}_{k|k-1} - \mathbf{K}_k\mathbf{P}_{z,k|k-1}\mathbf{K}_k^{\mathrm{T}} ,\end{aligned} \tag{5.16}$$

where $\mathbf{K}_k$ is the filter gain given by

$$\mathbf{K}_k = \mathbf{P}_{xz,k|k-1}\mathbf{P}_{z,k|k-1}^{-1} \tag{5.17}$$

and $\hat{\mathbf{z}}_{k|k-1}$ denotes a predicted measurement given by

$$\hat{\mathbf{z}}_{k|k-1} = \mathrm{E}\left\{\mathbf{h}_k(\mathbf{x}_k) \,\middle|\, \mathcal{Z}^{k-1}\right\} . \tag{5.18}$$

Finally, the remaining covariance matrices are given by the expected values

$$\begin{aligned}\mathbf{P}_{z,k|k-1} &= \mathrm{E}\left\{(\mathbf{h}_k(\mathbf{x}_k) - \hat{\mathbf{z}}_{k|k-1})(\mathbf{h}_k(\mathbf{x}_k) - \hat{\mathbf{z}}_{k|k-1})^{\mathrm{T}} \,\middle|\, \mathcal{Z}^{k-1}\right\} + \mathbf{R}_k \\ \mathbf{P}_{xz,k|k-1} &= \mathrm{E}\left\{(\mathbf{x}_k - \hat{\mathbf{x}}_{k|k-1})(\mathbf{z}_k - \hat{\mathbf{z}}_{k|k-1})^{\mathrm{T}} \,\middle|\, \mathcal{Z}^{k-1}\right\}\end{aligned} \tag{5.19}$$

5.3.2 Extended Kalman Filter

A well-known linearization technique to approximate the nonlinear functions in (5.15)–(5.19) is to use the first-order Taylor expansion, see e.g. [RAG04]. This leads to following equations for prediction and filtering, called *extended Kalman filter (EKF)*:

Prediction For prediction, the state and covariance are given by

$$\begin{aligned} \hat{\mathbf{x}}_{k|k-1} &= \mathbf{f}_{k-1}(\hat{\mathbf{x}}_{k-1|k-1}) \\ \mathbf{P}_{k|k-1} &= \widetilde{\mathbf{F}}_{k-1}\mathbf{P}_{k-1|k-1}\widetilde{\mathbf{F}}_{k-1}^{\mathrm{T}} + \mathbf{Q}_k \end{aligned} \tag{5.20}$$

with the Jacobian matrix resulting from first-order Taylor expansion at the previous estimate $\hat{\mathbf{x}}_{k-1|k-1}$

$$\widetilde{\mathbf{F}}_{k-1} = \frac{\partial \mathbf{f}_{k-1}(\hat{\mathbf{x}}_{k-1|k-1})}{\partial \hat{\mathbf{x}}_{k-1|k-1}} . \tag{5.21}$$

Filtering The following terms for filtering can be derived:

$$\begin{aligned} \hat{\mathbf{z}}_{k|k-1} &= \mathbf{h}_k(\hat{\mathbf{x}}_{k|k-1}) \\ \mathbf{P}_{z,k|k-1} &= \widetilde{\mathbf{H}}_k\mathbf{P}_{k|k-1}\widetilde{\mathbf{H}}_k^{\mathrm{T}} + \mathbf{R}_k \\ \mathbf{P}_{xz,k|k-1} &= \mathbf{P}_{k|k-1}\widetilde{\mathbf{H}}_k^{\mathrm{T}} \end{aligned} \tag{5.22}$$

which have to be inserted into (5.16) to complete the update scheme. Here,

$$\widetilde{\mathbf{H}}_k = \frac{\partial \mathbf{h}_k(\hat{\mathbf{x}}_{k|k-1})}{\partial \hat{\mathbf{x}}_{k|k-1}} , \tag{5.23}$$

is the Jacobian matrix of the measurement function evaluated at the predicted estimate resulting from the first-order Taylor approximation.

Rewriting the covariance update equations in information matrix form, i.e. the inverse form using the matrix inversion lemma, yields

$$\mathbf{P}_{k|k}^{-1} = \left(\widetilde{\mathbf{F}}_{k-1}\mathbf{P}_{k-1|k-1}\widetilde{\mathbf{F}}_{k-1}^{\mathrm{T}} + \mathbf{Q}_k\right)^{-1} + \widetilde{\mathbf{H}}_k^{\mathrm{T}}\mathbf{R}_k^{-1}\widetilde{\mathbf{H}}_k , \tag{5.24}$$

which is structurally identical to the recursive update of the Fisher information matrix (3.27) for calculating the CRLB. The differences are the presence of process noise due to matrix $\mathbf{Q}_k$ and that the partial derivatives are evaluated at the predicted/estimated states instead of the true states.

Especially in bearings-only tracking scenarios, the presented Cartesian coordinate EKF is known to diverge. This is due to the non-observability of target range before the first observer maneuver and subsequent collapse of the covariances which leads to amplification of estimation errors finally causing divergence [Aid79]. Alternatively, one can track in a different coordinate system so that the measurement equation is linear as performed in the modified polar coordinate (MPC) approach, where observable and unobservable states are decoupled [HJC78, HAGL83, Bec01]. The drawback is that the motion equation is nonlinear. However, using MPC has led to less filter divergence com-

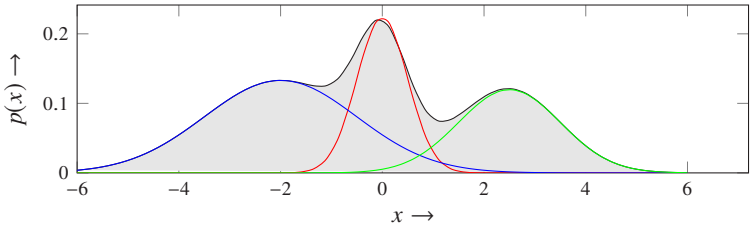

Figure 5.2: Gaussian mixture with 3 components. Each component is illustrated by different colors.

pared to the (Cartesian) EKF [AH83, vHF98]. Pseudo-linearization of the bearings-only measurement equation is another approach [LG78]. However, it leads to non-Gaussian measurement noise causing biased estimates [AN82]. Another variant is the range parameterized extended Kalman filter (RPEKF) [Kro98, KG05]. It consists of a bank of individual EKFs, each tuned to a certain range and is thus similar to following approach of bearings-only tracking via a Gaussian mixture filter using likelihood approximation.

5.4 Gaussian Mixture Filtering

The idea of Gaussian mixture filtering is that since the Bayesian recursions cannot generally be solved in closed-form when the system is nonlinear (see Subsection 5.3), density approximations based on Gaussian mixtures (or Gaussian sums) have been proposed [SA71]. Mušicki [Muš09] presents a Gaussian mixture likelihood approximation for bearings-only measurements which is intensively studied in this paper. Furthermore, in [DK10], a Gaussian mixture approximation has been developed which is used to localize emitters by means of time difference of arrival (TDoA) measurements as well as to estimate target altitude in a multistatic passive radar scenario.

5.4.1 Gaussian Mixture

A Gaussian mixture density is defined by a convex weighted sum of Gaussian densities (2.4) according to

$$p(\mathbf{x}) = \sum_{i=1}^{N} w_i \, \mathcal{N}(\mathbf{x}; \hat{\mathbf{x}}_i, \mathbf{P}_i) \,. \tag{5.25}$$

See Fig. 5.2 for an illustration of a Gaussian mixture with three components. The described Gaussian mixture has N components, which are themselves Gaussian densities with means $\hat{\mathbf{x}}_i$ and covariances $\mathbf{P}_i$. To assure that this Gaussian mixture is a valid probability density function, the weights w_i must be non-negative and add up to one.

One advantageous property of Gaussian mixtures is that they can be considered as universal approximator for an arbitrary density function, i.e. any density function can be approximated by means of a Gaussian mixture as closely as required [MS96, Hub15]. This property is exploited in the Gaussian mixture filter based on approximating the likelihood presented later in this section.

The overall mean and covariance of a Gaussian mixture can be calculated in closed form and are obtained by

$$\begin{aligned} \boldsymbol{\mu} &= \mathrm{E}\{\mathbf{x}\} = \sum_{i=1}^{N} w_i \, \hat{\mathbf{x}}_i \,, \\ \mathbf{C} &= \mathrm{Cov}\{\mathbf{x}\} = \sum_{i=1}^{N} w_i \left(\mathbf{P}_i + \hat{\mathbf{x}}_i \, \hat{\mathbf{x}}_i^{\mathrm{T}} \right) - \boldsymbol{\mu} \, \boldsymbol{\mu}^{\mathrm{T}} \,. \end{aligned} \tag{5.26}$$

5.4.2 Multi Hypothesis GM Filter Based on Likelihood Approximation

Gaussian mixture filtering can be classified into two groups, see also [Hub15]: Model approximation tries to approximate the transition density or the likelihood by means of a Gaussian mixture. Transition density approximation is, for example, covered in [HBH06], whereas likelihood approximation is the more common approach since in many practical filtering problems, the motion model is linear while the measurement model is nonlinear. Thus, likelihood approximation is proposed in this thesis as well as in [ME06, ALS07, Muš09]. On the other hand, density approximation approaches focus on directly approximating the true predicted or posterior density by means of Gaussian mixtures, as, for example, presented in [HF03].

Multi hypothesis tracking (MHT) has been attracted much interest for many practical applications in the past years. It is numerically very fast and flexible due to its mixture representation of a PDF [KvK97]. It certainly has the drawback that many parameters have to be modeled or estimated such as probability of detection p_D and spatial clutter density ρ_F. In this thesis, we assume that a single target shall be tracked. However, due to disturbances, false or missing detections can occur.

As mentioned above, consider for the multi hypothesis likelihood approximation Gaussian mixture filter (GMF) a linear state transition equation and a nonlinear measurement equation:

$$\begin{aligned} \mathbf{x}_k &= \mathbf{F}_{k-1} \mathbf{x}_{k-1} + \mathbf{w}_k \\ \mathbf{z}_k &= \mathbf{h}_k(\mathbf{x}_k) + \boldsymbol{\nu}_k \,. \end{aligned} \tag{5.27}$$

Hence, the state transition density $p(\mathbf{x}_k | \mathbf{x}_{k-1})$ is a Gaussian according to (5.7).

In contrast to the beginning of this chapter, we assume that now multiple measurements per time scan are allowed which means that the set of measurements up tp time t_k is given by

$$\mathcal{Z}^k = \{Z_0, Z_1, \ldots, Z_k\} \ . \tag{5.28}$$

Here, the measurement set at time t_k comprises m_k ambiguous measurements

$$Z_k = \left\{\mathbf{z}_k^1, \mathbf{z}_k^2, \ldots, \mathbf{z}_k^{m_k}\right\} \tag{5.29}$$

related to a single target. That means, at most one measurement originates from the target and the other measurements arise from imperfect detections or false measurements as from unwanted objects or clutter. Hence, (5.29) represents $m_k + 1$ hypotheses covering the case that each measurement comes from a hypothetical target location plus the case of no target measurement.

With m_k measurements at time t_k, we assume that each measurement $\mathbf{z}_k^j$ is approximated by a Gaussian mixture with L_k^j components that is linear in state $\mathbf{x}_k$.Incorporating probability of detection p_D and spatial clutter density ρ_F [Koc14] leads to the following multi hypothesis Gaussian mixture likelihood approximation:

$$p(Z_k|\mathbf{x}_k) \approx (1 - p_D)\rho_F + p_D \sum_{j=0}^{m_k} \sum_{i=1}^{L_k^j} \gamma_k^{i,j} \, \mathcal{N}\left(\mathbf{y}_k; \hat{\mathbf{y}}_k^{i,j}, \mathbf{\Sigma}_k^{i,j}\right) . \tag{5.30}$$

Since only single targets are considered – so that no track management is necessary which would mean that an association between hypotheses and per-measurement components must be kept – we can simplify the likelihood as follows:

$$p(Z_k|\mathbf{x}_k) \approx (1 - p_D)\rho_F + p_D \sum_{j=1}^{N_k} \gamma_k^j \, \mathcal{N}\left(\mathbf{y}_k; \hat{\mathbf{y}}_k^j, \mathbf{\Sigma}_k^j\right) \tag{5.31}$$

with $N_k = \sum_{j=0}^{m_k} L_k^j$. A detailed discussion and analysis on how to determine the weights γ_k^j, means $\hat{\mathbf{y}}_k^j$, and covariances $\mathbf{\Sigma}_k^j$ in case of bearings-only measurements is provided in Section 5.5. Note that $\mathbf{y}_k$ linearly depends on $\mathbf{x}_k$ and is obtained by a suitable coordinate transformation mapping from measurement to state coordinates. We assume, for now, that this transformation is possible, ignoring non-observable states as for bearings-only tracking. A solution to this problem will be presented later – it does not affect the general description of the GMF.

Filtering If we assume that the prior density $p\left(\mathbf{x}_k \middle| \mathcal{Z}^{k-1}\right)$ is given as a Gaussian mixture with G_{k-1} components, then according to the Bayes' theorem (5.3), we have for the filtering density

$$p\left(\mathbf{x}_k \middle| \mathcal{Z}^{k}\right) = c_k \, p(Z_k|\mathbf{x}_k) \underbrace{\left(\sum_{i=1}^{G_{k-1}} w_{k-1}^{i} \mathcal{N}\left(\mathbf{x}_k; \hat{\mathbf{x}}_{k|k-1}^{i}, \mathbf{P}_{k|k-1}^{i}\right)\right)}_{=p\left(\mathbf{x}_k \middle| \mathcal{Z}^{k-1}\right)} . \tag{5.32}$$

Component-wise multiplication and subsequent application of the product formula for Gaussians (see Subsection 2.2.1) leads to

$$p\left(\mathbf{x}_k \middle| \mathcal{Z}^{k}\right) = \sum_{j=0}^{N_k} \sum_{i=1}^{G_{k-1}} w_k^{i,j} \, \mathcal{N}\left(\mathbf{x}_k; \hat{\mathbf{x}}_{k|k}^{i,j}, \mathbf{P}_{k|k}^{i,j}\right) \tag{5.33}$$

with unnormalized weights

$$\bar{w}_k^{i,j} = \begin{cases} (1 - p_D)\rho_F \cdot w_{k-1}^{i} & \text{if } j = 0 \\ p_D \cdot w_{k-1}^{i} \gamma_k^{j} \, \mathcal{N}\left(\hat{\mathbf{y}}_k^{j}; \mathbf{H}_k \hat{\mathbf{x}}_{k|k-1}^{i}, \mathbf{S}_k^{i,j}\right) & \text{if } j > 0 \end{cases} \tag{5.34}$$

and their normalization

$$w_k^{i,j} = \frac{1}{\sum_{j=0}^{N_k} \sum_{i=1}^{G_{k-1}} \bar{w}_k^{i,j}} . \tag{5.35}$$

The innovation covariance $\mathbf{S}_k^{i,j}$ is given by

$$\mathbf{S}_k^{i,j} = \mathbf{H}_k \mathbf{P}_{k|k-1}^{i} \mathbf{H}_k^{\mathrm{T}} + \mathbf{\Sigma}_k^{j} . \tag{5.36}$$

Furthermore, in (5.33) each of the G_{k-1} components of the predicted Gaussian mixture is updated with N_k components of the Gaussian mixture likelihood performed by means of the standard Kalman filter update equations. Hence, for each component i of the prior and each component j of the likelihood, we update as follows:

$$\hat{\mathbf{x}}_{k|k}^{i,j} = \begin{cases} \hat{\mathbf{x}}_{k|k-1}^{i} & \text{if } j = 0 \\ \hat{\mathbf{x}}_{k|k-1}^{i} + \mathbf{K}_k^{i,j} \left(\hat{\mathbf{y}}_k^{j} - \mathbf{H}_k \hat{\mathbf{x}}_{k|k-1}^{i}\right) & \text{if } j > 0 \end{cases} \tag{5.37a}$$

$$\mathbf{P}_{k|k}^{i,j} = \begin{cases} \mathbf{P}_{k|k-1}^{i} & \text{if } j = 0 \\ \left(\mathbf{I} - \mathbf{K}_k^{i,j} \mathbf{H}_k\right) \mathbf{P}_{k|k-1}^{i} & \text{if } j > 0 \end{cases} \tag{5.37b}$$

with gain matrix

$$\mathbf{K}_k^{i,j} = \mathbf{P}_{k|k-1}^{i} \mathbf{H}_k^{\mathrm{T}} \left(\mathbf{S}_k^{i,j} \right)^{-1} . \tag{5.38}$$

Note that $j = 0$ reflects the "no measurement" case. Thus, state and covariance cannot be updated.

Component control According to (5.33), we obtain the posterior density as a Gaussian mixture of the form

$$p\left(\mathbf{x}_k \middle| \mathcal{Z}^k\right) = \sum_{i=1}^{G_{k-1}} \sum_{j=1}^{N_k} w_k^{i,j} \mathcal{N}\left(\mathbf{x}_k; \hat{\mathbf{x}}_{k|k}^{i,j}, \mathbf{P}_{k|k}^{i,j}\right) , \tag{5.39}$$

which can be rearranged and thus expressed in a simpler way as

$$p\left(\mathbf{x}_k \middle| \mathcal{Z}^k\right) = \sum_{i=1}^{G_k} w_k^{i} \mathcal{N}\left(\mathbf{x}_k; \hat{\mathbf{x}}_{k|k}^{i}, \mathbf{P}_{k|k}^{i}\right) \tag{5.40}$$

with $G_k = G_{k-1} \cdot N_k$. Since the number of components (hypotheses) grows exponentially in time, there will be a combinatorial disaster. In order to prevent this, the number if components has to be reduced [ME06]. A number of techniques exists to perform this task including pruning of components with low weight as well as sophisticated methods for merging several components. For details refer to [Sal89, BP99, Koc01, WM03, Run07].

Prediction According to the Bayesian prediction formula (5.2) and by means of the rearranged posterior (5.40) as well as the Gaussian state transition density (5.7), we receive for the predicted density

$$p\left(\mathbf{x}_k \middle| \mathcal{Z}^{k-1}\right) = \int_{\mathbb{R}^d} \mathcal{N}\left(\mathbf{x}_k; \mathbf{F}_{k-1}\mathbf{x}_{k-1}, \mathbf{Q}_k\right) \cdot \left(\sum_{i=1}^{G_{k-1}} w_{k-1}^{i} \mathcal{N}\left(\mathbf{x}_{k-1}; \hat{\mathbf{x}}_{k-1|k-1}^{i}, \mathbf{P}_{k-1|k-1}^{i}\right) \right) \mathrm{d}\mathbf{x}_{k-1} \tag{5.41}$$

with state transition matrix $\mathbf{F}_{k-1}$ and noise matrix $\mathbf{Q}_{k-1}$. Applying the product formula for Gaussians separates $\mathbf{x}_k$ and $\mathbf{x}_{k-1}$ leading to

$$p\left(\mathbf{x}_k \middle| \mathcal{Z}^{k-1}\right) = \sum_{i=1}^{G_{k-1}} w_{k-1}^{i} \mathcal{N}\left(\mathbf{x}_k; \hat{\mathbf{x}}_{k|k-1}^{i}, \mathbf{P}_{k|k-1}^{i}\right) \underbrace{\int_{\mathbb{R}^d} \mathcal{N}\left(\mathbf{x}_{k-1}, \cdot, \cdot\right) \mathrm{d}\mathbf{x}_{k-1}}_{=1} , \tag{5.42}$$

so that each component of the Gaussian mixture is predicted according to the standard Kalman filter prediction formulae, i.e.

$$\begin{aligned} \hat{\mathbf{x}}^i_{k|k-1} &= \mathbf{F}_{k-1}\hat{\mathbf{x}}^i_{k-1|k-1}\,, \\ \mathbf{P}^i_{k|k-1} &= \mathbf{F}_{k-1}\mathbf{P}^i_{k-1|k-1}\mathbf{F}^{\mathrm{T}}_{k-1} + \mathbf{Q}_{k-1}\,. \end{aligned} \tag{5.43}$$

Track output Having determined each component's estimated state and covariance, the overall estimate $\boldsymbol{\mu}_{k|k}$ and covariance $\mathbf{C}_{k|k}$ are found by means of (5.26).

5.5 Likelihood Approximation for Bearings-only Tracking

In this section, a discussion and analysis is given on how to determine a Gaussian mixture that is linear in target state and that approximates the likelihood (5.31) considering nonlinear bearings-only measurements. Also refer to the own paper [Hör14].

First, Streit's [SW09] likelihood function decomposition leading to a representation of the likelihood that is linear in target state is analyzed. Subsequently, Gaussian mixture approximations inspired by [Muš09] and Kronhamn [Kro98] are derived from Streit's likelihood decomposition. Both approaches are then analyzed.

5.5.1 Likelihood Function Decomposition

Here, we recap the likelihood function decomposition following Streit et al. [SW09]. Let $f, g : \mathbb{R}^d \to \mathbb{R}^d$ be continuously differentiable bijective functions with $f = g^{-1}$, i.e. f is the inverse of g. We assume that g maps state coordinates to measurement coordinates, so that for a d-dimensional state $\mathbf{x}$ and a d-dimensional measurement $\boldsymbol{\zeta}$ we have $\boldsymbol{\zeta} = g(\mathbf{x})$. Let the measurement errors be Gaussian distributed, then we can express the likelihood for state $\mathbf{x}$ as

$$p(\boldsymbol{\zeta}|\mathbf{x}) = \mathcal{N}(\boldsymbol{\zeta};\, g(\mathbf{x}), \mathbf{N})\,, \tag{5.44}$$

where $g(\mathbf{x})$ denotes the mean measurement in the absence of errors and $\mathbf{N}$ is the covariance matrix of the measurement errors. It can be shown (see Appendix B.1 or [SW09]) that

$$p(\boldsymbol{\zeta}|\mathbf{x}) \approx \det\left(\mathcal{D}f(\boldsymbol{\zeta})\right)\, \mathcal{N}\left(f(\boldsymbol{\zeta}); \mathbf{x}, \boldsymbol{\Sigma}\right)\,, \tag{5.45}$$

which is the decomposed likelihood that is linear in target state and has a Gaussian kernel. Here,

$$\mathcal{D}f(\boldsymbol{\zeta}) = \frac{\partial f(\boldsymbol{\zeta})}{\partial \boldsymbol{\zeta}} \tag{5.46}$$

is the Jacobian of f evaluated at $\boldsymbol{\zeta}$, see Appendix B.1 and

$$\boldsymbol{\Sigma} = \mathcal{D}f(\boldsymbol{\zeta})\,\mathbf{N}\,\mathcal{D}f(\boldsymbol{\zeta})^{\mathrm{T}} \tag{5.47}$$

is the converted covariance matrix, where $\det(\boldsymbol{\Sigma}) = \det(\mathbf{N})\det(\mathcal{D}f(\boldsymbol{\zeta}))^2$ holds.

Now additionally suppose that we have a measurement $\mathbf{z}$ of lower dimension than the state, i.e. $\mathbf{z}$ is s-dimensional, whereas $\mathbf{x}$ is d-dimensional, as above, with $s \leq d$. That means, $\mathbf{x}$ is not necessarily observable (see also Chapter 4). Furthermore, assume that $\mathbf{z}$ is a sub-vector of $\boldsymbol{\zeta}$ defined above, i.e. $\mathbf{z}$ comprises some, but not necessarily all elements of $\boldsymbol{\zeta}$. With this, let $\mathbf{z}^*$ be the vector of elements which are in $\boldsymbol{\zeta}$, but not in $\mathbf{z}$. Furthermore, let $\mathbf{h} : \mathbb{R}^d \to \mathbb{R}^s$ be the continuously differentiable measurement function, so that $\mathbf{z} = \mathbf{h}(\mathbf{x})$.

Using (5.45) and the technique of marginalizing out the elements in $\mathbf{z}^*$, we find an approximate term for the likelihood $p(\mathbf{z}|\mathbf{x})$ which is linear in target state as

$$p(\mathbf{z}|\mathbf{x}) = \mathcal{N}(\mathbf{z}; \mathbf{h}(\mathbf{x}), \mathbf{R}) \approx \int_U \det(\mathcal{D}f(\boldsymbol{\zeta}))\ \mathcal{N}(f(\boldsymbol{\zeta}); \mathbf{x}, \boldsymbol{\Sigma})\,\mathrm{d}\mathbf{z}^* = \tilde{p}(\mathbf{z}|\mathbf{x})\,, \tag{5.48}$$

where $\mathbf{R}$ is the covariance matrix of the measurement noise. The generally unbounded set $U = g\left(\mathbb{R}^{d-s}\right)$ has dimension $d - s$ and denotes the image of g restricted to the elements of $\mathbf{z}^*$.

Note that the integral over $\tilde{p}(\mathbf{z}|\mathbf{x})$ with respect to $\mathbb{R}$ has a finite value. Hence, in order to preserve this value if the approximation $\tilde{p}(\mathbf{z}|\mathbf{x})$ shall be restricted to a compact set C, we have to normalize it:

$$\tilde{p}_C(\mathbf{z}|\mathbf{x}) = \frac{1}{k}\int_C \det(\mathcal{D}f(\boldsymbol{\zeta}))\ \mathcal{N}(f(\boldsymbol{\zeta}); \mathbf{x}, \boldsymbol{\Sigma})\,\mathrm{d}\mathbf{z}^*\,, \tag{5.49}$$

where the normalization factor k is given by [SA71]

$$k = \int_C \mathbf{z}^*\,\mathrm{d}\mathbf{z}^*\,. \tag{5.50}$$

Bearings-only measurements To conduct the likelihood decomposition for bearings-only measurements, let

$$\begin{aligned} \mathbf{x} &= [x, y]^{\mathrm{T}} \\ \boldsymbol{\zeta} &= [r, \theta]^{\mathrm{T}} \\ \mathbf{z} &= \theta \\ g(\mathbf{x}) &= \left[\sqrt{x^2 + y^2}, \arctan(x/y)\right]^{\mathrm{T}}, \\ f(\boldsymbol{\zeta}) &= [r \sin\theta, r\cos\theta]^{\mathrm{T}} \\ \mathbf{h}(\mathbf{x}) &= \arctan(x/y) \\ \mathbf{N} &= \mathrm{diag}[\sigma_r^2, \sigma_\theta^2] \\ \mathbf{R} &= \sigma_\theta^2 \end{aligned} \tag{5.51}$$

with target position $[x, y]$, range r, and azimuth bearing θ. Obviously, $\mathbf{z}^* = r$ and since $\boldsymbol{\chi}$ and g correspond to locally orthogonal coordinate systems [SW09], $\mathcal{D}f(\boldsymbol{\zeta}) = \mathbf{TD}$ with rotation matrix

$$\mathbf{T} = \begin{bmatrix} \sin\theta & \cos\theta \\ \cos\theta & -\sin\theta \end{bmatrix} \tag{5.52}$$

and $\mathbf{D} = \mathrm{diag}[1, r]$ leading to $\det(\mathcal{D}f(\boldsymbol{\zeta})) = r$. Then the approximation of the bearings-only likelihood that is linear in target state is given by using (5.48) with marginalization of range r

$$\mathcal{N}(\mathbf{z}; \mathbf{h}(\mathbf{x}), \mathbf{R}) \approx \int_0^\infty r\mathcal{N}\left(f(\boldsymbol{\zeta}); \mathbf{x}, \boldsymbol{\Sigma}\right) \mathrm{d}r\,, \tag{5.53}$$

which is the general approximation scheme for a bearings-only likelihood. Furthermore, using (5.52), we can express $\boldsymbol{\Sigma}$ as

$$\boldsymbol{\Sigma} = \mathbf{TDND}^{\mathrm{T}}\mathbf{T}^{\mathrm{T}} = \mathbf{T}\begin{bmatrix} \sigma_r^2 & 0 \\ 0 & r^2\sigma_\theta^2 \end{bmatrix}\mathbf{T}^{\mathrm{T}}. \tag{5.54}$$

5.5.2 Gaussian Mixture Likelihood Approximations

Similar to Mušicki [Muš09], the aim is to approximate the likelihood $p(\mathbf{z}|\mathbf{x})$ by a Gaussian mixture with N components that is linear in target state, i.e.,

$$p(\mathbf{z}|\mathbf{x}) = \sum_{i=1}^{N} \gamma_i \mathcal{N}(\mathbf{y};\, \hat{\mathbf{y}}_i, \boldsymbol{\Sigma}_i)\,, \tag{5.55}$$

where $\mathbf{y} = [x, y]^{\mathrm{T}} = \mathbf{H}\mathbf{x} = f(\boldsymbol{\zeta})$ denotes the target position and depends linearly on the target state $\mathbf{x}$ by means of the projection matrix $\mathbf{H}$. Furthermore, $\boldsymbol{\zeta}$ and the coordinate transformation f are defined as in Subsection 5.5.1. The component weights, means, and covariances are denoted by γ_i, $\hat{\mathbf{y}}_i$, and $\boldsymbol{\Sigma}_i$, respectively. We demand that the weights add up to one.

Concerning range, we assume a compact range interval $[r_{\min}, r_{\max}]$ limited by minimum and maximum distance from sensor to target. Let $r_1 = r_{\min} < r_2 < \ldots < r_N < r_{N+1} = r_{\max}$ be an arbitrary partition of the interval $[r_{\min}, r_{\max}]$ into N subintervals. Length and mean range of any subinterval $[r_i, r_{i+1}]$ are defined as

$$\Delta r_i = r_{i+1} - r_i \tag{5.56}$$

and

$$\bar{r}_i = (r_{i+1} + r_i)/2\,. \tag{5.57}$$

Mušicki [Muš09] defines the means and covariances of the Gaussian mixture components depending on bearing θ and bearing standard deviation σ_θ as

$$\hat{\mathbf{y}}_i = \bar{r}_i \begin{bmatrix} \sin\theta \\ \cos\theta \end{bmatrix} \tag{5.58}$$

and

$$\boldsymbol{\Sigma}_i = \mathbf{T} \begin{bmatrix} \Delta r_i^2/4 & 0 \\ 0 & \bar{r}_i^2 \sigma_\theta^2 \end{bmatrix} \mathbf{T}^{\mathrm{T}}\,, \tag{5.59}$$

where $\mathbf{T}$ is given according to (5.52). Thus, we can interpret the likelihood (5.55) as a Gaussian mixture where each component is tuned to a certain range. That means, each component represents a range hypothesis. For Mušicki, the component weights denote the probability that subinterval i contains the target. Hence, he determines the weights to be proportional to the area covered by Gaussian mixture component i,

$$\gamma_i^{\mathrm{M}} = \frac{\sqrt{\det \boldsymbol{\Sigma}_i}}{\sum_{j=1}^{N} \sqrt{\det \boldsymbol{\Sigma}_j}}\,. \tag{5.60}$$

Note that the weights do not depend on σ_θ since it can be reduced.

On the other hand, Kronhamn [Kro98] defines the weights as proportional to the length of the range subinterval covered by Gaussian mixture component i, proposing

$$\gamma_i^{\mathrm{K}} = \frac{\Delta r_i}{\sum_{j=1}^{N} \Delta r_j}\,. \tag{5.61}$$

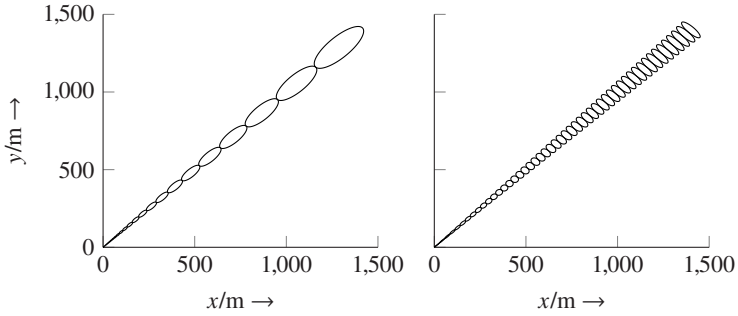

Figure 5.3: Gaussian mixture representation of bearings-only measurement likelihood for geometric (left) and equidistant (right) partition with $N = 50$, $r_{\min} = 0.1\,\text{m}$, $r_{\max} = 2000\,\text{m}$, $\theta = 45°$, and $\sigma_\theta = 3°$, © 2014 IEEE.

After some calculations involving telescoping series, the weights can be transformed to

$$\gamma_i^{\text{M}} = \frac{r_{i+1}^2 - r_i^2}{r_{\max}^2 - r_{\min}^2} \text{ and } \gamma_i^{\text{K}} = \frac{r_{i+1} - r_i}{r_{\max} - r_{\min}} . \tag{5.62}$$

With this, we can identify Mušicki's weights as a "quadratic version" of Kronhamn's weights. A relation between γ_i^{M} and γ_i^{K} can be established by

$$\gamma_i^{\text{M}} = \gamma_i^{\text{K}} \frac{2\bar{r}_i}{r_{\max} + r_{\min}} . \tag{5.63}$$

Note that γ_i^{M} and γ_i^{K} are defined for an arbitrary partition of the interval $[r_{\min}, r_{\max}]$. In the following, we will examine two types of partitions, a geometric partition and an equidistant partition of $[r_{\min}, r_{\max}]$.

Geometric partition Both Kronhamn and Mušicki use a common partition of the interval $[r_{\min}, r_{\max}]$ which is also employed in the RPEKF [KG05]: The range interval is divided into N subintervals in a geometric progression

$$r_{i+1} = \rho r_i \tag{5.64}$$

so that

$$\rho^N = \frac{r_{\max}}{r_{\min}} . \tag{5.65}$$

Fig. 5.3 shows such Gaussian mixture representation of the bearings-only measurement likelihood using geometric partition. With this approach, the non-linear effects are the

same for all subintervals and each ellipse has the same eccentricity which is an important numerical aspect [Kro98, Muš09].

Using geometric partition, the weights can be expressed as

$$\gamma_i^{\mathrm{M,g}} = \frac{r_i^2}{\sum_{j=1}^{N} r_j^2} = \rho^{2(i-1)} \frac{\rho^2 - 1}{\rho^{2N} - 1} \tag{5.66}$$

and

$$\gamma_i^{\mathrm{K,g}} = \frac{r_i}{\sum_{j=1}^{N} r_j} = \rho^{(i-1)} \frac{\rho - 1}{\rho^{N} - 1} \,. \tag{5.67}$$

Furthermore, $\gamma_i^{\mathrm{M,g}} = c(N,\rho) \left(\gamma_i^{\mathrm{K,g}}\right)^2$ holds. The proportionality constant c which only depends on N and ρ is given by

$$c(N,\rho) = \frac{\left(\rho^N - 1\right)(\rho + 1)}{\left(\rho^N + 1\right)(\rho - 1)} \,. \tag{5.68}$$

Equidistant partition Alternatively, one can divide the range interval into equidistant subintervals, see Fig. 5.3, so that the interval length Δr is constant, i.e.,

$$\Delta r = \Delta r_i = r_{i+1} - r_i = \frac{r_{\max} - r_{\min}}{N} = \text{const} \,. \tag{5.69}$$

With this, Mušicki's weights can be transformed to

$$\gamma_i^{\mathrm{M,q}} = \frac{\bar{r}_i}{\sum_{j=1}^{N} \bar{r}_j} \,. \tag{5.70}$$

Kronhamn's weights are constant and given by

$$\gamma_i^{\mathrm{K,q}} = \frac{1}{N} \,. \tag{5.71}$$

5.5.3 Derivation of the Likelihood Approximations

In this section, Mušicki's and Kronhamn's Gaussian mixture likelihood approximations will be derived from Streit's formulation of the approximate bearings-only likelihood which is linear in target state. If we restrict the range to the interval $[r_{\min}, r_{\max}]$, we can write (5.53) due to the symmetry of the Gaussian distribution as

$$\tilde{p}(\mathbf{z}|\mathbf{x}) = \frac{1}{k} \int_{r_{\min}}^{r_{\max}} r \mathcal{N}\left(\mathbf{y};\, f(\boldsymbol{\zeta}), \boldsymbol{\Sigma}\right) \mathrm{d}r \,, \tag{5.72}$$

where the definitions from Subsections 5.5.1 and 5.5.2 hold. According to (5.50), the normalizing factor k is given by

$$k = \int_{r_{\min}}^{r_{\max}} r \, \mathrm{d}r = \frac{1}{2}\left(r_{\max}^2 - r_{\min}^2\right). \tag{5.73}$$

It is well known that (5.72) can be approximated by a Riemann sum.

Riemann sum Let $f : D \to \mathbb{R}$ be a function defined on a subset D of $\mathbb{R}$. Let $[a, b] \subseteq D$ be a closed interval contained in D and let

$$P = \{[x_1, x_2), [x_2, x_3), \ldots, [x_N, x_{N+1}]\} \tag{5.74}$$

be a partition of $[a, b]$, where

$$a = x_1 < x_2 < x_3 < \ldots < x_N < x_{N+1} = b\,. \tag{5.75}$$

The *Riemann sum* of f over $[a, b]$ with partition P is defined as

$$S = \sum_{i=1}^{N} f(x_i^*)(x_{i+1} - x_i), \quad x_i \le x_i^* \le x_{i+1}\,. \tag{5.76}$$

Note that partition P is arbitrary as long as it complies with the condition given in (5.75). Especially it need not to be equidistant. Note further that the choice of x_i^* in $[x_i, x_{i+1}]$ is also arbitrary. If $x_i^* = (x_{i+1} + x_i)/2$, S is called a *middle Riemann sum*.

Therefore, expressing (5.72) as a middle Riemann sum leads to

$$S = \frac{2}{r_{\max}^2 - r_{\min}^2} \sum_{i=1}^{N} \bar{r}_i \mathcal{N}\left(\mathbf{y}; \hat{\mathbf{y}}_i, \mathbf{T}\begin{bmatrix}\sigma_r^2 & 0\\ 0 & \bar{r}_i^2\sigma_\theta^2\end{bmatrix}\mathbf{T}^{\mathrm{T}}\right)\Delta r_i \tag{5.77}$$

with $\hat{\mathbf{y}}_i$, $\bar{r}_i$, and Δr_i defined as in Subsection 5.5.2. Setting $\sigma_r = \Delta r_i/2$ and transforming the weights according to

$$\begin{aligned}\frac{2\bar{r}_i\Delta r_i}{r_{\max}^2 - r_{\min}^2} &= \frac{\bar{r}_i\Delta r_i}{\sum_{j=1}^{N}\bar{r}_j\Delta r_j}\\ = \frac{\sigma_\theta\bar{r}_i\Delta r_i/2}{\sum_{j=1}^{N}\sigma_\theta\bar{r}_j\Delta r_j/2} &= \frac{\sqrt{\det\mathbf{\Sigma}_i}}{\sum_{j=1}^{N}\sqrt{\det\mathbf{\Sigma}_j}}\,,\end{aligned} \tag{5.78}$$

we exactly obtain the parameters of Mušicki's Gaussian mixture approximation, see (5.60).

On the other hand, to gain Kronhamn's weights, we observe the following: Since the probability density function of the normal distribution is always greater than zero, we

can apply the *mean value theorem* for integration to (5.72) which says that there exists a $\xi(\mathbf{y}) \in [r_{\min}, r_{\max}]$ such that

$$\frac{1}{k}\int_{r_{\min}}^{r_{\max}} r\mathcal{N}\left(\mathbf{y};\,\hat{\mathbf{y}},\boldsymbol{\Sigma}\right)\mathrm{d}r = \xi(\mathbf{y})\frac{1}{k}\int_{r_{\min}}^{r_{\max}} \mathcal{N}\left(\mathbf{y};\,\hat{\mathbf{y}},\boldsymbol{\Sigma}\right)\mathrm{d}r = \psi(\mathbf{z}|\mathbf{x})\,. \tag{5.79}$$

Expressing (5.79) as middle Riemann sum yields

$$S = \frac{2\xi(\mathbf{y})}{r_{\max}^2 - r_{\min}^2}\sum_{i=1}^{N}\mathcal{N}\left(\mathbf{y};\,\hat{\mathbf{y}}_i,\mathbf{T}\begin{bmatrix}\sigma_r^2 & 0\\ 0 & \bar{r}_i^2\sigma_\theta^2\end{bmatrix}\mathbf{T}^{\mathrm{T}}\right)\Delta r_i \tag{5.80}$$

with $\hat{\mathbf{y}}_i$, $\bar{r}_i$, and Δr_i defined as in Subsection 5.5.2. If we choose ξ to be

$$\xi(\mathbf{y}) = \frac{r_{\max} + r_{\min}}{2}\,, \tag{5.81}$$

i.e., ξ is the interval center of $[r_{\min}, r_{\max}]$, and $\sigma_r = \Delta r_i/2$, then we obtain the weights as equal to Kronhamn's approach (5.61):

$$\frac{2\xi(\mathbf{y})\Delta r_i}{r_{\max}^2 - r_{\min}^2} = \frac{\Delta r_i}{r_{\max} - r_{\min}} = \frac{\Delta r_i}{\sum_{j=1}^{N}\Delta r_j}\,. \tag{5.82}$$

Choosing ξ as above to approximate (5.80) is one possibility. However, it leads to an approach which is widely used so that it is worth investigating. In the following section, we will highlight some convenient properties of this approach.

5.5.4 Analysis

In Section 5.5.3 we have chosen $\xi(\mathbf{y}) = (r_{\max} + r_{\min})/2$ to derive Kronhamn's weights. The open question is: Why is this reasonable? Due to (5.79) we can write

$$\xi(\mathbf{y}) = \frac{\int_{r_{\min}}^{r_{\max}} r\mathcal{N}\left(\mathbf{y};\,\hat{\mathbf{y}},\boldsymbol{\Sigma}\right)\mathrm{d}r}{\int_{r_{\min}}^{r_{\max}} \mathcal{N}\left(\mathbf{y};\,\hat{\mathbf{y}},\boldsymbol{\Sigma}\right)\mathrm{d}r}\,. \tag{5.83}$$

In Fig. 5.4 $\xi(\mathbf{y})$ is visualized as a contour plot for $\theta = 45°$, $r_{\min} = 0.1\,\mathrm{m}$, and $r_{\max} = 2000\,\mathrm{m}$. The figure indicates the following hypothesis: Let

$$\xi^{+}(\mathbf{y}) = \xi(\mathbf{y})\begin{bmatrix}\sin\theta\\ \cos\theta\end{bmatrix}\,. \tag{5.84}$$

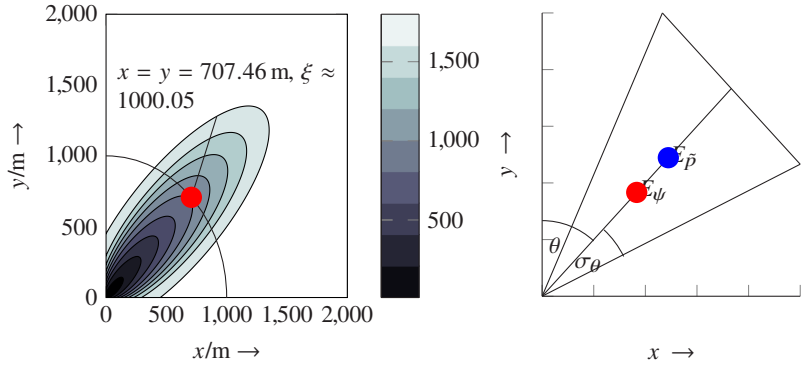

Figure 5.4: Left: Contour plot of $\xi(\mathbf{y})$. The red dot is plotted at coordinates $(r_{\max} + r_{\min})[\sin\theta, \cos\theta]^{\mathrm{T}}/2$ with $\theta = 45°$, $r_{\min} = 0.1\,\mathrm{m}$, $r_{\max} = 2000\,\mathrm{m}$. The function value at that coordinate is $(r_{\max} + r_{\min})/2$. Right: Visualization of E_ψ as centroid of the isosceles triangle and $\mathrm{E}_{\tilde{p}}$ as interval center, © 2014 IEEE.

Then

$$\mathbf{y}^* = \frac{r_{\max} + r_{\min}}{2} \begin{bmatrix} \sin\theta \\ \cos\theta \end{bmatrix} \tag{5.85}$$

is a fixed point of ξ^+, i.e., $\xi^+(\mathbf{y}^*) = \mathbf{y}^*$ or equivalently $\xi(\mathbf{y}^*) = (r_{\max} + r_{\min})/2$. The further analysis as well as the simulation study will support this hypothesis.

The expected value of $\tilde{p}(\mathbf{z}|\mathbf{x})$ (5.72) with respect to $\mathbf{z}$ is given by

$$\mathrm{E}_{\tilde{p}}\{\mathbf{z}\} = \frac{2}{3}\frac{r_{\max}^3 - r_{\min}^3}{r_{\max}^2 - r_{\min}^2} \begin{bmatrix} \sin\theta \\ \cos\theta \end{bmatrix} \approx \frac{2}{3} r_{\max} \begin{bmatrix} \sin\theta \\ \cos\theta \end{bmatrix} \tag{5.86}$$

for small $r_{\min}$. For a derivation, see Appendix B.2. Due to the calculations in Section 5.5.3, this is also the expected value for $\tilde{p}(\mathbf{z}|\mathbf{x})$, the approximated likelihood using Mušicki's method. Considering $\psi(\mathbf{z}|\mathbf{x})$ (5.79) the expected value with respect to $\mathbf{z}$ is

$$\mathrm{E}_{\psi}\{\mathbf{z}\} = \xi(\mathbf{y}) \begin{bmatrix} \sin\theta \\ \cos\theta \end{bmatrix} = \frac{r_{\max} + r_{\min}}{2} \begin{bmatrix} \sin\theta \\ \cos\theta \end{bmatrix}, \tag{5.87}$$

which is due to (5.81).

Interpreted geometrically, the expected value of Mušicki's Gaussian mixture corresponds to the centroid of an isosceles triangle spanned by σ_θ and $r_{\max}$, see Fig. 5.4, since

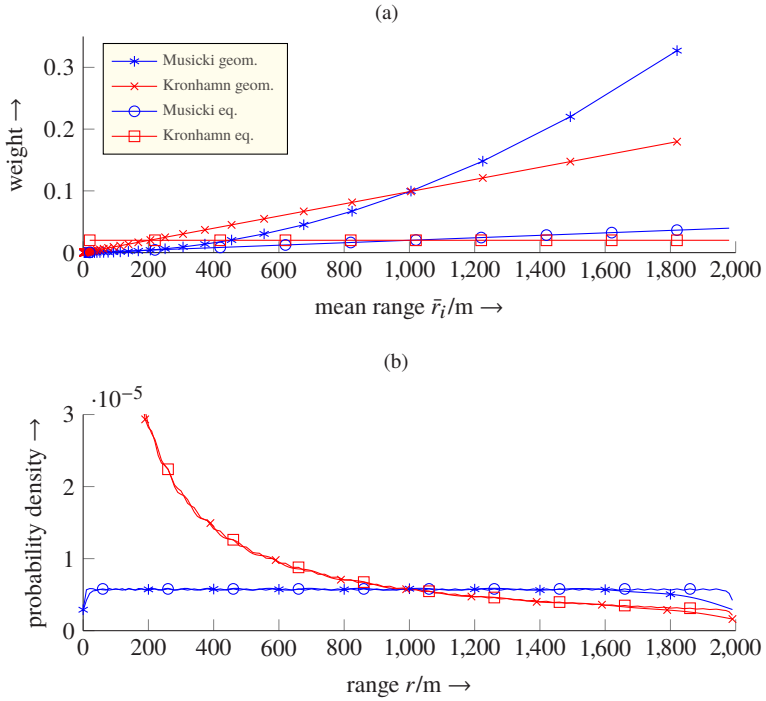

Figure 5.5: Gaussian mixture component weights (a) and Gaussian mixture probability density (b) vs. range for Mušicki's and Kronhamn's approach with geometric and equidistant partition, © 2014 IEEE.

Mušicki's approach considers the ellipses' areas. On the other hand, expected value of the Gaussian mixture with Kronhamn's weights is the center of the interval $[r_{\min}, r_{\max}]$.

For the further analysis, we assume that the number of Gaussian mixture components is $N = 50$, the minimum and maximum ranges are $r_{\min} = 0.1\,\text{m}$ and $r_{\max} = 2000\,\text{m}$, respectively, and the bearing θ is fixed to 45° with standard deviation $\sigma_\theta = 3°$.

Fig. 5.5 shows the Gaussian mixture component weights $\gamma_i^{\text{M,g}}$, $\gamma_i^{\text{K,g}}$, $\gamma_i^{\text{M,q}}$, and $\gamma_i^{\text{K,q}}$ versus mean range $\bar{r}_i$ for Mušicki's and Kronhamn's approach with geometric and equidistant partition. As indicated by the equations, Mušicki's weights with geometric partition increase quadratically. For equidistant partition we have a linear growth. Kronhamn's weights increase linearly with a geometric partition and are constant in the equidistant

case. Visually, the graphs of both approaches intersect at the center of the considered interval $[r_{\min}, r_{\max}]$. Analytically, for the intersection point in Fig. 5.5 $\gamma_i^{\mathrm{M}} = \gamma_i^{\mathrm{K}}$ holds. Using (5.63), this is solved by an r^* with

$$r^* = \frac{r_{\min} + r_{\max}}{2}, \tag{5.88}$$

which is equal to $\xi(\mathbf{z}^*)$ supporting the fixed point hypothesis.

Let

$$\tilde{p}_\theta(r) = \tilde{p}(\theta \mid r[\sin\theta, \cos\theta]^{\mathrm{T}}) = \tilde{p}(\mathbf{z}|\mathbf{x}) \tag{5.89}$$

be the PDF of the Gaussian mixture approximation depending only on range r with a fixed bearing θ. In Fig. 5.5, $\tilde{p}_\theta(r)$ is plotted against range for Mušicki's and Kronhamn's approach with geometric and equidistant partition. There are only slight differences between geometric and equidistant partition: Towards $r_{\max}$, the graphs using equidistant partition show a higher probability density. This is because the last geometric subinterval covers a big range whereas the same subinterval is covered by several segments using equidistant partition, see also Fig. 5.3. Comparing Mušicki's and Kronhamn's approach, we can see that the former initially has high probability density which is monotonically decreasing, whereas the latter basically remains constant over the whole range, close to a uniform distribution over $[r_{\min}, r_{\max}]$. Also here, we have an intersection meaning equal probability density at the interval center. This follows directly from the fixed point hypothesis.

Define

$$d_\theta(\mathbf{z}) = \tilde{p}^{\mathrm{M}}(\mathbf{z}|\mathbf{x}) - \tilde{p}^{\mathrm{K}}(\mathbf{z}|\mathbf{x}) \tag{5.90}$$

as difference between the likelihoods of Mušicki's and Kronhamn's approaches which is defined for geometric as well as equidistant partition. Fig. 5.6 depicts the difference $d_\theta(\mathbf{z})$ for geometric and equidistant partition as contour plot, respectively. Here, dark colors illustrate negative and bright colors positive values. The arcs show maximum range and the interval center. In both cases, the difference is negative in the first half of the interval and positive in the second half. Since Kronhamn's approach puts more weight on targets with a small range and Mušicki's approach does so with targets with a high range regarding cross-over point r^* (see also Fig. 5.5), we can conclude that Kronhamn's approach provides a better approximation of the bearings-only likelihood (5.53) if the target range is less than r^* and Mušicki's approach is superior when the target range is greater than r^*.

5.5.5 Simulation Study

The scenario is depicted in Fig. 5.7. A single sensor mounted on a vehicle follows a constant velocity trajectory for 50 s starting at position [65 m, 55 m] with speed 18 m/s and

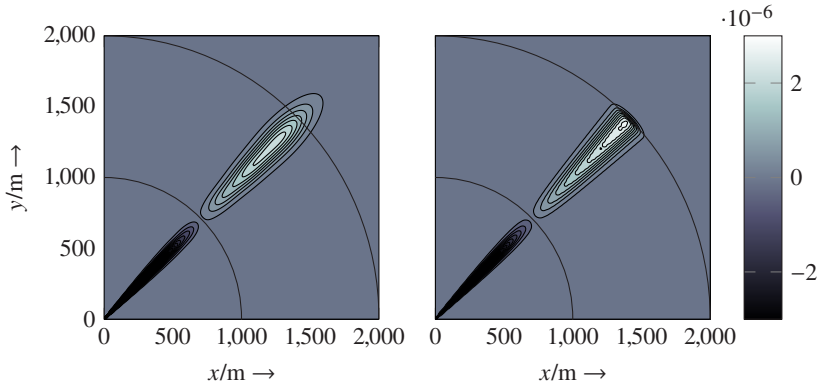

Figure 5.6: Contour plot of difference $d_\theta(\mathbf{z})$ from Mušicki's to Kronhamn's approach with geometric (left) and equidistant (right) partition. $r_{\max}$ and the interval half are depicted by the arcs, © 2014 IEEE.

heading 326°. The sensor scan time is 1 s and, as in the above sections, it is assumed that $r_{\min} = 0.1\,\text{m}$ and $r_{\max} = 2000\,\text{m}$. The measurements noise is assumed to be white and Gaussian distributed with zero mean and $\sigma_\theta = 3°$. Here, no missed and false detections are assumed, thus $p_D = 1$ and $\rho_F = 0$. In order to evaluate the performance of both approaches, two experiments are conducted: the first one with a static target near $r_{\min}$ at $[250\,\text{m}, 100\,\text{m}]$ and the second one with a static target near $r_{\max}$ at $[1400\,\text{m}, 1400\,\text{m}]$.

The Gaussian mixture likelihood approximation is performed with $N = 50$ components. 1000 Monte Carlo runs are carried out to produce the root mean square estimation error (RMSE) results illustrated in Fig. 5.8a for the nearby target and Fig. 5.8b for the distant target. Considering the nearby target, Kronhamn's approach clearly outperforms Mušicki's approach as predicted by the analysis in Section 5.5.4. The RMSE for geometric and equidistant partition which behave similarly is about 25 m after the initial phase. Mušicki's approach with geometric partition has an RMSE of about 70 m. An inferior performance is achieved by Mušicki's approach with equidistant partition which has an RMSE of about 600 m and is not depicted here. The situation is different for the distant target. Here, Mušicki's approach shows a better performance than Kronhamn's approach. Furthermore, equidistant partition has a slight advantage with an RMSE of about 110 m compared to the geometric partition with an RMSE of about 230 m. The results of this simulation study confirm the fixed point hypothesis. Furthermore, a similiar study is performend in Section 6.2.3 based on real sensor data and thus assuming a probability of detection p_D lower than one and a non-zero clutter density ρ_F since false and missed detections could occur when using a real sensor.

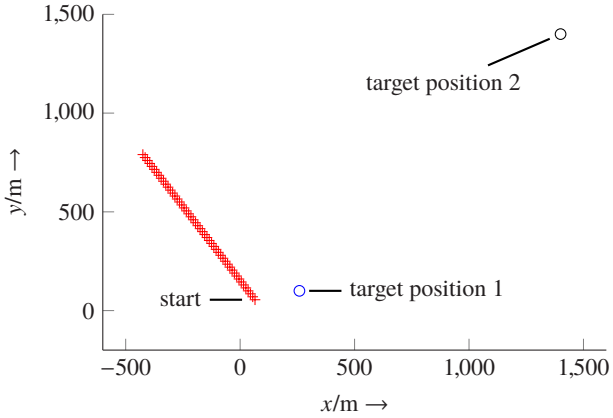

Figure 5.7: Scenario for GMF simulation study, © 2014 IEEE.

5.6 Non-Bayesian State Estimation

This section is dedicated to the central theme of bearings-only tracking for maneuvering targets as it introduces the maximum likelihood estimator which will be applied to the piecewise motion models presented in Chapter 2.

5.6.1 Maximum Likelihood Estimator

The maximum likelihood estimator (MLE) provides an estimate $\hat{\mathbf{x}}_{\ell|\ell}$ of a d-dimensional state vector $\mathbf{x}_\ell$ at time t_ℓ based on a measurement sequence up to time $t_k \geq t_\ell$, namely $\mathbf{Z}_{1:k} = \{\mathbf{z}_1, \ldots, \mathbf{z}_k\}$, by maximizing the likelihood function $p(\mathbf{Z}_{1:k}|\mathbf{x}_\ell)$, i.e.,

$$\hat{\mathbf{x}}_{\ell|\ell} = \arg\max_{\mathbf{x}_\ell} p(\mathbf{Z}_{1:k}|\mathbf{x}_\ell) \,. \tag{5.91}$$

In contrast to the Bayesian method, no prior of the state $\mathbf{x}_\ell$ is needed – the state is modeled as an unknown constant and not as a random variable. The estimate is solely based on the likelihood including a batch of all past measurements. Therefore, MLE approaches are often referred to as batch methods since the entire data has to be processed simultaneously for every time t_i. This makes batch methods computationally demanding. On the other hand, it does not need a proper initialization which is often the reason that filters diverge when applied for estimation problem which are not observable initially [LZJ02, HAGL83].

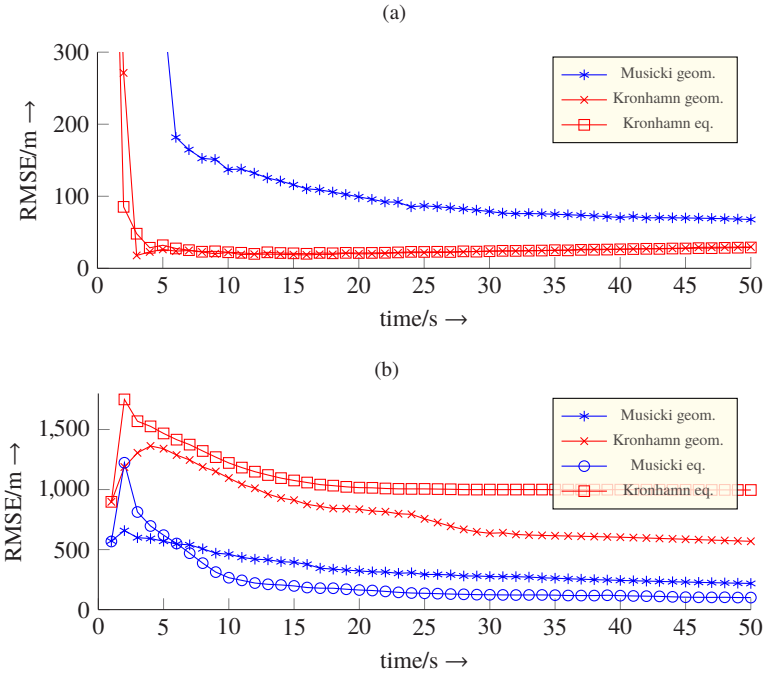

Figure 5.8: (a) RMSE for target at [250 m, 100 m] and (b) RMSE for target at [1400 m, 1400 m], © 2014 IEEE.

The maximum likelihood method has been introduced by Fisher in 1912 [Fis12] based on the least squares techniques by Gauss and Legendre. The MLE has been successfully applied in the domain of bearings-only tracking, see e.g. [HAGL83,Bec05b,Bec92,NLG84]. Similar to the pseudomeasurement filter, there is also a coordinate transformation technique leading to a pseudo-linear estimator (PLE) [LG78, HH93, NG97]. This results in a linear measurement equation so that the optimization can be performed in closed-form[2]. However, the PLE suffers from bias problems so that bias compensation techniques have been developed [Doğ06]. Regarding maneuvering targets, Kirubarajan et al. [KBSL01] have designed a MLE solution including the interacting multiple model (IMM) approach, until then only incorporated into recursive filters. The technique in this thesis is an alternative approach since we use a motion models that imply most other motion types as special cases, rather than different switching models.

[2] Under the assumption that the motion equation is also linear which is not the case in this thesis.

If we consider the nonlinear system (3.1) with deterministic trajectory and Gaussian measurement noise assumptions repeated here

$$\mathbf{x}_k = \mathbf{f}_{k-1}(\mathbf{x}_{k-1}) \tag{5.92a}$$

$$\mathbf{z}_k = \mathbf{h}_k(\mathbf{x}_k) + \boldsymbol{\nu}_k\,, \tag{5.92b}$$

the likelihood turns out to be Gaussian. To simplify matters, but without loss of generality, we assume that $\ell = 1$, i.e. the earliest state in chronologically order is estimated. Since the motion equation is deterministic, the state at t_k can be reconstructed uniquely by repeated application of the state transition function (cf. (2.42)),

$$\mathbf{x}_k = \mathbf{f}(\mathbf{x}_1; t_k, t_1) = \mathbf{f}_{k-1}(\mathbf{f}_{k-2}(\cdots \mathbf{f}_1(\mathbf{x}_1)))\,. \tag{5.93}$$

Since the exponent of a Gaussian is negative and since a Gaussian can be simplified using its logarithm, the MLE is equal to minimizing a cost function $Q(\mathbf{x}_1)$,

$$\hat{\mathbf{x}}_{1|k} = \arg\min_{\mathbf{x}_1} Q_k(\mathbf{x}_1)\,, \tag{5.94}$$

where the scalar $Q_k(\mathbf{x}_1)$ is given by a quadratic form

$$Q_k(\mathbf{x}_1) = \boldsymbol{\eta}_k(\mathbf{x}_1)^{\mathrm{T}} \mathbf{W}_k^{-1} \boldsymbol{\eta}_k(\mathbf{x}_1)\,. \tag{5.95}$$

Thus, it can be recognized that the MLE complies with the least squares solution [Sor70] for $\hat{\mathbf{x}}_{1|1}$. Here, $\boldsymbol{\eta}_k(\mathbf{x}_1)$ is the stacked vector of residuals

$$\boldsymbol{\eta}_k(\mathbf{x}_1) = \begin{bmatrix} \mathbf{z}_1 - \mathbf{h}_1(\mathbf{x}_1) \\ \mathbf{z}_2 - \mathbf{h}_2(\mathbf{f}_1(\mathbf{x}_1)) \\ \vdots \\ \mathbf{z}_k - \mathbf{h}_k(\mathbf{f}(\mathbf{x}_1; t_k, t_1)) \end{bmatrix}, \tag{5.96}$$

where $\mathbf{W}_k$ is a diagonal stacked matrix of measurement covariance matrices assuming that the measurements are uncorrelated,

$$\mathbf{W}_k = \begin{bmatrix} \mathbf{R}_1 & \mathbf{0} & \cdots & \mathbf{0} \\ \mathbf{0} & \mathbf{R}_2 & \cdots & \mathbf{0} \\ \vdots & \vdots & \ddots & \vdots \\ \mathbf{0} & \mathbf{0} & \cdots & \mathbf{R}_k \end{bmatrix}. \tag{5.97}$$

Due to the diagonal form of $\mathbf{W}_k$, the cost function can also be expressed as sum:

$$Q_k(\mathbf{x}_1) = \sum_{j=1}^{k} \left[\mathbf{z}_j - \mathbf{h}_j(\mathbf{f}(\mathbf{x}_1; t_j, t_1))\right]^{\mathrm{T}} \mathbf{R}_j^{-1} \left[\mathbf{z}_j - \mathbf{h}_j(\mathbf{f}(\mathbf{x}_1; t_j, t_1))\right] . \tag{5.98}$$

In general, there is no closed-form solution available to find the minimum in (5.94) since nonlinear functions are involved. Therefore, numerical optimization methods have to be applied. Popular examples are the Levenberg-Marquardt algorithm [Mor78], the Nelder-Mead simplex algorithm [NM65], or the the Gauss-Newton method [Wed74]. A more sophisticated approach is to find a coarse global optimum, for example by using controlled random search (CRS) with local mutation [Pri83, KA06] and polish this value to a greater accuracy with local optimization algorithms on a smaller region [Joh14]. Here, BOBYQA (bound optimization by quadratic approximation) [Pow09], a local derivative-free method, or MMA (method of moving asymptotes) [Sva02], a local gradient-based algorithm, can be applied. See also Chapter 6.

5.6.2 MLE for Bearings-only Tracking of Maneuvering Targets

We recall the measurement functions for bearing (2.12), bearing rate (2.14), and range measurements (3.63),

$$\alpha(\mathbf{x}_k) = \arctan \frac{\Delta x_k}{\Delta y_k} \tag{5.99a}$$

$$\dot{\alpha}(\mathbf{x}_k) = \frac{\Delta \dot{x}_k \Delta y_k - \Delta \dot{y}_k \Delta x_k}{\Delta x_k^2 + \Delta y_k^2} \tag{5.99b}$$

$$\rho(\mathbf{x}_k) = \sqrt{\Delta x_k^2 + \Delta y_k^2}\,, \tag{5.99c}$$

where Δ denotes the respective state component's difference from the target to the observer. Furthermore, α_k^{m}, $\dot{\alpha}_k^{\mathrm{m}}$, and ρ_k^{m} are the respective measurements, which are related to the measurement equations by means of a noise term with zero mean and standard deviations σ_α, $\sigma_{\dot{\alpha}}$, and σ_ρ, respectively.

As the measurements are assumed to be uncorrelated, the structure of the cost function Q_k (5.98) for the different measurement combinations (see also Section 3.3) is as follows:

$$Q_k(\mathbf{x}_1) = \begin{cases} Q_k^{\alpha}(\mathbf{x}_1) & \text{for bearings-only (BO)} \\ Q_k^{\alpha}(\mathbf{x}_1) + Q_k^{\dot{\alpha}}(\mathbf{x}_1) & \text{for bearing and bearing rate (B-BR)} \\ Q_k^{\alpha}(\mathbf{x}_1) + Q_k^{\rho}(\mathbf{x}_1) & \text{for bearing and range (BR)} \end{cases}, \tag{5.100}$$

where the individual cost functions are specified by

$$Q_k^{\psi}(\mathbf{x}_1) = \frac{1}{\sigma_{\psi}^2} \sum_{j=1}^{k} \left[\psi_j^{\mathrm{m}} - \psi(\mathbf{f}(\mathbf{x}_1; t_j, t_1)) \right]^2 \tag{5.101}$$

for $\psi = \{\alpha, \dot{\alpha}, \rho\}$.

Applying the piecewise inertial or piecewise curvilinear motion model from Chapter 2, the unknown maneuver change times are clearly part of the estimation problem. Note that with each maneuver change, the dimension of the state increases by three components, namely velocity in x- and y-direction and the maneuver change time in case of piecewise inertial motion, and tangential and normal acceleration as well as the maneuver change time for piecewise curvilinear motion.

In the literature, maneuver handling is commonly a testing or decision problem [LJ02]. In contrast to that, our approach tries to estimate the maneuver change time like estimating the target position or speed. As shown in Chapter 3, the CRLB can provide an estimation accuracy for the maneuver change time. This is an advantage over a decision-based approach where an explicit, hard decision about a maneuver change is taken without the possibility to provide an accuracy. Nevertheless, estimation and decision are strongly connected with each other [LJ02] since they both try to deduce an unknown quantity from available information. The difference is that decision uses a discrete set of possible solutions, whereas estimation is based on a continuous set. Hence, when assuming a discrete-time tracking problem, a decision-based approach has been preferred in the literature [BSLK01, BSF88, RJLB09] especially when a Bayesian estimator is used. In the own paper [HO11a] we have employed a decision-based method to detect course changes along with a Bayesian estimator, the particle filter. In this work, maneuver change time estimation is applied to a discrete-time tracking problem in order to evaluate its accuracy. Estimation is performed with a non-Bayesian approach.

For piecewise inertial or piecewise curvilinear motion, the aforementioned cost function is parameterized by a state vector with dimensions $(4 + 3M)$ or $(6 + 3M)$, respectively. including the unknown maneuver change times. It should be clear that the choice of the correct state vector dimension requires the knowledge of the number of maneuver change points M. However, in practice, this number is unknown. For the sake of simplicity, we assume that M is known a priori but the maneuver change times are unknown. This is a restricting condition, but it eases the estimation process since the estimation can be performed with a fixed sized state dimension. We emphasize that a state estimation concerning the target state with an increasing dimension when M is unknown is a hard and challenging task that is not covered in this thesis. Additionally, it is not necessary for a comparison with the CRLB. This estimator is a proof of concept to show that especially the maneuver change times can be estimated. The estimation results in Section 6.1 are based on this concept.

Alternatively, an estimation technique can be used that only considers one maneuver change. Thus, it tries to estimate the respective parameters from the current maneuver segment m (including the maneuver change time) and the parameters from the segment $m-1$. In the equations below, only the boxed elements are therefore part of the estimation process and the state dimension is constant. For piecewise inertial motion, we consider

$$\mathbf{x}_k = \left[\boxed{x_k, y_k};\ \dot{x}_0, \dot{y}_0, \ldots, \boxed{\dot{x}_{m-1}, \dot{y}_{m-1}, \dot{x}_m, \dot{y}_m};\ \tilde{t}_1, \ldots, \boxed{\tilde{t}_m}\right]^{\mathrm{T}} \tag{5.102}$$

and analogously, in case of piecewise curvilinear motion

$$\mathbf{x}_k = \left[\boxed{x_k, y_k, v_k, \varphi_k};\ a_{\mathrm{t},0}, a_{\mathrm{n},0}, \ldots, \boxed{a_{\mathrm{t},m-1}, a_{\mathrm{n},m-1}, a_{\mathrm{t},m}, a_{\mathrm{n},m}};\ \tilde{t}_1, \ldots, \boxed{\tilde{t}_m}\right]^{\mathrm{T}}. \tag{5.103}$$

The specific parameters of the other maneuver segments are regarded as nuisance parameters and are not estimated in this approach. Furthermore, it is not necessary to know the number of maneuver change points a priori. The algorithm detects the m-th maneuver change if the accuracy of the maneuver change time estimates is sufficiently precise and/or the acceleration estimates between the segments are sufficiently different. Finally, the results can be used as an initialization to estimate the full target state vector.

5.6.3 Combination of Bayesian and Non-Bayesian Estimation: Filter Initialization

We have learned that a Bayesian filter must be properly initialized by a prior density since it is a recursive scheme. More specifically, as only Gaussian assumptions are made in this thesis, an initial mean $\hat{\mathbf{x}}_{0|0}$ and covariance $\mathbf{P}_{0|0}$ has to be found somehow. As filters react "sluggish", meaning that outlying measurements do not affect a filter to a great extent since they are fused to a motion model, good initialization is crucial. Otherwise, the filter could diverge quickly. Hence, several techniques have been developed based on a small number of measurements, for example one-point or two-point initialization [BSLK01]. However, especially for bearings-only tracking this kind of initialization is not appropriate since the state is not observable before the first observer maneuver. To overcome this, one can use a batch MLE approach until the first observer maneuver and use the estimate as well as the CRLB for an initial mean and covariance [KBSL01]. This guarantees the best possible initialization for a recursive filter. On the other hand, likelihood approximation techniques as presented in Section 5.5 can be used without an initialization technique. However, a maximum range assumption needed for a finite number of Gaussian mixture components has to be made.

5.7 Summary of the Chapter

This chapter again combines the two central themes of this thesis. In the first part, several Bayesian filtering methods for linear and nonlinear systems have been derived which all base on the same scheme given by Bayes' rule which emerges into an iterative update scheme, called Kalman filter, for linear, Gaussian systems. Especially with bearings-only tracking in mind, the Gaussian mixture filter has been examined with its natural extension to multi-hypothesis tracking to account for missing and false observations. These usually occur in field tests. In order to find a strategy how to choose the Gaussian mixture components, two approaches based on the work of Kronhamn and Mušicki have been studied. The contribution is here that both approaches can be derived from a more general likelihood approximation introduced by Streit. The results of this comparison is that Kronhamn's and Mušicki's approaches are suitable for near and far targets, respectively. In the second part, non-Bayesian state estimation methods, namely the maximum likelihood estimator has been presented. It is intended for bearings-only tracking of maneuvering targets due to its robustness. Hence, similar to the CRLB in Chapter 3, the incorporation of piecewise motion models has been investigated. Having covered state estimation leads to its application to simulative as well as real scenarios in the following Chapter 6.

6 Experimental Results

6.1 Simulation Results for Bearings-only Tracking of Maneuvering Targets

In this section, the simulation results for a piecewise inertial and a piecewise curvilinear motion scenario are illustrated based on the aforementioned measurement combinations, bearings-only (BO), bearing and bearing rate (B-BR), and bearing and range (BR). For both motion models, first the CRLB is presented, and then the results of the estimation process using the maximum likelihood approach from Section 5.6 are presented. Here, 500 Monte Carlo runs are carried out in order to study the performance of the estimator. Finally, CRLB and estimation results are compared.

6.1.1 Piecewise Inertial Motion

For piecewise inertial motion we consider the 2D scenario depicted in Fig. 6.1. The target trajectory is given for 600 s by the initial state

$$[x(t_0), y(t_0)] = [1\,\text{km}, 5.5\,\text{km}] \tag{6.1}$$

and the following maneuver segments:

$$\begin{aligned} [t_0, v_0, \varphi_0] &= [0\,\text{s}, 15\,\text{m/s}, 60^\circ] \\ [\tilde{t}_1, v_1, \varphi_1] &= [200\,\text{s}, 15\,\text{m/s}, 150^\circ] \\ [\tilde{t}_2, v_2, \varphi_2] &= [400\,\text{s}, 15\,\text{m/s}, 90^\circ]\,. \end{aligned} \tag{6.2}$$

Thus, the target moves in three legs with a constant speed and performs two maneuver changes at times $\tilde{t}_1 = 200\,\text{s}$ and $\tilde{t}_2 = 400\,\text{s}$. Note that the maneuver segment parameters are given in polar coordinates due to readability. The observer moves according to the

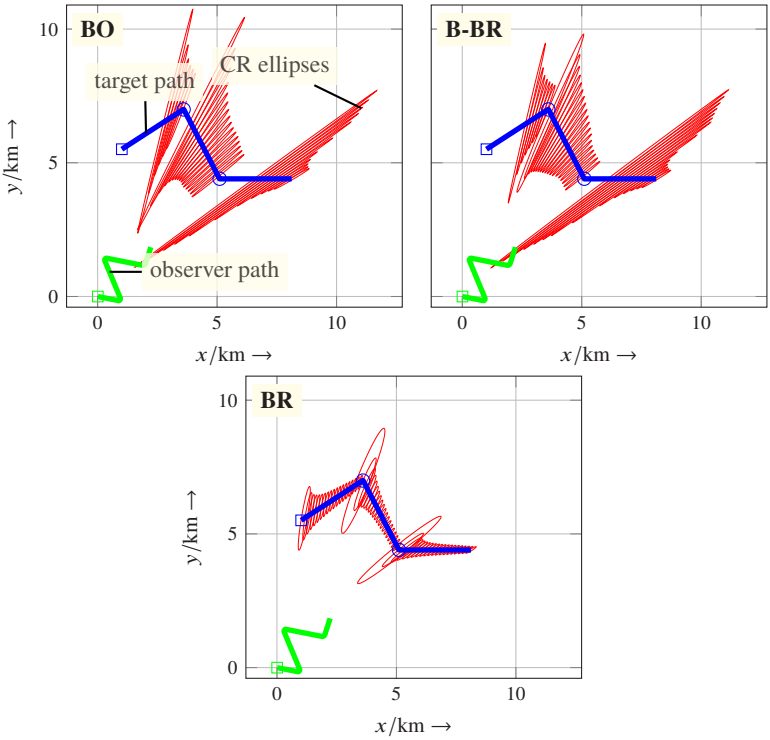

Figure 6.1: Piecewise inertial motion: Scenario and corresponding CRLB for BO, B-BR, and BR. The ellipses are scaled and drawn every 10 s. Ellipses with an with an extent of over 10 km are omitted, © 2014 IEEE.

depicted trajectory with four legs for 630 s from starting point [0 km, 0 km] with a constant speed of 8 m/s and the following maneuver segments:

$$\begin{aligned}
[t_0, \varphi_\mathrm{O}] &= [0\,\mathrm{s}, 100°] \\
[\tilde{t}_{\mathrm{O},1}, a_{\mathrm{O,n}}] &= [110\,\mathrm{s}, -0.87\,\mathrm{m/s^2}] \\
[\tilde{t}_{\mathrm{O},2}, \varphi_\mathrm{O}] &= [130\,\mathrm{s}, 335°] \\
[\tilde{t}_{\mathrm{O},3}, a_{\mathrm{O,n}}] &= [320\,\mathrm{s}, 0.87\,\mathrm{m/s^2}] \\
[\tilde{t}_{\mathrm{O},4}, \varphi_\mathrm{O}] &= [340\,\mathrm{s}, 100°] \\
[\tilde{t}_{\mathrm{O},5}, a_{\mathrm{O,n}}] &= [530\,\mathrm{s}, -0.56\,\mathrm{m/s^2}] \\
[\tilde{t}_{\mathrm{O},6}, \varphi_\mathrm{O}] &= [550\,\mathrm{s}, 20°]\,.
\end{aligned} \tag{6.3}$$

The observer's normal acceleration is zero in the segments 0, 2, 4, and 6. The observer collects measurements each second. Therefore, about 200 measurements are taken per target maneuver segment with the assumption that there are no missed detections. The standard deviations of the azimuth, the azimuth rate, and the range measurements are as follows:

$$\sigma_\alpha = 1^\circ, \quad \sigma_{\dot{\alpha}} = 1\,\text{mrad/s} \approx 0.057\,^\circ/\text{s}, \quad \sigma_\rho = 1000\,\text{m}. \tag{6.4}$$

Since the observer performs several maneuvers, the observability condition is fulfilled after the first observer maneuver in case of passive measurements (BO and B-BR).

Cramér-Rao Analysis

In Fig. 6.1, the CRLB for the target position using BO, B-BR, and BR is shown. The bounds are illustrated by means of uncertainty ellipses which are scaled in order to fit into the figures. The CRLB of BO, B-BR, and BR with respect to time is visualized in Fig. 6.2 and 6.3. This is carried out for the complete target state, namely position x, y, segment velocities, $\dot{x}_0$, $\dot{y}_0$, $\dot{x}_1$, $\dot{y}_1$, $\dot{x}_2$, $\dot{y}_2$, and maneuver change times $\tilde{t}_1$, $\tilde{t}_2$. Additionally, for clarification, the true maneuver change times of the target and the observer are shown in the referenced figures. The depicted bounds equal the square root of the respective diagonal elements of the inverted FIMs.

It can be recognized from Fig. 6.1, Fig. 6.2, and Fig. 6.3 that for all three segments of the target motion the estimation accuracy for the BO case is the lowest. Considering additional bearing rate measurements leads to an information gain, so that for the B-BR case, a better performance illustrated by smaller ellipses and bounds can be identified. For B-BR, the position accuracy is about 2 times higher than for BO, the velocity accuracy is at least 3 times higher, and the maneuver change time accuracy about 1.3 to 1.5 times. The highest accuracy is achieved when using bearing and range measurements (BR). It is about 13 times higher than for BO regarding position accuracy, at least 5 times higher regarding velocity accuracy, and about 1.5 to 3 times higher regarding maneuver change time accuracy. This makes clear that it is crucial whether range information is obtained directly (BR) or whether it has to be derived from passive measurements by means of a target motion analysis (BO and B-BR). Additionally, Fig. 6.2 and 6.3 illustrate that for BO and B-BR, a sufficient localization is possible only after the first observer maneuver. Before the first observer maneuver, the FIM is not invertible so that a reasonable bound cannot be provided. In contrast to that, for BR, observability is guaranteed from the beginning due to available range measurements. Therefore, a CRLB can be provided over the complete time.

At the target maneuver change times, the position CRLB rapidly increases for all three cases. This is because the state vector is augmented by three elements, namely the segment velocities in x and y direction as well as the maneuver change time, which contribute zero value entries to the FIM initially. Thus, only minimal information

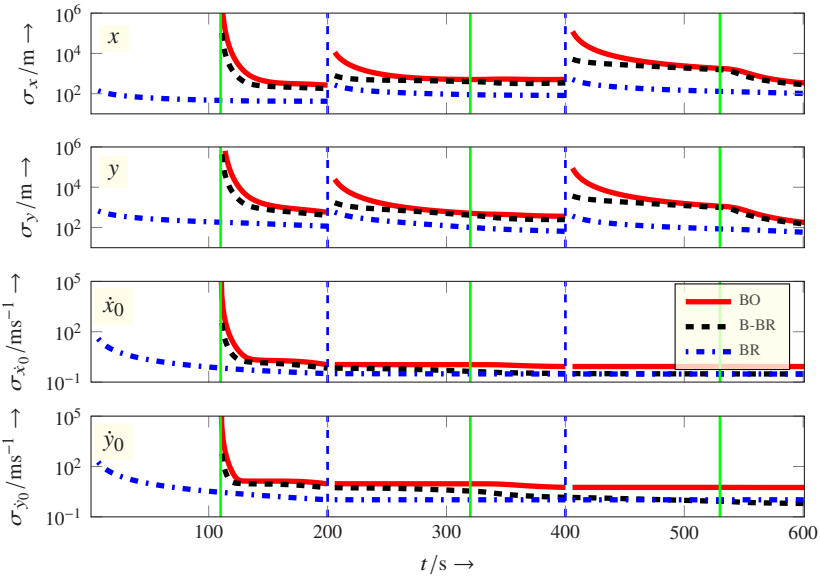

Figure 6.2: Piecewise inertial motion: Visualization of CRLB for target state components x, y, $\dot{x}_0$, and $\dot{y}_0$ regarding BO, B-BR, and BR. The solid vertical lines denote the observer maneuvers, the dashed vertical lines the target maneuvers, © 2014 IEEE.

about the current velocities is provided at the target maneuver change times. Due to the fact that the velocities could have arbitrary (high) values in theory, the uncertainty about the target position is high. Since no further constraints with respect to the target motion are considered, the target position might be unobservable shortly after a target maneuver. Mathematically, the inversion of the FIM with very small current segment velocity elements leads to a rapidly increasing position CRLB since all entries influence the position entries when performing the inversion. Since the segment velocities and the maneuver change times are constant estimation parameters and therefore they do not change with time, their bounds necessarily decrease monotonically. The velocities for segment m are not constant after the target has moved to segment $m+1$. One can recognize in Fig. 6.2 and 6.3 that the velocities from previous segments are nearly constant in later segments. The most variation can be seen for the B-BR case. This is because a bearing rate measurement carries information about the velocities which is not the case for BO and BR. Since we consider all past measurements for the CRLB, there is an influence on the velocity accuracy concerning a previous segment. However, the nearly constancy of the velocities shows that there is no absolute need to estimate them in later segments: they

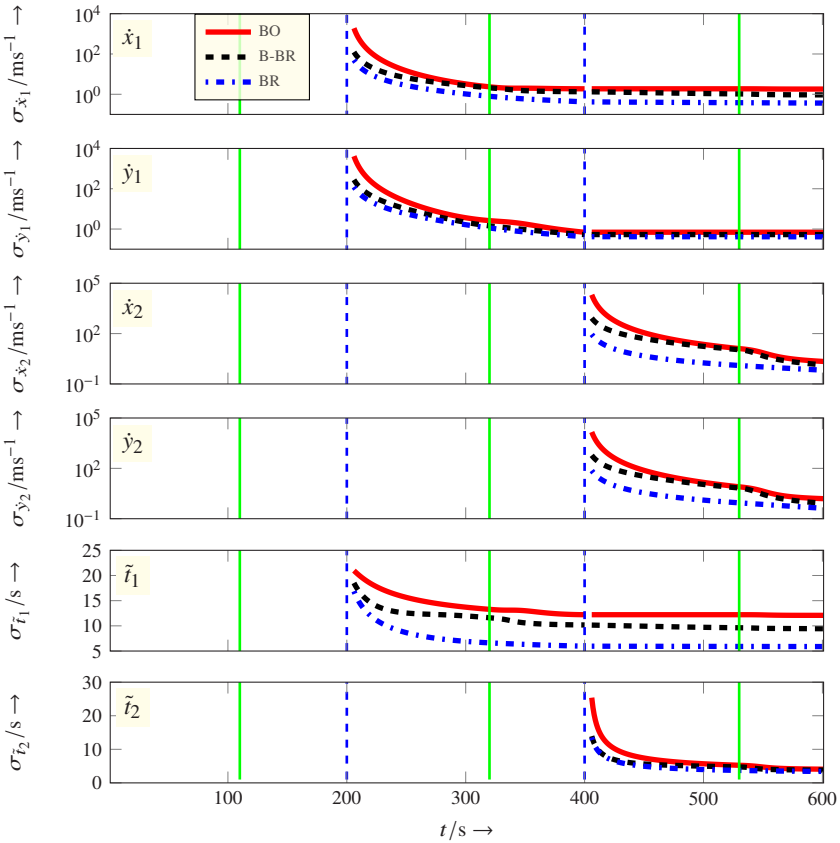

Figure 6.3: Piecewise inertial motion: Visualization of CRLB for target state components $\dot{x}_1$, $\dot{y}_1$, $\dot{x}_2$, $\dot{y}_2$, $\tilde{t}_1$, and $\tilde{t}_2$ regarding BO, B-BR, and BR. The solid vertical lines denote the observer maneuvers, the dashed vertical lines the target maneuvers, © 2014 IEEE.

can be identified as nuisance parameters and the estimation problem is therefore easier to solve. This approach has also been proposed in Section 5.6, see (5.102) and (5.103).

State Estimation

Here, the results of state estimation using a maximum likelihood estimator are compared to the CRLB. We assume the scenario illustrated in Fig. 6.1. For the considered scenario,

	Δx_k and Δy_k	Δx_k and $\Delta \dot{x}_1$
BO	1.9777	2.1987
BO bias corrected	1.9545	2.1094
B-BR	1.8752	1.9637
B-BR bias corrected	1.8328	1.9224
BR	2.0097	2.1297
BR bias corrected	2.0052	1.9910

Table 6.1: Piecewise inertial motion: NEES for BO, B-BR, and BR regarding the cases depicted in Fig. 6.4 and 6.5, © 2014 IEEE.

Monte Carlo simulations with 500 runs are carried out to study the performance of the ML estimator given in Section 5.6. In our simulations, we use the simplex method of Nelder and Mead [NM65] to find the minima of the respective cost functions (5.101) and we initialize every search with the true value. The results have been determined at time $t = 400\,\mathrm{s}$ which equals the first maneuver change time $\tilde{t}_2$.

The scattering of the Monte Carlo estimates around the true values is visualized in Fig. 6.4 and 6.5 by scatter plots of the estimation error. That means, estimation results are depicted as estimation errors so that the true target state is at $[0, 0]$. Here, the position error in x-direction, defined as $\Delta x_k = x_1 - \hat{x}_1$, i.e. the difference between true and estimated value, is compared to the position estimation error in y-direction, Δy_k, as well as the segment velocity estimation error in x-direction, $\Delta \dot{x}_1$, is shown regarding all three investigated tracking cases BO, B-BR, and BR. Assuming normally distributed estimation errors, the ellipse parameters have been chosen in such a way that the estimation error ellipses enclose 95.4% (2σ ellipse) of the sample values. We can recognize that the estimation error ellipses (sample covariance) and CRLB ellipses have a similar orientation and expansion, so the CRLB is mostly attained in the presented cases.

In Table 6.1 the normalized estimation error squared (NEES) for the cases depicted in Fig. 6.4 and 6.5 is given. The NEES indicates whether the estimator is efficient. The (single run) NEES at time t_k is defined as [BSLK01]

$$\epsilon_k = \Delta \mathbf{x}_k^{\mathrm{T}} \, \mathbf{J}_k \, \Delta \mathbf{x}_k \,, \tag{6.5}$$

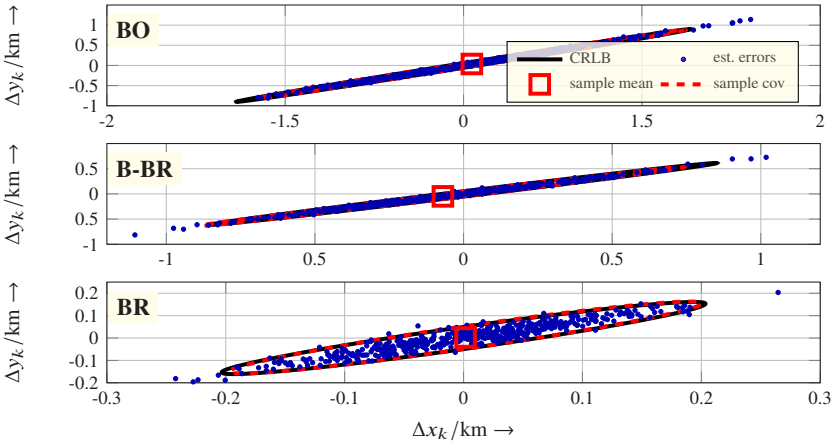

Figure 6.4: Piecewise inertial motion: Scatter plots of Monte Carlo estimation errors, corresponding estimation error ellipses, and CRLB ellipses plotted for Δx_k versus Δy_k regarding BO, B-BR, and BR at time $t = \tilde{t}_2 = 400\,\mathrm{s}$. The true target state is at $[0, 0]$, © 2014 IEEE.

where $\Delta\mathbf{x}_k$ comprises the errors of the respective parameters (in this case: Δx_k, Δy_k, and Δx_k, $\Delta \dot{x}_1$) and $\mathbf{J}_k$ is the FIM containing the respective entries. For N Monte Carlo runs, one has a sample average NEES as

$$\bar{\epsilon}_k = \frac{1}{N} \sum_{i=1}^{N} \epsilon_k^i \,, \tag{6.6}$$

where ϵ_k^i is the NEES (6.5) at time t_k for the i-th Monte Carlo run. The quantity $N\bar{\epsilon}_k$ is chi-square distributed with Nd degrees of freedom, where d is the dimension of the parameter set. Practically, one divides these values by N so that $\bar{\epsilon}_k$ hat to lie in an interval around d for the estimator to be efficient. Hence, if we consider a two-sided 95% acceptance region given by the interval $(1.8285, 2.1790)$ for two dimensions and $N = 500$ Monte Carlo runs, it can be seen that most NEES values, in particular all bias corrected NEES values, are within this range. That means that our estimator is consistent regarding the illustrated cases. The bias correction has been carried out in a way that the mean error over all Monte Carlo runs has been subtracted from the respective error for all parameters.

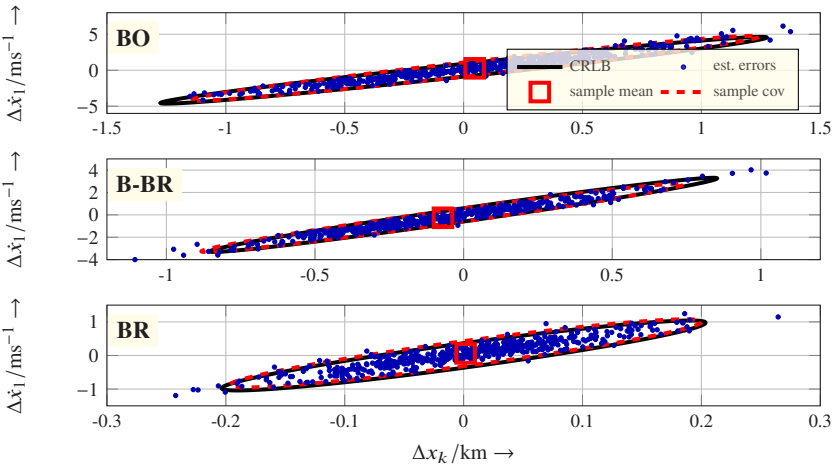

Figure 6.5: Piecewise inertial motion: Scatter plots of Monte Carlo estimation errors, corresponding estimation error ellipses, and CRLB ellipses plotted for Δx_k versus $\Delta\dot{x}_1$ regarding BO, B-BR, and BR at time $t = \tilde{t}_2 = 400\,\mathrm{s}$. The true target state is at $[0, 0]$, © 2014 IEEE.

6.1.2 Piecewise Curvilinear Motion

In this section, we consider the piecewise curvilinear motion scenario in Fig. 6.6. The target starts with the initial state

$$[x(t_0), y(t_0), v(t_0), \varphi(t_0)] = [-9\,\mathrm{km}, 12\,\mathrm{km}, 50\,\mathrm{m/s}, 90°] \tag{6.7}$$

and performs the maneuvers described by the following maneuver segments:

$$\begin{aligned} [t_0, a_{\mathrm{t},0}, a_{\mathrm{n},0}] &= [0\,\mathrm{s}, 0\,\mathrm{m/s^2}, 0\,\mathrm{m/s^2}] \\ [\tilde{t}_1, a_{\mathrm{t},1}, a_{\mathrm{n},1}] &= [400\,\mathrm{s}, 0\,\mathrm{m/s^2}, 0.5\,\mathrm{m/s^2}] \\ [\tilde{t}_2, a_{\mathrm{t},2}, a_{\mathrm{n},2}] &= [600\,\mathrm{s}, 0\,\mathrm{m/s^2}, 0\,\mathrm{m/s^2}]\,. \end{aligned} \tag{6.8}$$

So, the target moves inertially in the first and the last segment and performs a constant turn motion in the second segment. The maneuver change times are at $\tilde{t}_1 = 400\,\mathrm{s}$ and $\tilde{t}_2 = 600\,\mathrm{s}$. With each maneuver change the state dimension increases by three elements. Hence, the state consists of 6 elements at t_0 and 12 elements at $t_{\max} = 1000\,\mathrm{s}$. The observer moves for 1100 s counterclockwise along a circular path with a constant velocity. This is parameterized by $\mathbf{r}_{\mathrm{O}}(t_0) = [0\,\mathrm{km}, 0\,\mathrm{km}]^{\mathrm{T}}$, $|\dot{\mathbf{r}}_{\mathrm{O}}(t_0)| = 50\,\mathrm{m/s}$, $\varphi_{\mathrm{O}}(t_0) = 0°$, and $a_{\mathrm{O,n}} = -1.25\,\mathrm{m/s^2}$. The observer collects measurements each second with no missed

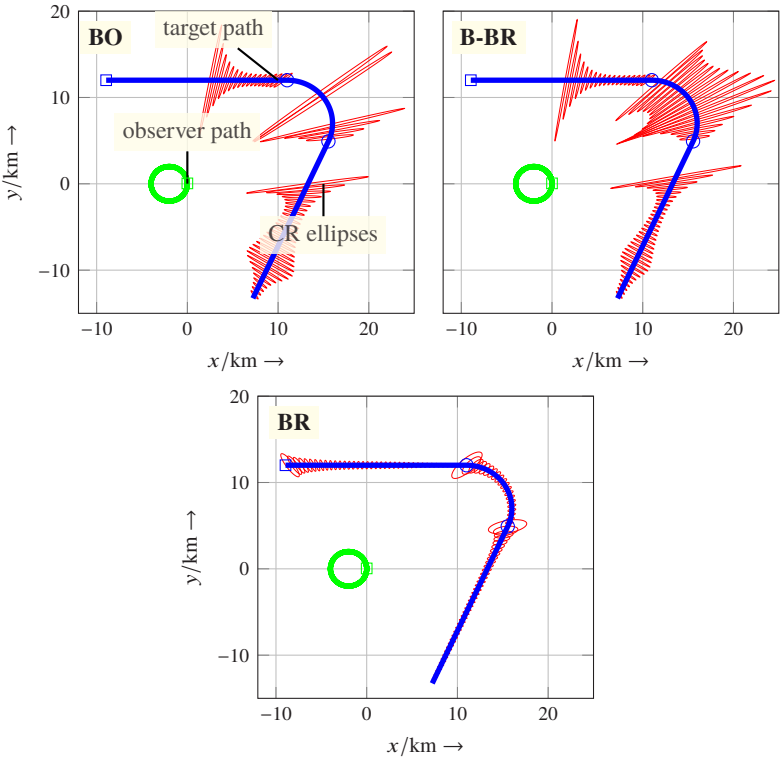

Figure 6.6: Piecewise curvilinear motion: Scenario and corresponding CRLB for BO, B-BR, and BR. The ellipses are scaled and drawn every 10 s. Ellipses with an extent of over 10 km are omitted, © 2014 IEEE.

detections. Hence, 400 measurements are taken in the first and the last segment and 200 in the middle segment. The standard deviations for bearing, bearing rate, and range measurements are the same as in Subsection 6.1.1,

$$\sigma_\alpha = 1^\circ, \quad \sigma_{\dot{\alpha}} = 1\,\text{mrad/s} \approx 0.057\,^\circ/\text{s}, \quad \sigma_\rho = 1000\,\text{m}. \tag{6.9}$$

From the observability condition established in [Bec96], it follows that the state of an inertial moving target can be determined from azimuth measurements obtained from a sensor moving on a circular path. So, for the considered scenario the uniqueness condition is already fulfilled in the first segment of the target trajectory.

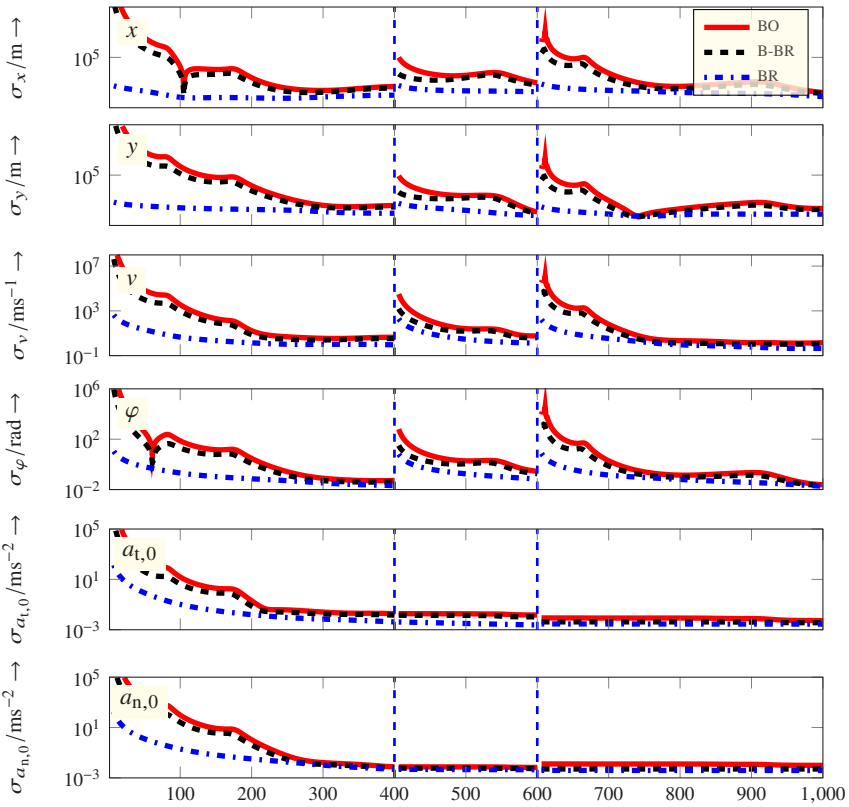

Figure 6.7: Piecewise curvilinear motion: Visualization of CRLB for x, y, v, φ, $a_{\mathrm{t},0}$, $a_{\mathrm{n},0}$ regarding BO, B-BR, and BR. The dashed vertical lines denote the target maneuvers, © 2014 IEEE.

Cramér-Rao Analysis

In Fig. 6.6, the ellipses representing the CRLB for target position considering BO, B-BR, and BR are depicted. Fig. 6.7 and 6.8 show the CRLB of BO, B-BR, and BR for the full target state with respect to time. This includes target position, speed, and course, as well as the tangential accelerations $a_{\mathrm{t},0}$, $a_{\mathrm{t},1}$, $a_{\mathrm{t},2}$, the normal accelerations $a_{\mathrm{n},0}$, $a_{\mathrm{n},1}$, $a_{\mathrm{n},2}$, and the maneuver change times $\tilde{t}_1$ and $\tilde{t}_2$ regarding the three segments. The depicted lines are the square roots of the respective diagonal elements of the inverted FIMs.

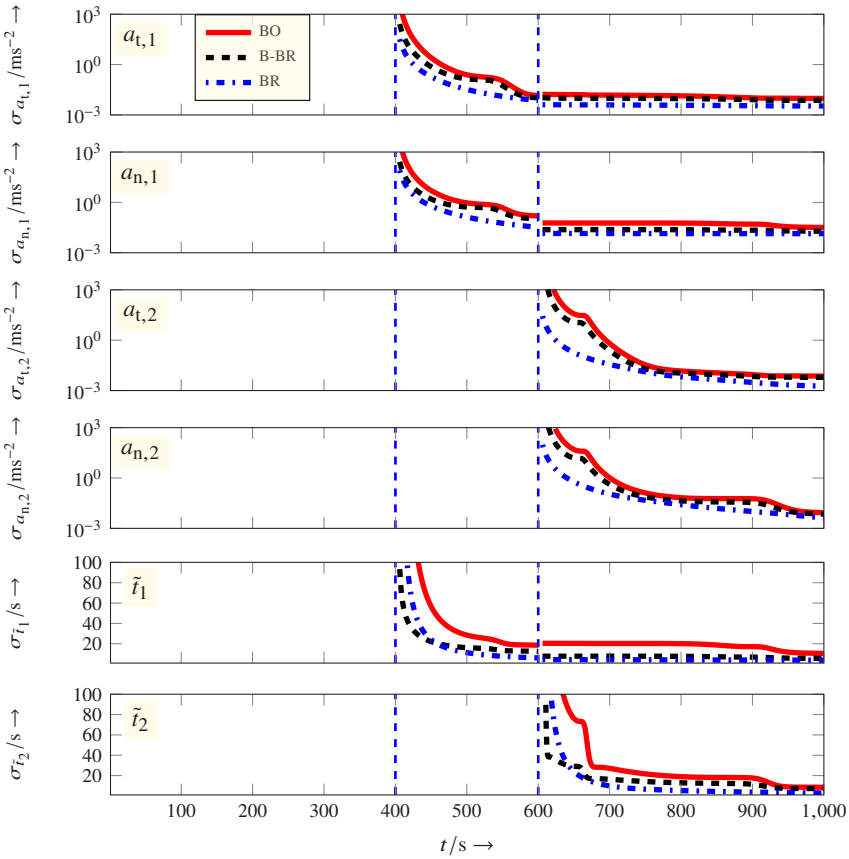

Figure 6.8: Piecewise curvilinear motion: Visualization of CRLB for $a_{t,1}$, $a_{n,1}$, $a_{t,2}$, $a_{n,2}$, $\tilde{t}_1$, $\tilde{t}_2$ regarding BO, B-BR, and BR. The dashed vertical lines denote the target maneuvers, © 2014 IEEE.

Since BO exploits the smallest amount of information, it carries the lowest estimation accuracy. If additional bearing rate measurements (B-BR) are considered, we can recognize a certain accuracy gain. This gain is about factor 3 to 4 for position, speed, course, tangential and normal accelerations as well as maneuver change times, see Fig. 6.7 and 6.8. Comparing BO and B-BR, a further accuracy gain can be identified. Here, the accuracy is about 15 times higher for position and course, about 7 times higher for speed, about 5 times higher for the segment accelerations, and about 4 to 7 times higher for the

maneuver change times. The figures show that no observability issues exist. Due to the circular motion of the observer, observability is ensured from the beginning regarding all three types of measurements.

It can be recognized that the estimation accuracy generally increases with a growing number of measurements. This is clear since the Fisher information is added up over all previous measurements, see also (3.19). At maneuver change points, particularly the position, speed, and course estimation accuracies decrease. This is due to a high uncertainty because the new segment accelerations are unknown. See also Subsection 6.1.1 for a similar explanation concerning the piecewise inertial case. Another effect is that the acceleration components as well as the respective maneuver change time stay nearly constant in the segment where they are not active any more. According to the last section, this supports an estimation approach which does not consider the complete $(6 + 3M)$-dimensional state with its $M + 1$ segments, but only the current segment and the segment before.

State Estimation

Here, the results of state estimation using a maximum likelihood estimator are compared to the CRLB. We assume the scenario illustrated in Fig. 6.6. Also here, Monte Carlo simulations with 500 runs are carried out and the minima of the respective cost functions are determined by the simplex method of Nelder and Mead [NM65]. We initialize every search with the true value. The time where the results are determined is $t = 600\,\mathrm{s}$ which is equal to the second maneuver change time $\tilde{t}_2$.

The scattering of the Monte Carlo estimates around the true values is visualized, by scatter plots of the estimation error. That means, estimation results are depicted as estimation errors so that the true target state is at $[0, 0]$. The resulting 2D estimation error ellipses (sample covariance) are compared with the corresponding CRLB ellipses. The ellipse parameters were chosen in such a way that, assuming normally distributed estimation errors, the ellipses enclose 95.4% (2σ ellipse) of the sample values.

In Fig. 6.9 and 6.10 the BO, B-BR, and BR case is shown for the target position error in x-direction, Δx_k, with respect to the target position error in y-direction, Δy_k as well as with respect to the estimation error of the first maneuver change time, $\Delta\tilde{t}_1$. The estimation error ellipses and bound ellipses have a similar orientation and expansion. The scatter plots display that the estimation results are mostly biased: The sample mean of the estimation errors (red quad) is only near $[0, 0]$. However, it is well-known that the MLE is asymptotically efficient: The estimates can be biased in the presence of noise and for a finite number of measurements N, but asymptotically they are not. Also here, the BR case shows the best performance with a negligible bias. Furthermore, the scatter plots prove that the target maneuvering time can be estimated, even if the error ellipse slightly deviates from the bound ellipses in the BO and B-BR case.

	Δx_k and Δy_k	Δx_k and $\Delta \tilde{t}_1$
BO	2.0405	1.7917
BO bias corrected	1.9690	1.6788
B-BR	1.9106	1.7937
B-BR bias corrected	1.8531	1.6939
BR	1.8947	1.9186
BR bias corrected	1.8926	1.9176

Table 6.2: Piecewise curvilinear motion: NEES for BO, B-BR, and BR regarding the cases depicted in Fig. 6.9 and 6.10, © 2014 IEEE.

In Table 6.2 the NEES (6.6) for the cases depicted in Fig. 6.9 and 6.10 is specified. Considering a two-sided 95% acceptance interval which is $(1.8285, 2.1790)$ for two dimensions and 500 Monte Carlo runs, it can be seen that the NEES values for Δx_k and Δy_k are all within that interval which means estimator consistency. However, besides the BR case, the NEES regarding $\Delta \tilde{t}_1$ is below the lower bound and therefore the estimator is pessimistic.

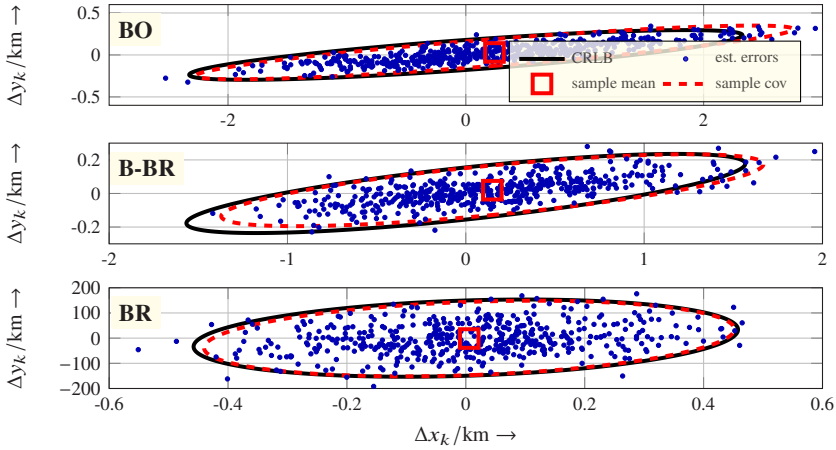

Figure 6.9: Piecewise curvilinear motion: Scatter plots of Monte Carlo estimation errors, corresponding estimation error ellipses, and CRLB ellipses plotted for Δx_k versus Δy_k regarding BO, B-BR, and BR at time $t = \tilde{t}_2 = 600\,\mathrm{s}$. The true target state is at $[0, 0]$, © 2014 IEEE.

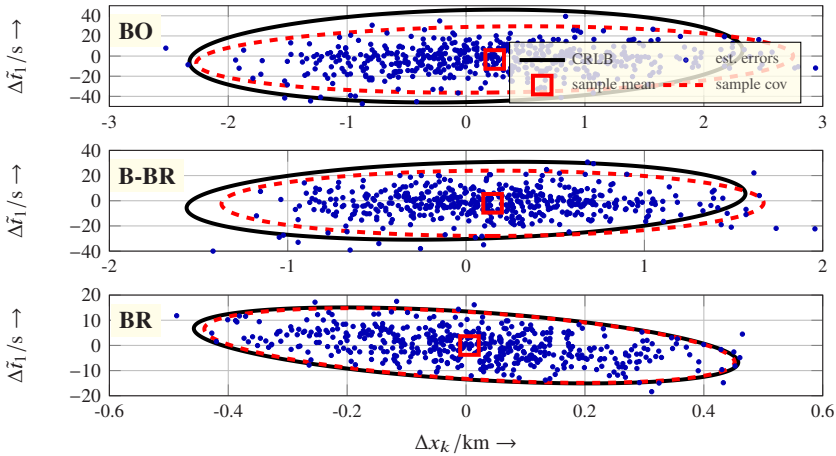

Figure 6.10: Piecewise curvilinear motion: Scatter plots of Monte Carlo estimation errors, corresponding estimation error ellipses, and CRLB ellipses plotted for Δx_k versus $\Delta \tilde{t}_1$ regarding BO, B-BR, and BR at time $t = \tilde{t}_2 = 600\,\mathrm{s}$. The true target state is at $[0, 0]$, © 2014 IEEE.

6.2 Field Test Results for BOT in a Vehicular Ad hoc Network Using Heterogeneous Sensors

In order to verify the BOT approach in a vehicular ad hoc network using heterogeneous sensors, several field tests have been carried out. First of all, communications and self-localization has been tested, see Subsection 6.2.1. In this context, all sensor input has been simulated. In a later phase, real sensors, namely a microphone array and a laser and radar detector, have been applied, see Subsection 6.2.2. The own reference paper is [HGR+16].

6.2.1 Communications Tests

The concept for the proposed mobile ad hoc network (MANET) includes a fusion center on each vehicle for reliability, see Section 1.4 and Fig. 1.3. The network architecture facilitates a full mesh of point-to-point connections, i.e. sending sensor data (plots) from each participant to another each time step a measurement is taken. With this, the setup for the vehicle-to-vehicle communications tests is as follows, see Fig. 6.11:

- A formation of two (later four) cars moves around a circuit with varying distances between 30 m and 200 m at speed 20 km/h to 40 km/h or stand at certain positions, see Fig. 6.12.
- Each car is equipped with a commercial-off-the-shelf (COTS) Wi-Fi device. Specifically, we employ Ubiquiti Bullet M5 Wi-Fi radios [Ubi11] operating at 5 GHz with an omni-directional antenna. The radios provide an IEEE 802.11n Wi-Fi and have OpenWRT installed as operating system. The nodes form a mobile wireless ad hoc network (MANET). As routing protocol OLSRv1 is used. Although a routing protocol is not mandatory when only two nodes are involved, we use this setup for performance evaluations considering different node-to-node distances and obstacles.
- Additionally, for self-localization purposes, each car is equipped with a GPS receiver. During these tests, we used both NovaTel and Garmin GPS receivers.
- On each car, a bearings-only sensor is simulated which generates angle-only measurements of a simulated threat.
- Communications device and GPS receiver are connected to a laptop on each car which acts as visualization device as well as a fusion center fusing information from the simulated sensors. The visualization software is based on NASA WorldWind Java SDK [Nat].

The first objective was to measure the communications performance for different vehicle distances. Therefore, the test has been carried out using two cars in four scenarios:

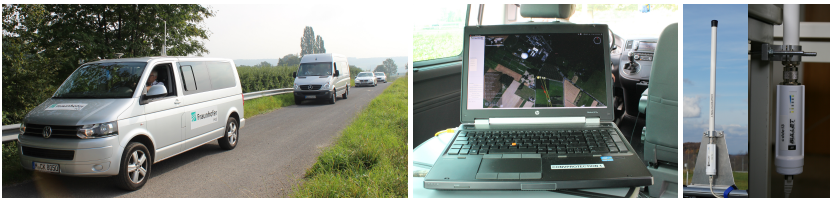

Figure 6.11: Formation of four cars during communications field tests with mounted communication devices (left), laptop with visualization and fusion software (center), and Ubiquiti Bullet M5 Wi-Fi radio device (right), © 2016 IEEE.

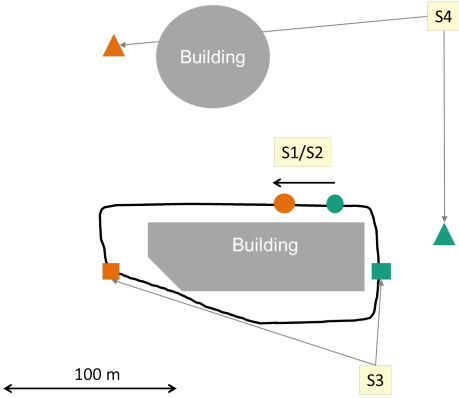

Figure 6.12: Schematic overview of test area and scenarios for communications tests with two cars (orange and green). The different shapes represent the scenarios S1-S4, © 2016 IEEE.

During the first two scenarios (S1 and S2), the cars move with low distances with an average of around 30 m to 50 m. For the third scenario (S3), we have chosen medium distances of about 100 m, and finally during the fourth run (S4), the maximal distance inside the test area of about 200 m has been used. Results for the scenarios S1 to S4 are shown in Fig. 6.13. Here, signal strength, bitrate, ETX, and car distance based on GPS measurements are depicted over time considering the communication between the first and the second car of the formation. ETX is the abbreviation for expected transmission count metric on (multi-hop) wireless networks and denotes expected number of transmissions required to send a packet successfully to its destination [DCABM05] used in OLSRv1. The plots clearly show that with low distances (S1 and S2) the signal strength and the bitrate are high while the ETX is one meaning only a single transmission

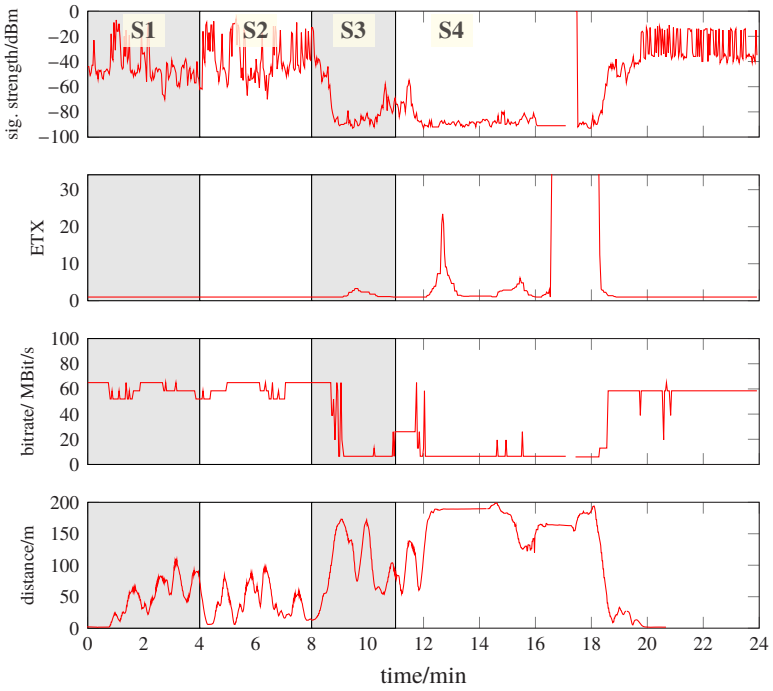

Figure 6.13: Results of communications tests for different scenarios S1-S4, © 2016 IEEE.

is needed for each packet indicating optimal connectivity. With higher distances (S3), the signal strength and the bitrate deteriorates while the ETX slightly increases. This is because of shadowing effects of a building depicted in Fig. 6.12. When the distance is maximized inside the test area (S4), and buildings are obstacles, the connectivity is interrupted, especially between minute 15 and 20 shown by no measurable signal strength and bitrate as well as indefinite ETX. This way we have evaluated the communications performance of the available hardware as a prerequisite for further tests.

The next test objective was to evaluate the performance of the distributed fusion algorithm over this wireless network in a simulated sensor environment. For that, we have chosen another test area north of Wachtberg-Werthhoven with no obstacles/buildings disturbing communications, see Fig. 6.14. Since a high bandwidth scenario is considered, where the bandwidth is sufficient to transmit most of the produced sensor data to the *fusion centers* on the different vehicles. This approach is called measurement-to-track fusion (M2TF). In Fig. 6.14, one can also recognize the location of the four cars, which have

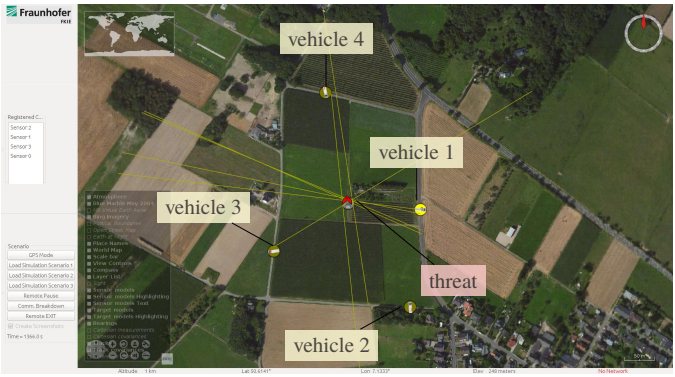

Figure 6.14: Fusion results from communications field tests with simulated sensors. Four vehicles with maximum distance at the test area. The estimated threat location (red) is near the true threat location. Screenshot from software based on NASA WorldWind Java SDK [Nat]. The test area is between the Fraunhofer campus Wachtberg and the village of Wachtberg-Werthhoven, © 2016 IEEE.

maximized their distance over the circuit, the current (simulated) angular measurements, and the fusion result for the simulated threat which is clearly near the true threat location.

6.2.2 Sensor Tests

After the communications test with simulated sensors have been carried out successfully, the next steps were to integrate several real sensors into the system. According to the scheme in Fig. 6.15, we have chosen two sensors to be integrated. Therefore the setup for these tests is given by the following changes to the setup described in Subsection 6.2.1:

- Two cars in a stationary and mobile scenario, see Fig. 6.16.
- Regarding the communications subsystem, no changes except an upgrade to OLSRv2 has been made.
- For the self-localization subsystem, we use u-blox EVK-6T GPS receivers on each car. Furthermore, since the GPS receivers cannot provide heading information while not in motion, we employ XSens MTi-G 700 INS devices. Vehicle heading is important to transform measurements from a sensor coordinate system to a global coordinate system.
- The following real sensors have been integrated:

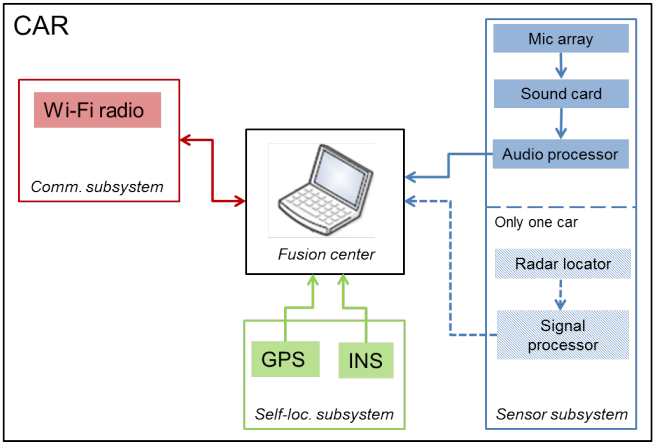

Figure 6.15: Schematic overview of components and subsystems mounted on a car, © 2016 IEEE.

Figure 6.16: Two cars fully mounted, © 2016 IEEE.

1. Eight-channel microphone array with eight channel TASCAM sound card which is able to provide an angular measurement to an object emitting sounds, in particular, acoustic shocks, e.g. from a gun or RPG. See Fig. 1.4 for an illustration.

2. COTS radar and laser detector "Valentine One", see [Val12] and Fig. 1.4. Usually, this device[1] is used to detect traffic radars in various bands: X, K,

[1] The inventor describes it as "a civilian version of what the military calls Electronic Warfare Support Measures (ESM)" [Val12]

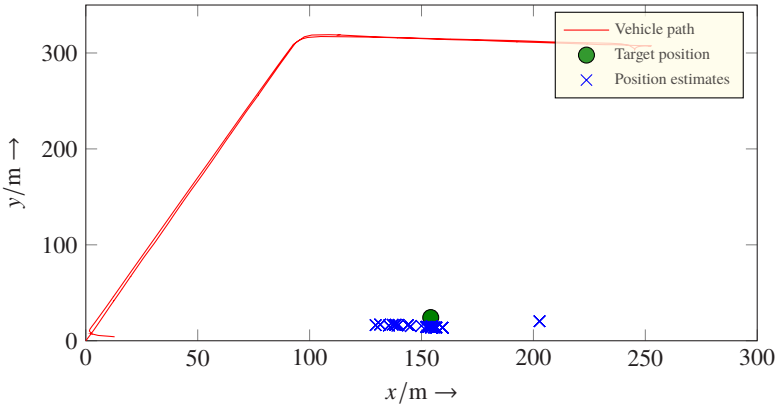

Figure 6.17: Field tests scenario and results using Kronhamn's weights.

Ka, and Ku band as well as laser between 820 nm and 950 nm. We are using it for detecting electromagnetic emissions from the simulated threat.

- In order to simulate a threat emitting sound as well as electromagnetic waves, we use the following trigger devices:

  1. Gas-powered stationary sonic blast-shock cannon "Purivox Triplex V", see Fig. 1.4 (right). This device is used to emulate a gun blast or similar. Usually, this cannon is used to expel birds from crops.

  2. Trigger device for the radar and laser detector. This device is commercially available for testing a traffic radar detector after installing it in a car. It is able to emit radar frequencies in X, K, Ka, and Ku band as well as laser.

6.2.3 Fusion Results from Sensor Tests

For each angular measurement of the threat produced by the microphone array by means of audio data processing, a plot message is generated which comprises the angular value of the bearing measurement as well as its standard deviation. The fusion center approximates the measurement likelihood (5.31) determined by the two transmitted parameters by means of a Gaussian mixture, where each mixture component represents a range hypothesis, see the analysis in Section 5.5 and applies a multi hypothesis Gaussian mixture filter in order to estimate the threat's location under potential missing detections and false alarms, see Section 5.4.

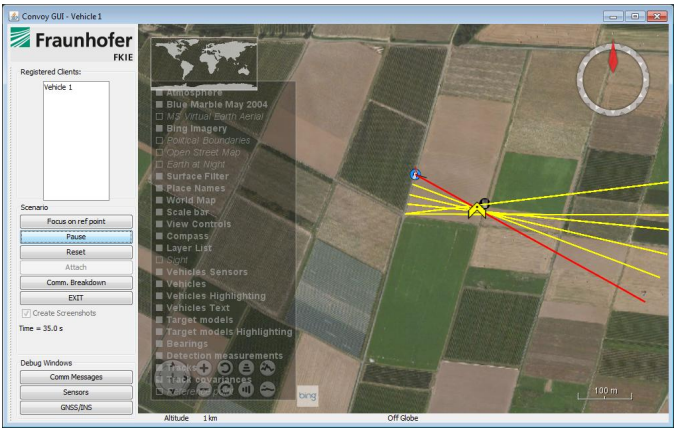

Figure 6.18: Field tests scenario and results using Kronhamn's weights (screenshot).

The test area is located north of Grafschaft-Oeverich and about 2 km south of the Fraunhofer campus Wachtberg, directly south of the border to the state of Rheinland-Pfalz, see Fig. 6.18 and 6.20. One vehicle equipped with a microphone array aligned to the right of the driving direction (see also Fig. 6.16) travels along a country road in northern direction and turns right at an intersection, see Fig. 6.17 and 6.19. The sonic blast-shock cannon is deployed at coordinates 50.599 183° N and 7.120 728° E about 150 m east of the starting position of the vehicle and is used as the source for audio measurements.

The first objective of this test is to verify the performance of the audio signal processing algorithm which calculates bearing measurements from the sound waves arriving at the microphone array. Nevertheless, signal processing is not part of this thesis, so that only the second objective is evaluated here: Verify the performance of the multi hypothesis Gaussian mixture filter with bearing-only measurements from a single platform. Of course, this strongly depends on the quality of the audio bearings which is high as we will see later. Due to these narrow test objectives, two other aspects have not been considered in these sensor tests: Multiple vehicles in order to test the communication and the detection of electromagnetic signals as intended by means of the laser/radar detector. The communications aspect has already been handled in the communications tests, see Subsection 6.2.1. However, the "fusional" integration of the detector stays an open question: It has only been considered for observability, see Chapter 4.

Hence, with the availability of audio bearings, the two likelihood approximation approaches from Section 5.5, namely Kronhamn's and Mušicki's approach, are compared in a real scenario. We remember that Kronhamn determined the Gaussian mixture com-

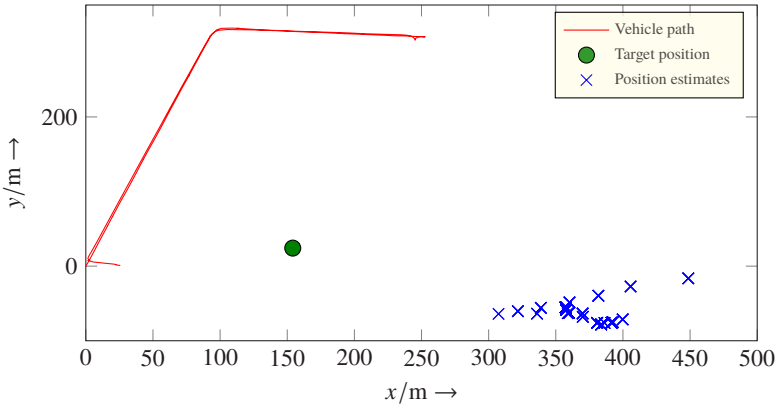

Figure 6.19: Field tests scenario and results using Mušicki's weights.

ponent weight as proportional to the length of the range subinterval covered by a Gaussian mixture component, whereas Mušicki proposed a method where the component weights are proportional to the area covered by a Gaussian mixture component. The simulations in Subsection 5.5.5 already have shown that, if the target is near, relative to the maximum range, Kronhamn's approach delivers better results, whereas Mušicki is more appropriate when the target is far away relative to the maximum range. For these tests, we have set the minimum range $r_{\min} = 0.1$ m and the maximum range $r_{\max} = 2000$ m, the probability of detection $p_D = 0.98$ and the clutter density $\rho_F = 1/2\pi$, the bearing standard deviation to $\sigma = 3°$. The results are as expected and predicted by the simulation in Subsection 5.5.5: For Kronhamn's approach, the position estimates are near the target, with a slight bias, see Fig. 6.17, whereas for Mušicki weights, the filter seems to diverge with position estimates around 200 m east of the true target location, see Fig. 6.19. Furthermore, the position error e_k^{pos} and the filter standard deviation in position coordinates σ_k^{pos} (cf. with root mean trace of the covariance, RMTC [DNK12]) given by

$$e_k^{\text{pos}} = \sqrt{\left(x_k^{\text{true}} - \hat{x}_{k|k}\right)^2 + \left(y_k^{\text{true}} - \hat{y}_{k|k}\right)^2} \tag{6.10a}$$

$$\sigma_k^{\text{pos}} = \sqrt{\text{tr}\left(\mathbf{P}_{k|k}\right)} \tag{6.10b}$$

is illustrated in Fig. 6.21. The bias corrected position error for time t_k is calculated by subtracting the median position error over time (which is about 10.27 m) from the respective position error at time t_k. The figure clearly reflects the findings. In both cases, the covariance is lower than the position error. This indicates problems with

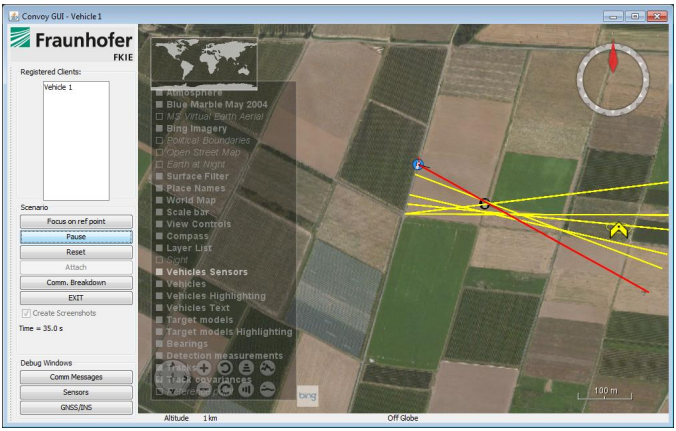

Figure 6.20: Field tests scenario and results using Mušicki's weights (screenshot).

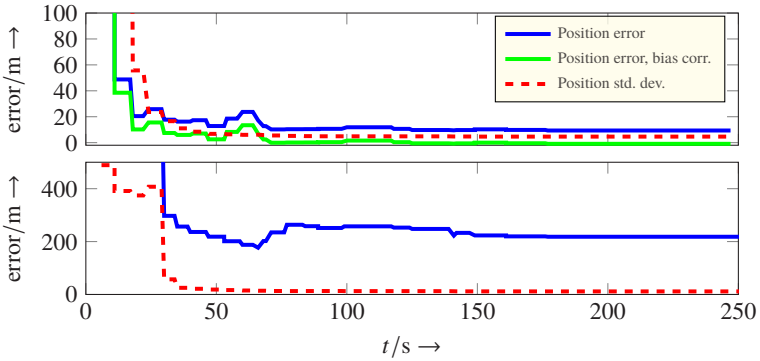

Figure 6.21: Position error and covariance using Kronhamn's (above) and Mušicki's (below) weights.

filter consistency, meaning the filter is optimistic. For Kronhamn's approach, there exist a certain estimation bias which seems to be explainable by a small measurement bias caused in the audio processing. Thus, the bias correction has been applied. With this, the bias corrected position error is lower than the covariance, so that for unbiased measurements, the filter shows appropriate performance. For Mušicki's approach, the general divergence is the cause. Thus, a bias correction makes no sense. Apparently, the audio signal processing algorithm has provided the filter with stable and mostly proper

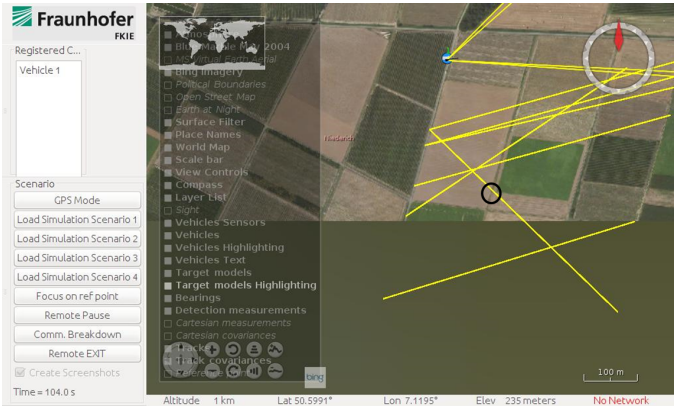

Figure 6.22: Acoustic bearings with false alarms for car speed $v = 40\,\mathrm{km/h}$ (screenshot from visualization software), © 2016 IEEE.

bearing measurements. It was able to suppress the most false detections, for example caused by driving about 40 km/h over a gravel path. This has been experienced in earlier campaigns, see Fig. 6.22, and has been successfully factored in. Nevertheless, there is always surrounding sound in an open area, so that false measurements may occur.

6.3 Summary of the Chapter

In this chapter, results for both central themes of this thesis have been presented. Concering the first theme, bearings-only tracking for maneuvering targets, a simulation study has been carried out. A major contribution is the ability to estimate a state with increasing dimensions due to the piecewise motion models especially including the maneuver change times. Furthermore, the presented estimator, which is in a proof of concept state, turned out to be predominantly efficient as it attained the CRLB for most of the state components. For the second central theme of this thesis, we have conducted field tests including several platforms interconnected by a wireless network. Putting the different technical components as sensors and their connection to the overall system to work has been a challenge itself. Thus, the field tests with fusion results have been narrowed to fuse bearings from an acoustic source in order to localize a threat. However, these real data experiments have been successful and were able to show the performance of the Gaussian mixture filter.

7 Summary and Conclusions

This thesis presented advances in two sub-themes of bearings-only tracking, namely bearings-only tracking for maneuvering targets, and bearings-only tracking using heterogeneous sensors. Both topics constitute the central themes which group this thesis into two vertical strands. In each chapter, the respective subject is discussed related to the central themes.

In Chapter 2 measurement and motion models essential for this thesis have been introduced and recapped. This includes bearings-only and bearing rate measurements, which play a role as additional measurements to improve the state estimation results. The presented motion models span different stages of complexity: From a simple constant-velocity model to the complex piecewise motion models, more specifically, piecewise inertial motion for maritime targets, and piecewise curvilinear models for agile targets like aircraft. These models are required to derive a Cramér-Rao lower bound for maneuvering targets, see Chapter 3, which is able to consider different maneuver segments as well as the times when a new maneuver segment is initiated. This is the first major theoretical contribution of this thesis.

The observability analysis in Chapter 4 is primarily related to the central theme of bearings-only tracking using heterogeneous sensors. However, it is strongly connected to the Cramér-Rao lower bound since the observability Gramian as main tool for any observability analysis has turned out to be algebraically equivalent to the Fisher information matrix as inverse of the CRLB besides the noise terms. Here, the proposed idea of heterogeneous bearings-only tracking, exploiting different signal propagation velocities has been investigated using acoustic and electromagnetic signals. The results showed that observability can be ensured for passive measurements involving moving targets from a single stationary observer using these heterogeneous sensor setup. This is in contrast to simple bearings-only tracking where an observer usually must maneuver to track a moving target and thus the second major contribution of this thesis.

With observability as requirement for state estimation and the CRLB as indication for maximum achievable estimator performance, state estimation methods have been presented in Chapter 5. We have distinguished between Bayesian and non-Bayesian state estimation methods. The non-Bayesian approach, namely the maximum likelihood estimator, has been the choice for bearings-only tracking of maneuvering targets. This is due to its robustness and the non-observability of the state before the first observer maneuver. Bayesian methods often diverge under these circumstances since a proper

initialization is challenging. If the filter is ill-initialized, all following estimates will base on these values due to the recursive Bayesian update scheme leading to divergence of the filter. On the other hand, non-Bayesian method often operate in batch mode for nonlinear problems so that they consider all past measurements for each estimate. This makes them more robust against divergence but also computationally demanding. For heterogeneous bearings-only tracking, Bayesian methods are used. The choice has been a linear Gaussian mixture filter which is based on a Gaussian mixture approximation of a bearings-only likelihood that is linear in target state. This likelihood approximation has been derived from a general technique for likelihood approximation. It turned out that the weights of the Gaussian mixture components can be obtained in two different ways which have been compared. This resulted in recommendations for the choice of weights depending on the target distance as third main theoretical contribution of this thesis.

Results for both central themes have been presented in the final technical chapter of this thesis, Chapter 6. Concerning the maneuvering target case, we have shown in a simulation study that a batch estimator can be specified which can estimate a state with increasing dimensions due to the target maneuvers modeled by the piecewise motion models. Furthermore, it has attained the CRLB, so it is predominantly efficient. Field tests featuring real sensors, i.e. a microphone array and a radar/laser detector have been conducted regarding the heterogeneous tracking part of this thesis. A system has been built up which is able to present a situation picture by means of modern communication and routing technology. The interaction of communication and data fusion has been shown. Furthermore, the performance of the Gaussian mixture filter has successfully been proven in these field tests for acoustic bearings-only measurements using a microphone array. Having set up and implemented such a system with relevance to distributed data fusion and communication is practical contribution of this thesis.

Future work Hence, in both central themes, relevant contributions have been made. However, there is always future work left. Concerning the maneuvering tracking part, the state estimation can be improved methodologically. At the moment it is in a proof of concept state. Since the state dimension is increasing with each maneuver segment, and therefore the computational complexity, one could research on methods to reduce that complexity. This could include identification of linear substructures, e.g. by means of appropriate coordinate transformations or further methods so that parts of the problem are linear and can be solved analytically. Concerning the heterogeneous tracking domain, the laser/radar detector must be integrated into the fusion process. This has only been examined theoretically for observability. Of course, exploiting different signal propagation velocities, using acoustic and electromagnetic signals ensures observability in situations where using only one signal type would suffer from non-observability. This alone would create a benefit for state estimation and possibly improve estimation accuracy. But there is even another item to think about: Since the detector only roughly detects direction, i.e. it

can give information whether the target is in front of the observer, at the side, or behind it, it could be used to pre-filter the acoustic bearings and thus suppress false detections from surrounding audio sources. Since the field test infrastructure with platforms and sensors is available, tests on this topic can be performed with real data.

A Partial Derivatives for Cramér-Rao Lower Bound

A.1 Partial Derivatives of Target Position for Inertial Motion

The target position is denoted as $\mathbf{r}_k = [x_k, y_k]^{\mathrm{T}}$. For t_k and t_{r} in the maneuver segment $m-1$, i.e., $\tilde{t}_{m-1} \leq t_k, t_{\mathrm{r}} \leq \tilde{t}_m$, we can express $\mathbf{r}_k$ by means of $\mathbf{r}_{\mathrm{r}}$:

$$\mathbf{r}_k = \mathbf{r}_{\mathrm{r}} + (t_k - t_{\mathrm{r}}) \begin{bmatrix} \dot{x}_{m-1} \\ \dot{y}_{m-1} \end{bmatrix} . \tag{A.1}$$

Therefore, the partial derivatives of the target position with respect to the velocities which are active in the maneuver segment $m-1$ are given by

$$\frac{\partial x_k}{\partial \dot{x}_{m-1}} = \frac{\partial y_k}{\partial \dot{y}_{m-1}} = t_k - t_{\mathrm{r}} . \tag{A.2}$$

The partial derivative of the target position at time t with respect to t can be expressed by

$$\frac{\partial \mathbf{r}(t)}{\partial t} = \dot{\mathbf{r}}(t) = \begin{bmatrix} \dot{x}_{m-1} \\ \dot{y}_{m-1} \end{bmatrix} . \tag{A.3}$$

Since t_{r} is subtracted in (A.1), the partial derivative of the target position at time t with respect to the reference time t_{r} yields

$$\frac{\partial \mathbf{r}(t)}{\partial t_{\mathrm{r}}} = - \begin{bmatrix} \dot{x}_{m-1} \\ \dot{y}_{m-1} \end{bmatrix} = - \frac{\partial \mathbf{r}(t)}{\partial t} . \tag{A.4}$$

A.2 Partial Derivatives of Target State for Curvilinear Motion

Using following definition from Chapter 2,

$$c_\mathrm{a} = \frac{1}{4a_\mathrm{t}^2 + a_\mathrm{n}^2} \tag{A.5a}$$

$$S(t) = (2a_\mathrm{t} \sin\varphi(t) - a_\mathrm{n} \cos\varphi(t))\, v^2(t) \tag{A.5b}$$

$$T(t) = (2a_\mathrm{t} \cos\varphi(t) + a_\mathrm{n} \sin\varphi(t))\, v^2(t) \tag{A.5c}$$

$$\Delta t_k = t_k - t_\mathrm{r} \tag{A.5d}$$

$$\Delta S_k = S(t_k) - S(t_\mathrm{r}) \tag{A.5e}$$

$$\Delta T_k = T(t_k) - T(t_\mathrm{r})\,. \tag{A.5f}$$

The derivative of the target state at time t_k with respect to the target state at reference time t_r is given by the following Jacobian matrix

$$\frac{\partial \mathbf{x}_k}{\partial \mathbf{x}_\mathrm{r}} = \frac{\partial \mathbf{f}(\mathbf{x}_\mathrm{r}; t_k, t_\mathrm{r})}{\partial \mathbf{x}_\mathrm{r}}\,, \tag{A.6}$$

which can be expressed by

$$\frac{\partial \mathbf{f}(\mathbf{x}_\mathrm{r}; t_k, t_\mathrm{r})}{\partial \mathbf{x}_\mathrm{r}} = \begin{bmatrix} 1 & 0 & \frac{\partial x_k}{\partial v_\mathrm{r}} & \frac{\partial x_k}{\partial \varphi_\mathrm{r}} & \frac{\partial x_k}{\partial a_\mathrm{t}} & \frac{\partial x_k}{\partial a_\mathrm{n}} \\ 0 & 1 & \frac{\partial y_k}{\partial v_\mathrm{r}} & \frac{\partial y_k}{\partial \varphi_\mathrm{r}} & \frac{\partial y_k}{\partial a_\mathrm{t}} & \frac{\partial y_k}{\partial a_\mathrm{n}} \\ 0 & 0 & 1 & 0 & \Delta t_k & 0 \\ 0 & 0 & \frac{\partial \varphi_k}{\partial v_\mathrm{r}} & 1 & \frac{\partial \varphi_k}{\partial a_\mathrm{t}} & \frac{\partial \varphi_k}{\partial a_\mathrm{n}} \\ 0 & 0 & 0 & 0 & 1 & 0 \\ 0 & 0 & 0 & 0 & 0 & 1 \end{bmatrix}. \tag{A.7}$$

For the partial derivatives of φ_k (2.28d) we have

$$\frac{\partial \varphi_k}{\partial v_\mathrm{r}} = -\frac{\Delta t\, a_\mathrm{n}}{v_\mathrm{r}(v_\mathrm{r} + \Delta t_k\, a_\mathrm{t})}\,, \tag{A.8a}$$

$$\frac{\partial \varphi_k}{\partial a_\mathrm{t}} = \begin{cases} \frac{a_\mathrm{n}}{a_\mathrm{t}} \left(-\frac{\partial \varphi_k}{\partial v_\mathrm{r}} + \frac{\Delta t_k}{v_\mathrm{r} + \Delta t_k\, a_\mathrm{t}} \right) & \text{for } a_\mathrm{t} \neq 0 \\ -\frac{\Delta t_k^2}{2} \frac{a_\mathrm{n}}{v_\mathrm{r}^2} & \text{for } a_\mathrm{t} = 0 \end{cases}, \tag{A.8b}$$

$$\frac{\partial \varphi_k}{\partial a_\mathrm{n}} = \begin{cases} \frac{1}{a_\mathrm{t}} \ln \left| 1 + \frac{a_\mathrm{t}}{v_\mathrm{r}} \Delta t_k \right| & \text{for } a_\mathrm{t} \neq 0 \\ \frac{1}{v_\mathrm{r}} \Delta t_k & \text{for } a_\mathrm{t} = 0 \end{cases}. \tag{A.8c}$$

Moreover, the derivatives of x_k (2.28a) are given by

$$\frac{\partial x_k}{\partial v_\mathrm{r}} = \begin{cases} c_\mathrm{a}\left(2\frac{S(t_k)}{v_k} + \frac{\partial \varphi_k}{\partial v_\mathrm{r}} T(t_k) - 2\frac{S(t_\mathrm{r})}{v_\mathrm{r}}\right) & \text{for } a_\mathrm{t} \neq 0 \text{ or } a_\mathrm{n} \neq 0 \\ \Delta t_k \ \sin\varphi_\mathrm{r} & \text{for } a_\mathrm{t} = 0 \text{ and } a_\mathrm{n} = 0 \end{cases}, \tag{A.9a}$$

$$\frac{\partial x_k}{\partial \varphi_\mathrm{r}} = \begin{cases} c_\mathrm{a}\,\Delta T_k & \text{for } a_\mathrm{t} \neq 0 \text{ or } a_\mathrm{n} \neq 0 \\ \Delta t_k\ v_\mathrm{r} \cos\varphi_\mathrm{r} & \text{for } a_\mathrm{t} = 0 \text{ and } a_\mathrm{n} = 0 \end{cases}, \tag{A.9b}$$

$$\frac{\partial x_k}{\partial a_\mathrm{t}} = \begin{cases} -8a_\mathrm{t}c_\mathrm{a}^2\,\Delta S_k + c_\mathrm{a}P(t_k) & \text{for } a_\mathrm{t} \neq 0 \text{ or } a_\mathrm{n} \neq 0 \\ \frac{\Delta t_k^2}{2}\sin\varphi_\mathrm{r} & \text{for } a_\mathrm{t} = 0 \text{ and } a_\mathrm{n} = 0 \end{cases}, \tag{A.9c}$$

$$\frac{\partial x_k}{\partial a_\mathrm{n}} = \begin{cases} -2a_\mathrm{n}c_\mathrm{a}^2\,\Delta S_k + c_\mathrm{a}Q(t_k) & \text{for } a_\mathrm{t} \neq 0 \text{ or } a_\mathrm{n} \neq 0 \\ \frac{\Delta t_k^2}{2}\cos\varphi_\mathrm{r} & \text{for } a_\mathrm{t} = 0 \text{ and } a_\mathrm{n} = 0 \end{cases}, \tag{A.9d}$$

where

$$P(t_k) = \frac{2\Delta t_k}{v_k} S(t_k) + \frac{\partial \varphi_k}{\partial a_\mathrm{t}} T(t_k) + 2v_k^2 \sin\varphi_k - 2v_\mathrm{r}^2 \sin\varphi_\mathrm{r}\,, \tag{A.10a}$$

$$Q(t_k) = \frac{\partial \varphi_k}{\partial a_\mathrm{n}} T(t_k) - v_k^2 \cos\varphi_k + v_\mathrm{r}^2 \cos\varphi_\mathrm{r}\,. \tag{A.10b}$$

Finally, we obtain for the partial derivatives of y_k (2.28b) by

$$\frac{\partial y_k}{\partial v_\mathrm{r}} = \begin{cases} c_\mathrm{a}\left(2\frac{T(t_k)}{v_k} + \frac{\partial \varphi_k}{\partial v_\mathrm{r}} S(t_k) - 2\frac{T(t_\mathrm{r})}{v_\mathrm{r}}\right) & \text{for } a_\mathrm{t} \neq 0 \text{ or } a_\mathrm{n} \neq 0 \\ \Delta t_k \ \cos\varphi_\mathrm{r} & \text{for } a_\mathrm{t} = 0 \text{ and } a_\mathrm{n} = 0 \end{cases} tc \tag{A.11a}$$

$$\frac{\partial y_k}{\partial \varphi_\mathrm{r}} = \begin{cases} -c_\mathrm{a}\Delta S_k & \text{for } a_\mathrm{t} \neq 0 \text{ or } a_\mathrm{n} \neq 0 \\ -\Delta t_k\ v_\mathrm{r} \sin\varphi_\mathrm{r} & \text{for } a_\mathrm{t} = 0 \text{ and } a_\mathrm{n} = 0 \end{cases}, \tag{A.11b}$$

$$\frac{\partial y_k}{\partial a_\mathrm{t}} = \begin{cases} -8a_\mathrm{t}c_\mathrm{a}^2\Delta T_k + c_\mathrm{a}U(t_k) & \text{for } a_\mathrm{t} \neq 0 \text{ or } a_\mathrm{n} \neq 0 \\ \frac{\Delta t_k^2}{2}\cos\varphi_\mathrm{r} & \text{for } a_\mathrm{t} = 0 \text{ and } a_\mathrm{n} = 0 \end{cases}, \tag{A.11c}$$

$$\frac{\partial y_k}{\partial a_\mathrm{n}} = \begin{cases} -2a_\mathrm{n}c_\mathrm{a}^2\Delta T_k + c_\mathrm{a}V(t_k) & \text{for } a_\mathrm{t} \neq 0 \text{ or } a_\mathrm{n} \neq 0 \\ \frac{\Delta t_k^2}{2}\sin\varphi_\mathrm{r} & \text{for } a_\mathrm{t} = 0 \text{ and } a_\mathrm{n} = 0 \end{cases}, \tag{A.11d}$$

with

$$U(t_k) = \frac{2\Delta t_k}{v_k} T(t_k) + \frac{\partial \varphi_k}{\partial a_\mathrm{t}} S(t_k) + 2v_k^2 \cos\varphi_k - 2v_\mathrm{r}^2 \cos\varphi_\mathrm{r}\,, \tag{A.12a}$$

$$V(t_k) = \frac{\partial \varphi_k}{\partial a_\mathrm{n}} S(t_k) - v_k^2 \sin\varphi_k + v_\mathrm{r}^2 \sin\varphi_\mathrm{r}\,. \tag{A.12b}$$

Finally, the derivative of $\mathbf{y}(t)$ with respect to t is given by

$$\frac{\partial \mathbf{y}(t)}{\partial t} = \left[v(t)\sin\varphi(t), v(t)\cos\varphi(t), a_{\mathrm{t}}, \frac{a_{\mathrm{n}}}{v(t)} \right]^{\mathrm{T}} , \tag{A.13}$$

If t and t_{r} are in the same maneuver segment, i.e., $\tilde{t}_{m-1} \leq t, t_{\mathrm{r}} \leq \tilde{t}_m$, the derivative of $\mathbf{y}(t)$ with respect to t_{r} is given by

$$\frac{\partial \mathbf{y}(t)}{\partial t_{\mathrm{r}}} = -\frac{\partial \mathbf{y}(t)}{\partial t} . \tag{A.14}$$

A.3 Partial Derivatives of Measurement Equations

In case of bearing measurements, the measurement equation (2.12) only depends on the position components $\mathbf{p}_k = [x_k, y_k]^{\mathrm{T}}$ of the state. Thus, the partial derivatives with respect to the other components are zero and therefore omitted here. Thus, the partial derivative of $\alpha(\mathbf{x}_k)$ with respect to the position components of the state is given by [RA03]

$$\frac{\partial \alpha(\mathbf{x}_k)}{\partial \mathbf{p}_k} = \frac{1}{r_k^2} \left[\Delta y_k, -\Delta x_k \right] = \frac{1}{r_k} \left[\cos\alpha(\mathbf{x}_k), -\sin\alpha(\mathbf{x}_k) \right] , \tag{A.15}$$

where r_k denotes the distance between observer and target.

For bearing rate measurements, the measurement equation (2.14) depends on the position and the velocity components of the state. Due to different motion models, we have to consider the partial derivatives with respect to both Cartesian and polar velocity components here. For the other components, the partial derivatives yield zero and are therefore not considered. Hence, the partial derivative of $\dot{\alpha}(\mathbf{x}_k)$ with respect to the position components of the state is given according to

$$\frac{\partial \dot{\alpha}(\mathbf{x}_k)}{\partial \mathbf{p}_k} = \frac{1}{r_k^2} \left(\begin{bmatrix} -\Delta \dot{y}_k \\ \Delta \dot{x}_k \end{bmatrix} - 2\dot{\alpha}(\mathbf{x}_k) \begin{bmatrix} \Delta x_k \\ \Delta y_k \end{bmatrix} \right)^{\mathrm{T}} . \tag{A.16}$$

Furthermore, for the partial derivative with respect to the Cartesian velocity components $\dot{\mathbf{p}}_k = [\dot{x}_k, \dot{y}_k]^{\mathrm{T}}$, we easily obtain the result from (A.15) since $\partial\dot{\alpha}(\mathbf{x}_k)/\partial\dot{\mathbf{p}}_k = \partial\alpha(\mathbf{x}_k)/\partial\mathbf{p}_k$. Note that in case of piecewise inertial motion and $\tilde{t}_{m-1} \leq t_k \leq \tilde{t}_m$, $[x_k, y_k]^{\mathrm{T}} = [x_{m-1}, y_{m-1}]^{\mathrm{T}}$ for $m = 1, \ldots, M+1$. With respect to polar velocity components $\boldsymbol{\upsilon}_k = [v_k, \varphi_k]^{\mathrm{T}}$, the partial derivative is given by

$$\frac{\partial \dot{\alpha}(\mathbf{x}_k)}{\partial \boldsymbol{\upsilon}_k} = \frac{1}{r_k^2} \left(\Delta y_k \begin{bmatrix} \sin\varphi_k \\ v_k \cos\varphi_k \end{bmatrix} + \Delta x_k \begin{bmatrix} -\cos\varphi_k \\ v_k \sin\varphi_k \end{bmatrix} \right)^{\mathrm{T}} . \tag{A.17}$$

Finally, if range measurements are considered, the measurement equation (3.63) only depends on the position components so that the derivations with respect to other components yield zero. Hence, we have

$$\frac{\partial \rho(\mathbf{x}_k)}{\partial \mathbf{p}_k} = -\frac{\Delta \mathbf{p}_k^{\mathrm{T}}}{r_k}\,, \tag{A.18}$$

where $\Delta \mathbf{p}_k = \left[\Delta x_k, \Delta y_k\right]^{\mathrm{T}}$.

B Calculations for Likelihood Decomposition

B.1 Derivation of the Decomposed Likelihood

Let $h : \mathbb{R}^n \to \mathbb{R}^n$ be a continuously differentiable function with $h(\mathbf{x}) = [h_1(\mathbf{x}), \ldots, h_n(\mathbf{x})]$ and let $\mathcal{D}h(\mathbf{x})$ be the Jacobian of h evaluated at $\mathbf{x}$

$$\mathcal{D}h(\mathbf{x}) = \begin{bmatrix} \frac{\partial h_1(\mathbf{x})}{\partial x_1} & \cdots & \frac{\partial h_1(\mathbf{x})}{\partial x_n} \\ \vdots & \ddots & \vdots \\ \frac{\partial h_n(\mathbf{x})}{\partial x_1} & \cdots & \frac{\partial h_n(\mathbf{x})}{\partial x_n} \end{bmatrix} \tag{B.1}$$

with $\mathbf{x} = [x_1, \ldots, x_n]$. Then the first-order (linear) multivariate Taylor series expansion of h around $\mathbf{a}$ is given by

$$h(\mathbf{x}) = h(\mathbf{a}) + \mathcal{D}h(\mathbf{a})(\mathbf{x} - \mathbf{a}) + O\left((\mathbf{x} - \mathbf{a})^2\right). \tag{B.2}$$

The following equation holds with f and g defined in Section 5.5.1:

$$\begin{aligned} \boldsymbol{\zeta} - g(\mathbf{x}) &= g(f(\boldsymbol{\zeta})) - g(\mathbf{x}) && \text{(B.3)} \\ &\approx \{\mathcal{D}g(f(\boldsymbol{\zeta}))\}(f(\boldsymbol{\zeta}) - \mathbf{x}) && \text{(B.4)} \\ &= \{\mathcal{D}f(\boldsymbol{\zeta})\}^{-1}(f(\boldsymbol{\zeta}) - \mathbf{x}), && \text{(B.5)} \end{aligned}$$

where (B.4) is due to applying the Taylor expansion of g around $f(\boldsymbol{\zeta})$ and truncating it after the linear term. We receive (B.5) by using the generalized chain rule. With this, we can approximate the likelihood (5.44) by

$$\begin{aligned} p(\boldsymbol{\zeta}|\mathbf{x}) &= c \, \exp\left(-(\boldsymbol{\zeta} - g(\mathbf{x}))^{\mathrm{T}} \mathbf{N}^{-1} (\boldsymbol{\zeta} - g(\mathbf{x}))/2\right) && \text{(B.6)} \\ &\approx c \, \exp\left(-(f(\boldsymbol{\zeta}) - \mathbf{x})^{\mathrm{T}} \boldsymbol{\Sigma}^{-1} (f(\boldsymbol{\zeta}) - \mathbf{x})/2\right) && \text{(B.7)} \\ &= \det(\mathcal{D}f(\boldsymbol{\zeta})) \, \mathcal{N}(f(\boldsymbol{\zeta}); \mathbf{x}, \boldsymbol{\Sigma}), && \text{(B.8)} \end{aligned}$$

where

$$c = (2\pi)^{-n/2} \det(\mathbf{N})^{-1/2} \tag{B.9}$$

and

$$\boldsymbol{\Sigma} = \mathcal{D}f(\boldsymbol{\zeta}) \, \mathbf{N} \, \mathcal{D}f(\boldsymbol{\zeta})^{\mathrm{T}}. \tag{B.10}$$

The step from (B.6) to (B.7) is due to inserting (B.5) into (B.6). Furthermore, (B.8) holds since

$$\det(\boldsymbol{\Sigma}) = \det(\mathbf{N}) \det(\mathcal{D} f(\boldsymbol{\zeta}))^2 . \tag{B.11}$$

B.2 Derivation of Expected Values

The expected value of $\tilde{p}(\mathbf{z}|\mathbf{x})$ (5.72) with respect to $\mathbf{z}$ is given by

$$E_{\tilde{p}}\{\mathbf{z}\} = \int_{-\infty}^{\infty} \mathbf{z}\, \tilde{p}(\mathbf{z}|\mathbf{x})\, \mathrm{d}\mathbf{z} . \tag{B.12}$$

Thus, with $\boldsymbol{\Sigma}$ from (5.54) we have

$$E_{\tilde{p}}\{\mathbf{z}\} = \int_{-\infty}^{\infty} \mathbf{z} \frac{1}{k} \int_{r_{\min}}^{r_{\max}} r \mathcal{N}\left(\mathbf{z}; r \begin{bmatrix} \sin\theta \\ \cos\theta \end{bmatrix}, \boldsymbol{\Sigma}\right) \mathrm{d}r\, \mathrm{d}\mathbf{z} \tag{B.13}$$

$$= \frac{1}{k} \int_{r_{\min}}^{r_{\max}} r \underbrace{\int_{-\infty}^{\infty} \mathbf{z} \mathcal{N}\left(\mathbf{z}; r \begin{bmatrix} \sin\theta \\ \cos\theta \end{bmatrix}, \boldsymbol{\Sigma}\right) \mathrm{d}\mathbf{z}}_{= r[\sin\theta, \cos\theta]^{\mathrm{T}}} \mathrm{d}r \tag{B.14}$$

$$= \frac{2}{r_{\max}^2 - r_{\min}^2} \begin{bmatrix} \sin\theta \\ \cos\theta \end{bmatrix} \int_{r_{\min}}^{r_{\max}} r^2\, \mathrm{d}r \tag{B.15}$$

$$= \frac{2}{3} \frac{r_{\max}^3 - r_{\min}^3}{r_{\max}^2 - r_{\min}^2} \begin{bmatrix} \sin\theta \\ \cos\theta \end{bmatrix} . \tag{B.16}$$

The expected value of $\psi(\mathbf{z}|\mathbf{x})$ (5.79) with respect to $\mathbf{z}$ can be calculated in a similar way.

List of Figures

List of Tables

Bibliography

[ACV07] M. S. Arulampalam, M. Clark, and R. Vinter. Performance of the Shifted Rayleigh Filter in Single-sensor Bearings-only Tracking. In *Proc. ISIF 10th International Conference on Information Fusion*, Québec City, Québec, Canada, July 2007.

[AH83] V. J. Aidala and S. Hammel. Utilization of Modified Polar Coordinates for Bearings-Only Tracking. *IEEE Trans. Automat. Contr.*, 28(3):283–294, March 1983.

[Aid79] V. J. Aidala. Kalman Filter Behavior in Bearings-Only Tracking Applications. *IEEE Trans. Aerosp. Electron. Syst.*, 15(1):29–39, January 1979.

[ALS07] S. Ali-Löytty and N. Sirola. Gaussian mixture filter in hybrid navigation. In *Proc. The European Navigation Conference GNSS*, pages 831–837, Geneva, Switzerland, May 2007.

[AMGC02] M. S. Arulampalam, S. Maskell, N. Gordon, and T. Clapp. A Tutorial on Particle Filters for Online Nonlinear/Non-Gaussian Bayesian Tracking. *IEEE Trans. Signal Processing*, 50(2):174–188, February 2002.

[AN82] V. J. Aidala and S. C. Nardone. Biased Estimation Properties of the Pseudolinear Tracking Filter. *IEEE Trans. Aerosp. Electron. Syst.*, 18(4):432–441, July 1982.

[AR00] M. S. Arulampalam and B. Ristic. Comparison of the Particle Filter with Range-Parameterised and Modified Polar EKFs for Angle-Only Tracking. In *Proc. SPIE 4048, Signal and Data Processing of Small Targets*, July 2000.

[Bar49] E. W. Barankin. Locally best unbiased estimates. *The Annals of Mathematical Statistics*, 20(4):477–501, 1949.

[Bay63] T. Bayes. An Essay towards Solving a Problem in the Doctrine of Chances. *Philosophical Transactions (1683-1775)*, 1763.

[Bec92] K. Becker. An Efficient Method of Passive Emitter Location. *IEEE Trans. Aerosp. Electron. Syst.*, 28:1091–1104, October 1992.

[Bec93] K. Becker. Simple Linear Theory Approach to TMA Observability. *IEEE Trans. Aerosp. Electron. Syst.*, 29:575–578, April 1993.

[Bec96] K. Becker. A General Approach to TMA Observability from Angle and Frequency Measurements. *IEEE Trans. Aerosp. Electron. Syst.*, 32:487–494, January 1996.

[Bec01] K. Becker. Target Motion Analysis (TMA). In S. Stergiopoulos, editor, *Advanced Signal Processing Handbook: Theory and Implementation for Radar, Sonar, and Medical Imaging Real-Time Systems*, chapter 9. CRC Press, 2001.

[Bec05a] K. Becker. Passive Aufklärung manövrierender Ziele aus Winkel- und Frequenzmessungen. FKIE Report 95, Research Establishment of Applied Science (FGAN), Wachtberg, April 2005. In German language.

[Bec05b] K. Becker. Three-Dimensional Target Motion Analysis using Angle and Frequency Measurements. *IEEE Trans. Aerosp. Electron. Syst.*, 41:284–301, January 2005.

[BFK+15] C. Barz, C. Fuchs, J. Kirchhoff, J. Niewiejska, and H. Rogge. OLSRv2 for Community Networks: Using Directional Airtime Metric with external radios. *Computer Networks*, 93:324–341, December 2015.

[BH09] K. Brinkmann and J. Hurka. Broadband Passive Sonar Tracking. In *Proc. 4th German Workshop on Sensor Data Fusion: Trends, Solutions, Applications (SDF 2009), 39th Annual Conference of the Gesellschaft für Informatik e.V. (GI)*, pages 2397–2404, Lübeck, Germany, October 2009.

[Bha48] A. Bhattacharyya. On Some Analogues of the Amount of Information and Their Use in Statistical Estimation (Concluded). *Sankhyā: The Indian Journal of Statistics*, pages 315–328, 1948.

[BM88] C. I. Byrnes and C. F. Martin. Global Observability and Detectability: an overview. In *Modelling and Adaptive Control*, pages 71–89. Springer, 1988.

[BN97] R. A. Best and J. P. Norton. A New Model and Efficient Tracker for a Target with Curvilinear Motion. *IEEE Trans. Aerosp. Electron. Syst.*, 33:1030–1037, July 1997.

[BP99] S. S. Blackman and R. Popoli. *Design and Analysis of Modern Tracking Systems*. Artech House, Norwood, MA, 1999.

[Bro74] W. L. Brogan. *Modern Control Theory*. Quantum, New York, 1974.

[BSF88] Y. Bar-Shalom and T. E. Fortmann. *Tracking and Data Association*. Academic-Press, Boston, 1988.

[BSL95] Y. Bar-Shalom and X. R. Li. *Multitarget-Multisensor Tracking: Principles and Techniques*. YBS Publishing, 1995.

[BSLK01] Y. Bar-Shalom, X. R. Li, and T. Kirubarajan. *Estimation with Applications to Tracking and Navigation: Theory, Algorithms, and Software*. John Wiley & Sons, Inc., 2001.

[BZ75] B. Z. Bobrovsky and M. Zakai. A Lower Bound on the Estimation Error for Markov Processes. *IEEE Trans. Automat. Contr.*, 20(6):785–788, December 1975.

[BZ83] D. Bestle and M. Zeitz. Canonical form observer design for non-linear time-variable systems. *International Journal of Control*, 38(2):419–431, 1983.

[CDDA09] T. Clausen, C. Dearlove, J. Dean, and C. Adjih. RFC 5444: Generalized Mobile Ad Hoc Network (MANET) Packet/Message Format. RFC, Internet Engineering Task Force (IETF), February 2009.

[CDJH14] T. Clausen, C. Dearlove, P. Jacquet, and U. Herberg. RFC 7181: The Optimized Link State Routing Protocol Version 2. RFC, Internet Engineering Task Force (IETF), April 2014.

[Che99] C.-T. Chen. *Linear System Theory and Design*. Oxford University Press, 1999.

[CJ03] T. Clausen and P. Jacquet. RFC 3626: The Optimized Link State Routing Protocol (OLSR). RFC, Internet Engineering Task Force (IETF), October 2003.

[Col94] P. F. Coll. Target Motion Analysis from a Diesel Submarine's Perspective. Master's thesis, Naval Postgraduate School, Monterey, CA, USA, September 1994.

[CPPJ11] J. Clavard, D. Pillon, A.-C. Pignol, and C. Jauffret. Bearings-Only Target Motion Analysis of a Source in a Circular Constant Speed Motion from a Non-Maneuvering Platform. In *Proc. ISIF 14th International Conference on Information Fusion*, Chicago, IL, USA, July 2011.

[CPPJ13] J. Clavard, D. Pillon, A.-C. Pignol, and C. Jauffret. Target Motion Analysis of a Source in a Constant Turn from a Nonmaneuvering Observer. *IEEE Trans. Automat. Contr.*, 49(3):1760–1780, July 2013.

[Cra46] H. Cramér. A contribution to the theory of statistical estimation. *Scandinavian Actuarial Journal*, 1946(1):85–94, 1946.

[CVY07] J. M. C. Clark, R. B. Vinter, and M. M. Yaqoob. Shifted Rayleigh Filter: A New Algorithm for Bearings-Only Tracking. *IEEE Trans. Aerosp. Electron. Syst.*, 43(4):1373–1384, 2007.

[Dau05] F. E. Daum. Nonlinear Filters: Beyond the Kalman Filter. *IEEE Aerosp. Electron. Syst. Mag.*, 20(8):57–69, August 2005.

[DCABM05] D. S. J. De Couto, D. Aguayo, J. Bicket, and R. Morris. A High-throughput Path Metric for Multi-hop Wireless Routing. *Wirel. Netw.*, 11(4):419–434, July 2005.

[DdFG01] A. Doucet, N. de Freitas, and N. Gordon. An Introduction to Sequential Monte Carlo Methods. In *Sequential Monte Carlo Methods in Practice*, pages 3–14. Springer, 2001.

[DGH+16] S. Davey, N. Gordon, I. Holland, M. Rutten, and J. Williams. *Bayesian Methods in the Search for MH370*. Springer, 2016.

[DK10] M. Daun and R. Kaune. Gaussian Mixture Initialization in Passive Tracking Applications. In *Proc. ISIF 13th International Conference on Information Fusion*, Edinburgh, UK, July 2010.

[DM85] L. Drager and C. Martin. Global observability of a class of nonlinear discrete time systems. *Systems & Control Letters*, 6(1):65–68, June 1985.

[DNK12] M. Daun, U. Nickel, and W. Koch. Tracking in multistatic passive radar systems using DAB/DVB-T illumination. *Signal Processing*, 92(6):1365–1386, June 2012.

[Doğ06] K. Doğançay. Bias Compensation for the Bearings-Only Pseudolinear Target Track Estimator. *IEEE Trans. Signal Processing*, 54(1):59–68, January 2006.

[dVGM92] J. H. de Vlieger and R. H. J. Gmelig Meyling. Maximum Likelihood Estimation for Long-Range Target Tracking Using Passive Sonar Measurements. *IEEE Trans. Signal Processing*, 40(5):1216–1225, May 1992.

[DW08] B. Demissie and P. Willett. Subspace approach to direction finding of rapidly moving sources with an uniform linear array. In *Proc. IEEE 25th Convention of Electrical and Electronics Engineers in Israel*, pages 664–668, Eilat, Israel, December 2008.

[Eke58] J. J. Ekelund. A Means of Passive Range Determination. *Commander Submarine Forces, Atlantic Fleet, Quarterly Information Bulletin*, 1958.

[Far99] A. Farina. Target tracking with bearings-only measurements. *Elsevier Signal Processing*, 78(1):61–78, October 1999.

[FG88] E. Fogel and M. Gavish. Nth-Oder Dynamics Target Observability From Angle Measurements. *IEEE Trans. Aerosp. Electron. Syst.*, 24(3):305–308, May 1988.

[Fis12] R. A. Fisher. On an absolute criterion for fitting frequency curves. *Messenger of Math.*, 41:155, 1912.

[Fit72] J. M. Fitts. On the Observability of Non-linear Systems with Applications to Non-linear Regression Analysis. *Elsevier Information Sciences*, 4(2):129–156, 1972.

[Gau09] C. F. Gauss. *Theoria motus corporum coelestium in sectionibus conicis solem ambientium*. Hamburgi Sumtibus Frid. Perthes et I. H. Besser, 1809.

[GC82] P. M. Grant and J. H. Collins. Introduction to electronic warfare. *IEE Proceedings F (Communications, Radar, and Signal Processing)*, 129(3):113–132, June 1982.

[GGB+02] F. Gustafsson, F. Gunnarsson, N. Bergman, U. Forssell, J. Jansson, R. Karlsson, and P.-J. Nordlund. Particle Filters for Positioning, Navigation, and Tracking. *IEEE Trans. Signal Processing*, 50(2):425–437, February 2002.

[GMBI92] D. Goshen-Meskin and I. Y. Bar-Itzhack. On the Connection Between Estimability and Observability. *IEEE Trans. Automat. Contr.*, 37:1225–1226, August 1992.

[Gov13] F. Govaers. *Enhanced Data Fusion in Communication Contstrained Multi Sensor Applications*. Number 1 in Fraunhofer Series Advances in Sensor Data and Information Fusion. GCA-Verlag, Waabs, Germany, 2013. PhD thesis, University of Bonn, Germany.

[GSS93] N. J. Gordon, D. J. Salmond, and A. F. Smith. Novel approach to nonlinear/non-Gaussian Bayesian state estimation. In *IEE Proceedings F (Radar and Signal Processing)*, volume 140, pages 107–113. IET, April 1993.

[HAGL83] S. Hammel, V. J. Aidala, K. F. Gong, and A. G. Lindgren. Recursive versus Batch Processing Algorithms for Bearings-Only Tracking. In *Proc. OCEANS '83*, pages 50–61, San Francisco, CA, USA, September 1983.

[Hau05] A. J. Haug. A Tutorial on Bayesian Estimation and Tracking Techniques Applicable to Nonlinear and Non-Gaussian Processes. Technical report, The MITRE Corporation, McLean, VA, USA, January 2005.

[HBH06] M. Huber, D. Brunn, and U. D. Hanebeck. Closed-Form Prediction of Nonlinear Dynamic Systems by Means of Gaussian Mixture Approximation of the Transition Density. In *2006 IEEE International Conference on Multisensor Fusion and Integration for Intelligent Systems (MFI)*, pages 98–103, Heidelberg, Germany, September 2006.

[HF03] U. D. Hanebeck and O. Feiermann. Progressive Bayesian Estimation for Nonlinear Discrete-Time Systems: The Filter Step for Scalar Measurements and Multidimensional States. In *Proc. 42nd IEEE Conference on Decision and Control (CDC)*, pages 5366–5371, Maui, Hawaii, USA, December 2003.

[HH93] A. Holtsberg and J. H. Holst. A Nearly Unbiased Inherently Stable Bearings-Only Tracker. *IEEE J. Oceanic Eng.*, 18(2):138–141, April 1993.

[HJC78] H. D. Hoelzer, G. W. Johnson, and A. O. Cohen. Modified Polar Coordinates – The Key to Well Behaved Bearings Only Ranging. IR & D Report, IBM Federal Systems Division Shipboard and Defense Systems, Manassas, VA, USA, August 1978.

[HK77] R. Hermann and A. J. Krener. Nonlinear Controllability and Observability. *IEEE Trans. Automat. Contr.*, 22(5):728–740, 1977.

[Hu01] L. Hu. Bearings-Only Target Motion Analysis Using a Dual-Waveband Infrared System. In *International Journal of Infrared and Millimeter Waves*, volume 22, pages 237–246. Springer, February 2001.

[Hub15] M. Huber. *Nonlinear Gaussian Filtering: Theory, Algorithms, and Applications*. Number 19 in Karlsruher Schriften zur Anthropomatik. KIT Scientific Publishing, Karlsruhe, Germany, 2015.

[Jau07] C. Jauffret. Observability and Fisher Information Matrix in Nonlinear Regression. *IEEE Trans. Aerosp. Electron. Syst.*, 43(2):756–759, April 2007.

[Jaz70] A. H. Jazwinski. *Stochastic Processes and Filtering Theory*. Academic Press, 1970.

[Joh14] S. G. Johnson. The NLopt nonlinear-optimization package. `http://ab-initio.mit.edu/nlopt`, 2014. Accessed: 2017-07-14.

[JP96] C. Jauffret and D. Pillon. Observability in Passive Target Motion Analysis. *IEEE Trans. Aerosp. Electron. Syst.*, 32(4):1290–1300, October 1996.

[JPP10] C. Jauffret, D. Pillon, and A.-C. Pignol. Bearings-only Maneuvering Target Motion Analysis from a Nonmaneuvering Platform. *IEEE Trans. Aerosp. Electron. Syst.*, 46(4):1934–1949, October 2010.

[JPP14] C. Jauffret and A.-C. Pérez-Pignol. Cramér-Rao-type Lower Bound for a Time of Abrupt Change. In *Proc. ISIF 17th International Conference on Information Fusion*, Salamanca, Spain, July 2014.

[JU04] S. J. Julier and J. K. Uhlmann. Unscented Filtering and Nonlinear Estimation. *Proc. IEEE*, 92(3):401–422, March 2004.

[JUDW95] S. J. Julier, J. K. Uhlmann, and H. Durrant-Whyte. A New Approach for Filtering Nonlinear Systems. In *Proc. 1995 American Control Conference*, volume 3, pages 1628–1632, June 1995.

[KA06] P. Kaelo and M. M. Ali. Some variants of the controlled random search algorithm for global optimization. *Journal of Optimization Theory and Applications*, 130(2):253–264, 2006.

[Kai80] T. Kailath. *Linear Systems*. Prentice-Hall, 1980.

[Kal60] R. E. Kalman. A New Approach to Linear Filtering and Prediction Problems. *Transactions of the ASME–Journal of Basic Engineering*, 82(Series D):35–45, 1960.

[KBSL01] T. Kirubarajan, Y. Bar-Shalom, and D. Lerro. Bearings-only Tracking of Maneuvering Targets Using a Batch-Recursive Estimator. *IEEE Trans. Aerosp. Electron. Syst.*, 37:770–780, July 2001.

[Ker89] T. H. Kerr. Status of CR-Like Lower Bounds for Nonlinear Filtering. *IEEE Trans. Aerosp. Electron. Syst.*, 25(5):590–601, September 1989.

[KET73] S. R. Kou, D. L. Elliott, and T. J. Tarn. Observability of Nonlinear Systems. *Information and Control*, 22(1):89–99, 1973.

[KG05] R. Karlsson and F. Gustafsson. Recursive Bayesian Estimation: Bearings-only Applications. *IEE Proceedings Radar, Sonar and Navigation*, 152(5):305–313, 2005.

[Koc01] W. Koch. Target Tracking. In S. Stergiopoulos, editor, *Advanced Signal Processing Handbook: Theory and Implementation for Radar, Sonar, and Medical Imaging Real-Time Systems*, chapter 8. CRC Press, 2001.

[Koc14] W. Koch. *Tracking and Sensor Data Fusion: Methodological Framework and Selected Applications*. Springer, 2014.

[Kro98] T. R. Kronhamn. Bearings-only Target Motion Analysis based on a Multihypothesis Kalman Filter and Adaptive Ownship Motion Control. *IEE Proceedings Radar, Sonar and Navigation*, 145(4):247–252, 1998.

[KvK97] W. Koch and G. van Keuk. Multiple Hypothesis Track Maintenance with Possibly Unresolved Measurements. *IEEE Trans. Aerosp. Electron. Syst.*, 33(3):883–892, July 1997.

[Lap80] P. S. Laplace. Mémoire sur la détermination des orbites des comètes. *Mémoires de l'Académie Royale des Sciences de Paris*, 1780.

[LCJ97] J. P. Le Cadre and C. Jauffret. Discrete-Time Observability and Estimability Analysis for Bearings-Only Target Motion Analysis. *IEEE Trans. Aerosp. Electron. Syst.*, 33(1):178–201, January 1997.

[LCT98] J. P. Le Cadre and O. Trémois. Bearings-only Tracking for Maneuvering Sources. *IEEE Trans. Aerosp. Electron. Syst.*, 34:179–193, January 1998.

[Leg06] A. M. Legendre. Nouvelles méthodes pour la détermination des orbites des comètes. *Imprimeur-Libraire pour les Mathématiques, Paris*, 1806.

[LG78] A. G. Lindgren and K. F. Gong. Position and Velocity Estimation Via Bearing Observations. *IEEE Trans. Aerosp. Electron. Syst.*, 14(4):564–577, July 1978.

[Li12] Q. Li. *Digital Sonar Design In Underwater Acoustics: Principles and Applications*. Springer, 2012.

[LJ02] X. R. Li and V. P. Jilkov. A Survey of Maneuvering Target Tracking–Part IV: Decision-Based Methods. In *Proc. SPIE 4728, Signal and Data Processing of Small Targets*, August 2002.

[LJ03] X. R. Li and V. P. Jilkov. Survey of Maneuvering Target Tracking. Part I: Dynamic Models. *IEEE Trans. Aerosp. Electron. Syst.*, 39(4):1333–1364, 2003.

[LJ08] D. Laneuville and C. Jauffret. Recursive Bearings-Only TMA via Unscented Kalman Filter: Cartesian vs. Modified Polar Coordinates. In *IEEE Aerospace Conference*, Big Sky, MT, USA, March 2008.

[LKBSM02] X. Lin, T. Kirubarajan, Y. Bar-Shalom, and S. Maskell. Comparison of EKF, Pseudomeasurement, and Particle Filters for a Bearing-only Target Tracking Problem. In *Proc. SPIE 4728, Signal and Data Processing of Small Targets*, pages 240–250, August 2002.

[LSK06] T. Leinmüller, E. Schoch, and F. Kargl. Position Verification Approaches for Vehicular Ad Hoc Networks. *IEEE Wireless Communications*, 13(5):16–21, October 2006.

[LSM08] B. La Scala and M. Morelande. An Analysis of the Single Sensor Bearings-Only Tracking Problem. In *Proc. ISIF 11th International Conference on Information Fusion*, Cologne, Germany, July 2008.

[LWBL16] X. Li, P. Willett, M. Baum, and Y. Li. PMHT Approach for Underwater Bearing-Only Multisensor–Multitarget Tracking in Clutter. *IEEE J. Oceanic Eng.*, 41(4):831–839, October 2016.

[LWGH09] D. Lindgren, O. Wilsson, F. Gustafsson, and H. Habberstad. Shooter Localization in Wireless Sensor Networks. In *Proc. ISIF 12th International Conference on Information Fusion*, Seattle, WA, USA, July 2009.

[LZJ02] X. R. Li, Z. Zhao, and V. P. Jilkov. Estimator's Credibility and its Measures. In *Proc. IFAC 15th World Congress*, Barcelona, Spain, July 2002.

[May82] P. S. Maybeck. *Stochastic Models, Estimation, and Control*, volume 3 of *Mathematics in Science and Engineering*. Acadamic Press, 1982.

[MBS05] W. Montlouis, O. Bayat, and B. Shafai. DOA and angular velocity estimation using planar array with subspace based initialization. In *Proc. IEEE Military Communications Conference (MILCOM)*, pages 2797 – 2801, Atlantic City, NJ, USA, October 2005.

[McG11] S. B. McGrayne. *The Theory That Would Not Die: How Bayes' Rule Cracked the Enigma Code, Hunted Down Russian Submarines, and*

Emerged Triumphant from Two Centuries of Controversy. Yale University Press, 2011.

[ME06] D. Mušicki and R. J. Evans. Measurement Gaussian Sum Mixture Target Tracking. In *Proc. ISIF 9th International Conference on Information Fusion*, Florence, Italy, July 2006.

[Mor78] J. J. Moré. The levenberg-marquardt algorithm: implementation and theory. In *Numerical Analysis*, pages 105–116. Springer, 1978.

[MS96] V. Maz'ya and G. Schmidt. On approximate approximations using Gaussian kernels. *IMA Journal of Numerical Analysis*, 16(1):13–29, 1996.

[Muš09] D. Mušicki. Bearings only single-sensor target tracking using gaussian mixtures. *Automatica*, 45(9):2088–2092, 2009.

[NA81] S. C. Nardone and V. J. Aidala. Observability Criteria For Bearings-Only Target Motion Analysis. *IEEE Trans. Aerosp. Electron. Syst.*, 17(2):162–166, March 1981.

[Nat] National Aeronautics and Space Administration (NASA). World Wind Java SDK. `http://worldwind.arc.nasa.gov/java/`. Accessed: 2015-12-04.

[NG97] S. C. Nardone and M. L. Graham. A Closed-Form Solution to Bearings-Only Target Motion Analysis. *IEEE J. Oceanic Eng.*, 22(1):168–178, January 1997.

[Nij82] H. Nijmeijer. Observability of autonomous discrete time non-linear systems: a geometric approach. *International Journal of Control*, 36(5):867–874, 1982.

[NLG84] S. C. Nardone, A. G. Lindgren, and K. F. Gong. Fundamental Properties and Performance of Conventional Bearings-Only Target Motion Analysis. *IEEE Trans. Automat. Contr.*, 29:775–787, September 1984.

[NM65] J. A. Nelder and R. Mead. A simplex method for function minimization. *Computer Journal*, 7:308–313, January 1965.

[Ois14] M. Oispuu. *Passive Emitter Localization by Direct Position Determination with Moving Array Sensors*. Number 5 in Fraunhofer Series Advances in Sensor Data and Information Fusion. GCA-Verlag, Waabs, Germany, 2014. PhD thesis, University of Siegen, Germany.

[OLS] OLSR. olsr.org. `http://www.olsr.org/`. Accessed: 2016-01-21.

[Pap84] A. Papoulis. *Probability, Random Variables, and Stochastic Processes*. McGraw-Hill, New York, 1984.

[Pea95] N. Peach. Bearings-only tracking using a set of range-parameterised extended Kalman filters. In *IEE Proc. Control Theory and Applications*, volume 142, pages 73–80, January 1995.

[Pow09] M. J. D. Powell. The BOBYQA algorithm for bound constrained optimization without derivatives. DAMTP 2009/NA06, Department of Applied Mathematics and Theoretical Physics, Cambridge University, June 2009.

[Pri83] W. L. Price. Global optimization by controlled random search. *Journal of Optimization Theory and Applications*, 40(3):333–348, 1983.

[PT08] M. Preuss and S. Thomas. Wireless, Mesh & Ad Hoc Networks; Military Convoy Location and Situation Awareness. In *2008 IEEE Sarnoff Symposium*, pages 1–5. IEEE, 2008.

[RA03] B. Ristic and M. S. Arulampalam. Tracking a manoeuvring target using angle-only measurements: algorithms and performance. *Elsevier Signal Processing*, 83:1223–1238, January 2003.

[RAG04] B. Ristic, M. S. Arulampalam, and N. Gordon. *Beyond the Kalman Filter: Particle Filters for Tracking Applications*. Artech House, Boston, MA, USA, 2004.

[Rao45] C. R. Rao. Information and accuracy attainable in the estimation of statistical parameters. *Bull. Calcutta. Math. Soc.*, 37:81–91, 1945.

[RB13] H. Rogge and E. Baccelli. Packet Sequence Number based directional Airtime Metric for OLSRv2. Internet Draft, Internet Engineering Task Force (IETF), June 2013.

[RGYU99] K. Reif, S. Günther, E. Yaz, and R. Unbehauen. Stochastic Stability of the Discrete-Time Extended Kalman Filter. *IEEE Trans. Automat. Contr.*, 44(4):714–728, April 1999.

[RJLB09] J. Ru, V. P. Jilkov, X. R. Li, and A. Bashi. Detection of Target Maneuver Onset. *IEEE Trans. Aerosp. Electron. Syst.*, 45(2):536–554, April 2009.

[RN05] S. Reece and D. Nicholson. Tighter Alternatives to the Cramér-Rao Lower Bound for Discrete-Time Filtering. In *Proc. ISIF 8th International Conference on Information Fusion*, Philadelphia, PA, USA, July 2005.

[Run07] A. R. Runnalls. Kullback-Leibler Approach to Gaussian Mixture Reduction. *IEEE Trans. Aerosp. Electron. Syst.*, 43(3):989–999, July 2007.

[SA71] H. W. Sorenson and D. L. Alspach. Recursive Bayesian Estimation using Gaussian Sums. *Automatica*, 7(4):465 – 479, 1971.

[Sal89] D. J. Salmond. Mixture Reduction Algorithms for Target Tracking. In *IEE Colloquium on State Estimation in Aerospace and Tracking Applications*, London, UK, December 1989.

[Sär13] S. Särkkä. *Bayesian Filtering and Smoothing*. Cambridge University Press, 2013.

[Sch91] L. L. Scharf. *Statistical Signal Processing: Detection, Estimation, and Time Series Analysis*. Prentice Hall, 1991.

[SDŠ11] O. Straka, J. Duník, and M. Šimandl. Performance Evaluation of Local State Estimation Methods in Bearings-only Tracking Problems. In *Proc. ISIF 14th International Conference on Information Fusion*, Chicago, IL, USA, July 2011.

[SG92] Y. Song and J. W. Grizzle. The Extended Kalman Filter as a Local Asymptotic Observer for Nonlinear Discrete-Time Systems. In *American Control Conference*, pages 3365–3369, Chicago, IL, USA, June 1992.

[ŠKT01] M. Šimandl, J. Královec, and P. Tichavský. Filtering, predictive, and smoothing Cramér-Rao bounds for discrete-time nonlinear dynamic systems. *Automatica*, 37:1703–1716, April 2001.

[Son84] E. D. Sontag. A concept of local observability. *Systems & Control Letters*, 5(1):41–47, 1984.

[Son96] T. L. Song. Observability of Target Tracking with Bearings-Only Measurements. *IEEE Trans. Aerosp. Electron. Syst.*, 32(4):1468–1472, October 1996.

[Sor70] H. W. Sorenson. Least-squares estimation: from Gauss to Kalman. *IEEE spectrum*, 7(7):63–68, July 1970.

[SS85] T. L. Song and J. L. Speyer. A Stochastic Analysis of a Modified Gain Extended Kalman Filter with Applications to Estimation with Bearings Only Measurements. *IEEE Trans. Automat. Contr.*, 30(10):940–949, October 1985.

[Sva02] K. Svanberg. A class of globally convergent optimization methods based on conservative convex separable approximations. *SIAM Journal on Optimization*, 12(2):555–573, 2002.

[SW09] R. L. Streit and R. L. Wojtowicz. A General Likelihood Function Decomposition that is Linear in Target State. In *IEEE Aerospace Conference*, pages 1–8, Big Sky, MT, USA, March 2009.

[Tay79] J. H. Taylor. The Cramér-Rao Estimation Error Lower Bound Computation for Deterministic Nonlinear Systems. *IEEE Trans. Automat. Contr.*, 24(2):343–344, April 1979.

[TMN98] P. Tichavský, C. H. Muravchik, and A. Nehorai. Posterior Cramér-Rao Bounds for Discrete-Time Nonlinear Filtering. *IEEE Trans. Signal Processing*, 46(5):1386–1396, May 1998.

[TPH99] W. I. Tam, K. N. Plataniotis, and D. Hatzinakos. An adaptive gaussian sum algorithm for radar tracking. *Signal processing*, 77(1):85–104, 1999.

[Tsc14] W. Tschirk. *Statistik: Klassisch oder Bayes: Zwei Wege im Vergleich*. Springer, 2014. In German language.

[Ubi11] Ubiquiti Networks, Inc. Bullet M Datasheet. `https://dl.ubnt.com/datasheets/bulletm/bm_ds_web.pdf`, 2011. Accessed: 2015-12-07.

[Val12] Valentine Research, Inc. Valentine One Radar Locator Owner's Manual. `http://www.valentine1.com/v1info/pdf/manual_2012/Manual_V1.pdf`, 2012. Accessed: 2015-12-07.

[vHF98] D. van Huyssteen and M. Farooq. Performance analysis of bearings-only tracking algorithm. In *Proc. SPIE 3365, Acquisition, Tracking, and Pointing XII*, pages 139–149, July 1998.

[VT68] H. L. Van Trees. *Detection, Estimation, and Modulation Theory, Part I: Detection, Estimation, and Linear Modulation Theory*. John Wiley & Sons, Inc., 1968.

[VTB07] H. L. Van Trees and K. L. Bell. *Bayesian Bounds for Parameter Estimation and Nonlinear Filtering/Tracking*. John Wiley & Sons, Inc., 2007.

[WE95] T. Wigren and A. Eriksson. Accuracy Aspects of DOA and Angular Velocity Estimation in Sensor Array Processing. *IEEE Signal Processing Lett.*, 2:60–62, April 1995.

[Wed74] R. W. M. Wedderburn. Quasi-Likelihood Functions, Generalized Linear Models, and the Gauss-Newton Method. *Biometrika*, 61(3):439–447, December 1974.

[WM03] J. L. Williams and P. S. Maybeck. Cost-Function-Based Gaussian Mixture Reduction for Target Tracking. In *Proc. ISIF 6th International Conference on Information Fusion*, Cairns, Queensland, Australia, July 2003.

[WW88] E. Weinstein and A. J. Weiss. A General Class of Lower Bounds in Parameter Estimation. *IEEE Trans. Inform. Theory*, 34(2):338–342, March 1988.

[YNBS15] R. Yang, G. W. Ng, and Y. Bar-Shalom. Bearings-Only Tracking with Fusion from Heterogenous Passive Sensors: ESM/EO and Acoustic. In *Proc. ISIF 18th International Conference on Information Fusion*, pages 1810–1816, Washington D.C., USA, July 2015.

Own References

[HK16] J. Hörst and W. Koch. Observability Analysis for Heterogeneous Passive Sensors Exploiting Signal Propagation Velocities. In *Proc. 2016 IEEE International Conference on Multisensor Fusion and Integration for Intelligent Systems (MFI 2016)*, Baden-Baden, Germany, September 2016.

[HGR+16] J. Hörst, F. Govaers, B. Rehbein, C. Barz, and P. Sevenich. Joint Protection of a Military Formation Using Heterogeneous Sensors in a Mobile Ad hoc Network: Concept and Field Tests. In *International Conference on Military Communications and Information Systems (ICMCIS)*, Brussels, Belgium, May 2016.

[Hör14] J. Hörst. Analysis of Likelihood Approximations for Bearings-Only Measurements. In *Proc. ISIF 17th International Conference on Information Fusion*, Salamanca, Spain, July 2014.

[HOK14] J. Hörst, M. Oispuu, and W. Koch. Accuracy Study for a Piecewise Maneuvering Target with Unknown Maneuver Change Times. *IEEE Trans. Aerosp. Electron. Syst.*, 50(1):737–755, January 2014.

[UWH+13] M. Ulmke, K. Wild, J. Hörst, and M. Mertens. Sensor Data Fusion for Agile UAVs in a Network-centric Environment. In *2012 Annual Military Scientific Research Report*. German Federal Ministry of Defence, April 2013.

[Hör12] J. Hörst. Target Maneuver Detection using a Particle Filter with Spawn Model and Particle Labeling. In *Proc. 7th German Workshop on Sensor Data Fusion*, pages 93–98, Bonn, Germany, September 2012.

[HO11a] J. Hörst and M. Oispuu. Target Localization and Course Change Detection Using Bearing and Bearing Rate Measurements. In *Proc. ISIF 14th International Conference on Information Fusion*, Chicago, IL, USA, July 2011.

[HO11b] J. Hörst and M. Oispuu. Accuracy Study and State Estimation for Piecewise Maneuvering Targets with Unknown Maneuver Change Times. FKIE Report 214, Fraunhofer FKIE, Wachtberg, July 2011.

[KHK11] R. Kaune, J. Hörst, and W. Koch. Accuracy Analysis for TDOA Localization in Sensor Networks. In *Proc. ISIF 14th International Conference on Information Fusion*, Chicago, IL, USA, July 2011.

[HO10] J. Hörst and M. Oispuu. Localization of Piecewise Curvilinearly Moving Targets Using Azimuth and Azimuth Rates. In *Proc. 5th German Workshop on Sensor Data Fusion*, Leipzig, Germany, September 2010.

[OH10] M. Oispuu and J. Hörst. Azimuth-only Localization and Accuracy Study for Piecewise Curvilinearly Moving Targets. In *Proc. ISIF 13th International Conference on Information Fusion*, Edinburgh, UK, July 2010.

[Hör09] J. Hörst. Extension of the Sliced Gaussian Mixture Filter with Application to Cooperative Passive Target Tracking. Diploma thesis, Universität Karlsruhe (TH), 2009.

[HSK+09] J. Hörst, F. Sawo, V. Klumpp, U. D. Hanebeck, and D. Fränken. Extension of the Sliced Gaussian Mixture Filter with Application to Cooperative Passive Target Tracking. In *Proc. ISIF 12th International Conference on Information Fusion*, Seattle, WA, USA, July 2009.